Addis Ababa University
Addis Ababa Institute of Technology
School of Electrical & Computer Engineering

Optimization of Millimeter Wave Microstrip Antenna for Wireless Application Using Genetic Algorithm

---

A PhD Dissertation submitted to the School of Graduate Studies of Addis Ababa University in partial fulfillment of the requirements for the Degree of Doctor of Philosophy in Communication Engineering

By:

Arebu Dejen

Supervisors

Prof. Jaume Anguera

Prof. Jeevani Jayasinghe

Dr. Murad Ridwan

December, 2023

Approval Page

A PhD Dissertation entitled **"Optimization of Millimeter Wave Microstrip Antenna for Wireless Application Using Genetic Algorithm"** is submitted to the School of Graduate Studies of Addis Ababa University in partial fulfillment of the requirements for the Degree of Doctor of Philosophy in Communication Engineering.

Arebu Dejen	_____
Name	Signature

Approved by Board of Examiners

Prof. Jaume Anguera	_____
Supervisor	Signature
Prof. Jeevani Jayasinghe	_____
Supervisor	Signature
Dr. Murad Ridwan	_____
Supervisor	Signature
Dr. Bisrat Derebssa	_____
Dean, SECE, AAiT	Signature
Prof. Mohammed Abdo	_____
Internal Examiner	Signature
Prof. Vedula VSS Sameer Chakravarthy	_____
External Examiner	Signature

Declaration

This PhD Dissertation is a presentation of my own original research work, and that any content derived from other sources is clearly identified, properly acknowledged, and cited.

Arebu Dejen Abdela _____

Name Signature

Date of submission: **December, 2023**

This PhD Dissertation has been submitted with the approval of my supervisors

Prof. Jaume Anguera _____

Supervisor Signature

Prof. Jeevani Jayasinghe _____

Supervisor Signature

Dr. Murad Ridwan _____

Supervisor Signature

Abstract

In the telecommunications industry, wireless communications have progressed very rapidly in the last two decades. The requirement for high data rates and the paucity of spectrum in existing wireless communication drive next-generation communication technology to mm-wave frequencies, which also require adequate and efficient antenna technology for successful operation. These signals, however, have a high path loss and are susceptible to blocking. These mm-wave signal propagation challenges can be overcome by using high-directivity, wide-band, and multi-band antennas. Nonetheless, creating such a high-performance antenna in every way is a challenging endeavor. This dissertation discourses on the modeling, optimizing, and synthesizing of a rectangular microstrip patch antenna with dual-band and multi-band service for mm-wave communication using a binary-coded genetic algorithm to improve the directivity and bandwidth. The algorithm iteratively creates new models of patch surfaces by employing an iterative combination of HFSS and MATLAB software, and then returns the best antenna model. Accordingly, the dissertation exhibits improvements in the directivity, bandwidth, and multi-functionality of a single microstrip antenna. With patch geometry optimization, a dual-band antenna was optimized and resonated at 28.0 GHz and 46.6 GHz with acceptable performance. Another optimization was carried out on a single microstrip antenna for triple band operation and directivity improvement. The optimized antenna resonated at three distinct frequency bands centered at 28.0 GHz, 40.0 GHz, and 47.0 GHz, and demonstrates broadside radiation patterns with peak directivities of 7.7 dB, 12.1 dB, and 8.2 dB, respectively. On the other hand, bandwidth melioration was achieved by a genetically optimized quad-band antenna, which was resonated at four frequencies centered at 28.3 GHz, 38.1 GHz, 46.6 GHz, and 60.0 GHz, and a total operating bandwidth of 11.5 GHz. The dissertation also presents a penta-band mm-wave antenna for wearable applications. The proposed antenna designed on PTFE fabric substrate and resonates at five distinct frequencies: 27.8 GHz, 30.3 GHz, 40.1 GHz, 47.2 GHz, and 56.7 GHz. In free space, the antenna achieves a wide bandwidth of 0.69, 2.32, 2.22, 1.76, and 8.11 GHz and an improved broadside directivity of 10.3, 8.5, 7.8, 9.6, and 8.9 dB, respectively. Overall, the optimized antennas performances were suitable for multi-functional mm-wave applications.

Keyword: mm-wave communication, microstrip antenna, genetic algorithm optimization, dual-band antenna, triple band antenna, quad-band antenna, penta-band antenna, directivity improvement, bandwidth enhancement

Acknowledgment

First and foremost, I would like to extend my utmost gratitude and appreciation to my dissertation supervisor, Prof. Jaume Anguera (Universitate of Roman Llull, Barcelona, Spain). He provided excellent oversight, and his insightful remarks, advice, and guidance were very helpful in advancing my study. I also want to extend my gratefulness and deep respect to my advisor, Prof. Jeevani Jayasinghe (Wayamba University of Sri Lanka). Her unwavering encouragement, essential assistance with constructive feedback, and ideas throughout the study have all been credited with the accomplishment of this dissertation.
I wanted to express my thankfulness and admiration for my instructor and dissertation advisor, Dr. Murad Ridwan (AAU, AAiT). He was really helpful and provided great advice, support, remarks, and assistance during my entire PhD life.
I would also like to convey my thanks to the members of the school of electrical and computer engineering staff at the Addis Ababa Institute of Technology (AAiT). I wish to express my special thanks to Dr. Ephrem Teshale, and Dr. Bisrat for their administrative and technical support to complete this study.
I also appreciate the moral support provided by my pals, Dr. Abdureuf Misgea and Mr. Ahmed Dagne. Last but not least, I want to thank my parents, Dejene Abdella and Alem Gizaw, for their unending love and understanding. Finally, I would like to express my gratitude to my wife, Remla Hussen, for her support and patience during the PhD process.

List of Publications

1. A. Dejen, J. Jayasinghe, M. Ridwan, and J. Anguera, "Genetically optimized quadband mm-wave microstrip patch antenna," *in Advances in Signal Processing, Embedded Systems and IoT, Lecture Notes in Electrical Engineering*, vol 992, Springer, Singapore, May 2023

2. A. Dejen, J. Anguera, J. Jayasinghe, and M. Ridwan, "Bandwidth improvement of dual-band microstrip mm-wave antenna using genetic algorithm," *Inter Journal of Computing and Digital Systems*, Vol. 13, pp. 1-8, 2023

3. A. Dejen, J. Jayasinghe, M. Ridwan, and J. Anguera, "Synthesis of quadband mm-wave microstrip antenna using genetic algorithm for wireless application," *Technologies*, vol. 11, pp. 1–14, 2023.

4. A. Dejen, M. Ridwan, J. Anguera, and J. Jayasinghe, "Millimeter wave cellular communication performances and challenges: A survey," *EAI Endorsed Transactions on Mobile Communications and Applications*, vol. 7, pp. 1–8, 2022

5. A. Dejen, M. Ridwan, J. Jayasinghe, and J. Anguera, "Multi-band mm-wave wearable antenna synthesized with a genetic algorithm," *International Journal of Antennas and Propagation*, vol. 2022, pp. 1–17, 2022

6. A. Dejen, J. Jayasinghe, M. Ridwan, and J. Anguera, "Genetically engineered triband microstrip antenna with improved directivity for mm-wave wireless application,"*AIMS Electronics and Electrical Engineering*, vol. 6, pp. 1–15, 2022

7. A. Dejen, J.Jayasinghe, M.Ridwan, J. Anguera, "Optimization of dualband microstrip mm-wave antenna with improved directivity for mobile application using genetic algorithm," *International Conference on Advances of Science and Technology*, vol 441. Bahir Dar, Ethiopia, 2021

8. A. Dejen, J. Anguera, M. Ridwan, and J. Jayasinghe, "Genetically engineered dualband microstrip antenna with improved directivity for 5g mm-wave mobile applications," *1st IEEE International Women in Engineering Symposium*, Sir Lanka, 2020.

Contents

Abstract iv

Acknowledgment v

List of Publications vi

List of Figures x

List of Tables xiii

List of abbreviations xiv

1 Introduction 2

1.1 Millimeter wave communication: A background . . . 3
1.2 Statement of the problem . . . 5
1.3 Objectives . . . 6
1.3.1 General objective . . . 6
1.3.2 Specific objectives . . . 6
1.4 Methodology . . . 7
1.5 Thesis Contribution . . . 7
1.6 Thesis structure . . . 9

2 A Comprehensive Survey on Microstrip Antenna 11

2.1 Introduction . . . 11
2.2 Microstrip Antenna . . . 12
2.2.1 Method of analysis . . . 14
2.3 Performance Metrics . . . 19
2.3.1 Radiation pattern . . . 19
2.3.2 Directivity and Gain . . . 20
2.3.3 Efficiency . . . 21
2.3.4 Return loss and Bandwidth . . . 21
2.3.5 Input impedance . . . 22
2.4 Performance Improvement Techniques . . . 25
2.4.1 Gain and Directivity Improvement Methods . . . 25
2.4.2 Bandwidth Enhancement . . . 27
2.4.3 Multi-band Creation Techniques . . . 30
2.5 Current State of the Art . . . 34
2.6 Chapter Summary . . . 35

3 Genetic Algorithm Optimization for Microstrip Antenna Design 37
3.1 Introduction . . . 37
3.2 Genetic Algorithm Optimization . . . 37
3.2.1 Binary-Coded GA Terminologies . . . 38
3.2.2 Fitness Function . . . 38
3.3 GA Operators and Procedures . . . 38
3.3.1 Selection . . . 39
3.3.2 Crossover . . . 40
3.3.3 Mutation . . . 42
3.4 The Schema Theorem . . . 42
3.5 GA for Microstrip Antenna Optimization . . . 45
3.6 Interfacing Ansys HFSS and MATLAB . . . 46
3.6.1 HFSS computation methods . . . 46
3.6.2 Implementing GA . . . 48
3.7 Chapter Summary . . . 49

4 Synthesis of Dual-band Microstrip Antenna based on GA 51
4.1 Introduction . . . 51
4.2 Dual-band with Improved Directivity . . . 51
4.2.1 Employing Small-rectangular Cells . . . 52
4.2.2 Employing Circular Cells . . . 56
4.2.3 Comparison with Related Works . . . 59
4.3 Dual-band Antenna with Enhanced Bandwidth . . . 62
4.3.1 Antenna Modeling . . . 63
4.3.2 GA Optimization Setup . . . 63
4.3.3 Results and Discussion . . . 67
4.4 Chapter Summary . . . 70

5 Synthesis of Multi-band Microstrip Antenna with Improved Directivity and Bandwidth based on GA 72
5.1 Introduction . . . 72
5.2 Tri-band Antenna with Directivity Improvement . . . 73
5.2.1 Antenna Modeling . . . 73
5.2.2 GA Optimization Setup . . . 75
5.2.3 Results and Discussion . . . 77
5.2.4 Comparison with Related Works . . . 82
5.3 Bandwidth Enhancement of Quad-band Antenna . . . 84
5.3.1 Antenna Modeling . . . 84
5.3.2 GA Optimization Setup . . . 85

5.3.3 Results and Discussion . . . 87
5.3.4 Comparison with Related Works . . . 92
5.4 Penta-band Antenna with Bandwidth Improvement for Wearable Applications . . . 94
5.4.1 Antenna Modeling . . . 95
5.4.2 GA Optimization Setup . . . 96
5.4.3 Results and Discussion . . . 98
5.4.4 Comparison with Related Works . . . 106
5.5 Chapter Summary . . . 108

6 Conclusion and Recommendation for Future work 110
6.1 Conclusions . . . 110
6.2 Challenges and Limitations . . . 113
6.3 Recommendation for Future Work . . . 113
6.3.1 Increasing Efficiency and Effectiveness of GA . . . 113
6.3.2 Further Improving Performance of mm-wave antenna . . . 114

References 116

List of Figures

1.1 Predicted spectrum of mm wave for wireless communication [16] 4

2.1 Structure of rectangular microstrip patch antenna 13
2.2 Physical and effective length of a microstrip antenna 14
2.3 Electric field lines from the radiating patch 14
2.4 magnetically wall model of microstrip antenna 16
2.5 Charge distribution and current density on microstrip antenna 16
2.6 The radiating patch surface and the equivalent transmission line model . 23
2.7 Rectangular microstrip antenna with transitional impedance matching line 24
2.8 Summary of peak average directivity vs patch area (λ^2) of single patch element 34

3.1 Process of reproducing next generation in genetic algorithm [171] 39
3.2 Example of single point crossover operation 41
3.3 Genetic algorithm flowchart 42
3.4 Gridded rectangular patch surface 46
3.5 Iterative implementation GA using HFSS and MATLAB 48
3.6 The proposed Genetic Algorithm optimization flowchart 50

4.1 Single patch antenna top view at 28.0 GHz on finite substrate 53
4.2 8 x 8 division of the reference microstrip patch surface 53
4.3 Genetically optimized proposed patch geometry 54
4.4 Simulated results of reference antenna magnitude of S11 resonating at 28.0 GHz 55
4.5 Radiation pattern plot of reference antenna at 28.0 GHz 55
4.6 S_{11} result of genetically optimized patch antenna 56
4.7 Directivity of genetically optimized patch antenna (a) at 28.0 GHz and (b) directivity at 46.6 GHz 56
4.8 Reference patch antenna element operating at 28.0 GHz printed on a substrate (a) top view and (b) side view. 57
4.9 Placement of 100 circular cells on rectangular patch surface 58
4.10 average fitness value of a generation vs number of generation 59
4.11 genetically optimized microstrip radiating patch geometry 59
4.12 Simulated S11 of the GAO dual-band patch antenna resonates at 28.0 GHz and 31.1 GHz 60
4.13 Directivity of genetically optimized patch antenna a) at 28.0 GHz b) at 31.1 GHz 60

4.14 Surface Current distribution: a) reference antenna at 28 GHz, b) GAO antenna at 28 GHz, and c) GAO antenna at 31.1 GHz 61
4.15 patch antenna element operating at 39.0GHz printed on a substrate (a) top view and (b) side view. 64
4.16 Placement of 100 rectangular cells on the patch surface 65
4.17 average fitness-value vs number of generation 66
4.18 Genetically optimized radiating patch geometry (fittest individual candidate) 66
4.19 Simulated S_{11} of the GAO dual-band patch antenna resonates at 39.1 GHz and 50.2 GHz 67
4.20 Directivity versus frequency plot of genetically optimized antenna ϕ='90^0' and θ='0^0' 68
4.21 3D gain plot of the optimized antenna (a) at 39.1 GHz and (b) at 50.2 GHz 68
4.22 E-plane and H-plane 2D radiation pattern cut of the optimized antenna (a) at 39.1 GHz and (b) at 50.2 GHz 68
4.23 total and radiation efficiency of engineered antenna 69
4.24 Surface Current distribution of genetically optimized antenna (a) at 39.1 GHz and (b) 50.2 GHz 70

5.1 The front and perspective view of reference microstrip patch antenna on finite ground plane 74
5.2 (a) Conventional building blocks with infinitesimal connections. (b) Proposed overlapping outline, (c) cell distribution on the patch surface . . . 76
5.3 (a) convergence rate of genetic algorithm and (b) The best fitted individual patch antenna structure 78
5.4 Simulated S11 results of both reference model and genetically optimized antenna 78
5.5 Directivity in dB Versus frequency plot at ϕ=90^0 and θ=0^0 80
5.6 Polar plot of directivity in dB at three resonant frequencies when ϕ=90^0 80
5.7 Optimized antenna total and radiation efficiency plot in different tangent loss. 81
5.8 Polar plot of gain in dB when $\phi = 0^0$ and $\phi = 90^0$ 81
5.9 Surface current distribution of (a) reference antenna at 28GHZ and optimized antenna (b) at 28GHZ, (c) at 40GHz and (d) at 47GHz 82
5.10 Reference patch antenna model on a substrate (h=0.5 mm,ϵr =2.2, tanδ= 0.0009) (a) top view, (b) side view. 85
5.11 Divided patch surface in rectangular cells 86
5.12 a) genetically optimized proposed patch geometry, b) fitness value vs. number generation 88

5.13 Simulated results of S11 for genetically optimized antenna and reference model . . . 88
5.14 VSWR result of genetically optimized antenna . . . 89
5.15 Real and imaginary impedance plot . . . 89
5.16 The 3D gain plot of the proposed antenna in dB (a) at 28.3 GHz (b) at 38.1 GHz, (c) at 46.6 GHz, (d) at 60.0 GHz. . . . 90
5.17 The 2D radiation pattern plot of the proposed antenna in dB (a) at 28.3 GHz (b) at 38.1 GHz, (c) at 46.6 GHz, (d) at 60.0 GHz. . . . 90
5.18 Total efficiency and radiation efficiency of the optimized antenna . . . 91
5.19 Current distribution on the surface of the optimized antenna (a) 28.3GHz (b) 38.1GHz, (c) 46.6 GHz, (d) 60.0 GHz. . . . 92
5.20 Proposed reference microstrip antenna model on finite ground plane . . . 96
5.21 Division of patch surface for binary-coded genetic algorithm . . . 97
5.22 (a) The fitted genetically optimized patch geometry (b) Fitness value versus number of generation . . . 99
5.23 S11 curve for the genetically optimized antenna and the reference antenna 100
5.24 The 3D gain of the optimized antenna at all five resonance frequencies (a) 27.2 GHz, (b) 30.3 GHz, (c) 40.0 GHz, (d) 47.2 GHz, and (e) 56.7 GHz . 100
5.25 S11 result of the genetically optimized antenna with various fabric substrates 101
5.26 2D gain pattern in E-plane of the optimized antenna in various fabric substrate . . . 103
5.27 2D gain pattern in H-plane of the optimized antenna in various fabric substrate . . . 103
5.28 Current distribution on the patch surface of the optimized antenna with PTFE substrate at different resonance frequencies . . . 104
5.29 (a) Human body model and its dimensions [229] (b) placement of the optimized antenna in variable proximity(S) . . . 105
5.30 S_{11} performance of the optimized antenna at various proximity from the human model . . . 105
5.31 On-body H-plane 2D gain pattern of in various distances from human body model . . . 107
5.32 On-body H-plane 2D gain pattern of in various distances from human body model . . . 107

List of Tables

2.1 Comparison summary of gain and directivity enhancement techniques . . 28
2.2 Summary of bandwidth improvement techniques with their achievement . 30
2.3 Parasitic element method literature summary 32

4.1 summary of dimensions of reference microstrip patch antenna 52
4.2 Summary of performance of proposed and reference antenna 55
4.3 Proposed antenna dimension summary 57
4.4 Overall performance of genetically optimized proposed antenna 60
4.5 Comparison of proposed works with related simulated results 62
4.6 Summary of optimization setup 65
4.7 Performance comparison of this work and related works 69

5.1 Summary of dimensions for the referenced antenna model 75
5.2 Summary of genetic algorithm optimization setup 77
5.3 Performance of the reference and optimized antennas 79
5.4 performance comparison of this work with other related works 83
5.5 Optimization setup for genetic algorithm 86
5.6 Performance comparison of this work with related simulated works 93
5.7 Summary of the size of reference antenna 95
5.8 The dielectric constant and the loss tangent value of the selected fabric substrates 101
5.9 performance of the optimized antennas 102
5.10 On-body simulation performance of the optimized antenna at various distances from the body model 106
5.11 Performance comparison of this work with similar works in the literature 108

List of abbreviations

1G (AMPS)	First Generation (Advanced Mobile Phone System)
5G	Fifth Generation
AMC	Artificial Magnetic Conductors
DGS	Defected Ground Structure
EBG	Electromagnetic Band Gap
FCC	Federal Communications Commission
FSPL	Free Space Path Loss
GPS	Global Positioning system
GSM	Global System for Mobile Communications
GA	Genetic Algorithm
HD TV	High definition Television
HFSS	High-frequency Structure Simulator
FEM	Finite Element Method
FDTD	Finite Difference Time Domain
FSS	Frequency-Selective Surface
ICT	Information Communication Technology
ITU	International Telecommunication Union
IMT	International Mobile Telecommunications
LTE	Long Term Evolution
MIMO	Multiple-Input and Multiple-Output
MMIC	Monolithic Microwave Integrated Circuit
MEMS	Microelectromechanical Systems
MoM	Method of Moments
PCS	Broadband Personal Communications Service
PTFE	Polytetrafluoroethylene
PBG	Photonic Band Gap

PIFA	Planar Inverted F Antenna
RAM	Random-access memory
RF	Radio Frequency
SAGSIN	Space-Air-Ground-Sea Integrated Network
SRR	Split-ring resonator
TM	Transverse Magnetic
UMTS	Universal Mobile Telecommunications System
UE	User Equipment
VNA	Vector network analyzer
VSWR	Voltage Stands Wave Ratio
Wi-MAX	Worldwide Interoperability for Microwave Access
WLAN	Wireless Local Area Network

IEEEexample:BSTcontrol

Chapter 1

Introduction

The global economy is currently being boosted by the effective and efficient use of information and communication technologies [1]. Wireless communication systems are arguably the most significant aspect that supports many sectors directly or indirectly as part of the world's ICT strategy. It is one of the world's most rapidly developing, vibrant, and dynamic places [2]. The advancement of wireless communication technology has significantly altered people's lifestyles in terms of communication, business, and social activities. The exponential surge in technical innovation may presage the success of wireless communication technology.

The wireless communication sector has advanced quickly, from analog 1G (AMPS) to the recently implemented 5G. Currently, the rapid growth of data-centric intelligent systems requires effective wireless connectivity. However, spectrum scarcity is one of the most challenging aspects of today's wireless communication industry. Next-generation wireless communication technologies will provide worldwide coverage and use the space-air-ground-sea integrated network (SAGSIN) to connect communication systems from the sky to the deep sea [3]. It will have low power consumption, low latency, high reliability, privacy, and security, along with better quality service. To deal with it developing technologies must employ mm-wave frequencies, which offer a large amount of bandwidth for faster data rate transmission [4]. Whatever advancements are achieved by newly released wireless technologies, the goal of every wireless communication system is to transmit and receive data in the form of electromagnetic signals. This is not possible without an antenna, hence, the antenna is vital and can impact how the system performs overall [5]. Such critical attributes motivate numerous antenna design and optimization studies to enhance antenna parameters such as radiation properties, size miniaturization, multi-functionality, and affordability to satisfy the needs of the rapid development of wireless technologies [6]. Creating a qualified multi-band, broadband, and high-directive small antenna is challenging work for the research community.

Multi-band antenna performances are necessary to accommodate many wireless services spread across a wide frequency range. The inclusion of many communication protocols in a single compact system has piqued the interest of many researchers [7]. However, as an antenna is a hardware device that operates on a fixed resonance frequency, there are a few critical limitations in exploring other working bands. Even though the multi-band functioning of an antenna is accomplished via the use of various techniques, it is

difficult to achieve high performance while clearing bandwidth constraints and meeting possible gain in all coverage bands with a compact antenna size in classical antenna design technologies and conventional antennas. In particular, procured methodologies are required to drive appropriate performance in the case of microstrip antennas, which this dissertation chose as an intriguing alternative. In this regard, numerous performance enhancement approaches and optimization algorithms have been created [8]. Iterative search optimization techniques are needed to provide new solutions that incorporate the enhancement of antenna qualities while reducing design complexity. Researchers have utilized a variety of bio-inspired and other algorithms to improve microstrip patch antennas. Optimizing the dimensions of the antenna, the feeding point and shorting pin location, the slot and slit sizes, and the slot position on the antenna will enable the microstrip antenna to achieve its particular purpose [9]. The common algorithms used in the literature are genetic algorithms and particle swarm optimization. This dissertation will optimize and synthesize a microstrip patch antenna using a genetic algorithm because it does not require prior knowledge about the problem, does not use derivative information on the cost function, and can be applied to complex and poorly defined problems [10]. Even though a genetic algorithm is computationally expensive and time-consuming, it is more accurate at handling different electromagnetic difficulties.

1.1 Millimeter wave communication: A background

In wireless communication, more and more bandwidth-intensive applications are emerging. Millions of wireless devices, including HD TVs, cameras, laptops, household appliances, smartphones, sensors, video surveillance systems, wearable devices, and robots, will be able to connect, with exponential growth expected soon. Simultaneously, technologies related to smart grids, smart cities, virtual reality, machine-to-machine communication, autonomous driving, and e-health are emerging [11]. These new and developing technologies need tremendous bandwidth to enable the simultaneous movement of massive volumes of data. Because of bandwidth constraints, the existing microwave spectrum does not include all of these elements, but millimeter wave (mm-wave) frequencies offer ample capacity and are projected to meet such high-end needs.

The frequency ranges with a wavelength in millimeters (1–10 mm) are referred to as "mm-wave frequencies," which encompasses 30-300 GHz. However, because their propagation behavior is similar to that of mm-wave signals, certain frequencies less than 30 GHz are included in the mm-wave spectrum; hence, mm-wave frequencies span from 20 GHz to 300 GHz [12, 13]. On the other hand, spectrum allocation is the most pressing issue in wireless communication. International standard-setting bodies such as the ITU, IMT, and FCC have advocated a 20–100 GHz prime mm-wave spectrum for wireless applications [14, 15]. The behavior of mm-wave bands in wireless communications is

being investigated. Some frequencies are unsuitable for wireless applications due to a variety of issues. For land mobile applications, the following mm-wave frequencies have previously been identified: 27.5-29.5 GHz, 30.0–31.3 GHz, 37.4–42.5 GHz, 43.5–47.2 GHz, and 47.9–51.4 GHz [16, 17]. Unlicensed spectrum in the 57–66 GHz range is reserved for high data-rate short-range wireless communication systems [18]. Other potential candidate frequency bands include 71–76 GHz and 81–86 GHz, which are allocated for radio navigation-satellite service, radio-location service, mobile-satellite service, broadcasting service , broadcasting-satellite service, and space research service [19]. Figure 1.1 more elaborates on the specified allocation of mm-wave frequencies for terrestrial land based cellular, vehicular, and mobile terminal applications.

Following the exploration and allocation of large amounts of bandwidth for different wireless applications, a communication system has been efficiently employed to utilize the available amount of bandwidth. High-performance antenna design is critical in wireless communication for transmitting signals via electromagnetic waves [20]. The mm-wave antennas and equipment are intrinsically smaller in size than their counterparts in the lower microwave range. In addition, the communication link at the mm-wave spectrum is naturally secure and has less user interference. However, communication lengths in the mm-wave frequency ranges are limited by significant attenuation due to atmospheric absorption, are sensitive to blockages, and have tighter fabrication tolerances, which impede wireless network performance [21]. The Friis equation, presented in equation (1.1) states that the square of carrier frequency (f_c) is directly proportional to free space path loss (FSPL) [22]. As a result, higher transmission frequencies suffer from more path loss, resulting in reduced cell coverage in mm-wave communication.

$$FSPL = \left(\frac{4\pi d}{c}\right)^2 f_c^2 \tag{1.1}$$

where d is the transmission distance and c is the speed of light.
Furthermore, wireless communications in this band are susceptible to shadowing any ob-

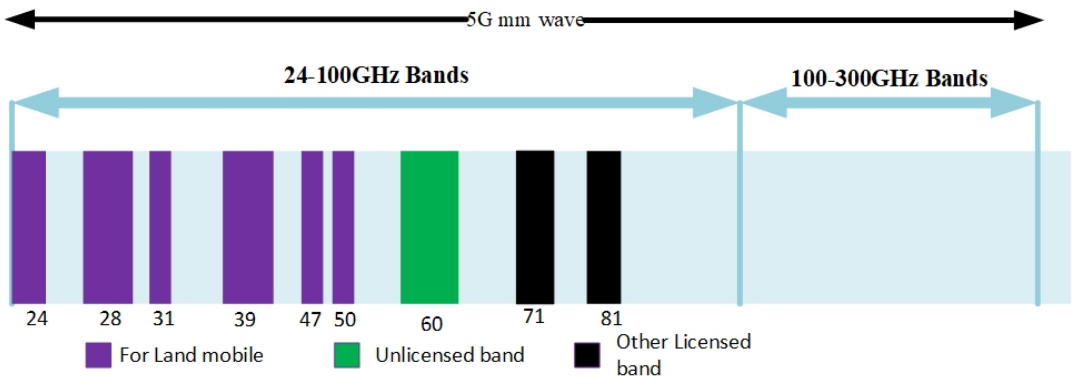

Figure 1.1: Predicted spectrum of mm wave for wireless communication [16]

structions in the line-of-sight path and causing a significant fluctuation in the strength of the signal that the user equipment receives [23, 24]. By employing directional antennas from both UE and base station terminals, shadowing losses, path losses, and multi-path fading can be reduced, as proposed in [25,26]. As a result, antennas with a high directive, excellent gain, and wide bandwidths are required for successful mm-wave communication, which offers high-data-rate wireless communication [27].

Because mm-wave signals have a short wavelength, additional antenna components may be incorporated into an array to offer high directivity and gain in a physically limited space [28]. The intricate feeding system, associated mutual coupling, and spurious radiation, on the other hand, are impeding inspiration. In this regard, microstrip patch antennas have particular importance for end-user terminal devices due to their low profile. This dissertation focuses on the design, optimization, and synthesis of mm-wave microstrip antennas with improved performance.

1.2 Statement of the problem

The proliferation of bandwidth-hungry services leads to the current microwave wireless link in spectrum scarcity. In order to overcome the bandwidth shortage difficulties, the ITU recommends using the mm-wave spectrum. Following that, researchers are striving to attain the inquiries of next-generation wireless communication at mm-wave frequency. Particularly, antenna technologies at mm-wave have faced several expectations and challenges. This dissertation identified the following articulated problems around the mm-wave antenna.

Challenges of mm-wave signal propagation: Environmental factors have a significant impact on the transmission of mm-wave signals. In contrast to microwave signal transmission, mm-wave antennas will confront additional environmental obstacles such as high atmospheric absorption, shadowing, susceptibility to blocking, large-scale attenuation, and significant propagation loss. Experts in the field advise employing high gain and high-directivity antennas to address some of these issues. However, modeling and optimization of high-gain, directional antennas is a difficult problem as well.

Antenna performance: Antennas used for user equipment (UE) terminal applications must be low profile, compact, and planar-configured; the optimum alternative is a microstrip patch antenna. However, the traditional microstrip antenna has inferior gain, reduced directivity, limited functionality, and is less effective. Meanwhile, emerging wireless technologies consider only a high data rate with low latency communication. The emerging wireless inquiries are a highly challenging paradox that requires perpetual research to reconcile. Therefore, it is vital to maintain high efficiency and appropriate antenna performance to support emerging technologies.

Demand for multi-functional services: Nowadays, multiple services are expected

from a single device. Multi-band antenna enhancements are essential to meet such high-end demands. The challenge is determining how a single microstrip patch antenna may work at many frequencies while maintaining acceptable performance. This dissertation will look at re-engineering a single-patch antenna for multiple-frequency operation.
The dissertation aims to utilize a binary-coded genetic algorithm to optimize mm-wave microstrip antennas, resulting in enhanced performance in terms of multiple-band operation, directivity, and bandwidth. This unique approach in the band able to achieve antenna performance improvement, and has the potential to significantly advance mm-wave antenna technology and broaden its applications across various disciplines. By employing the genetic algorithm, the dissertation seeks to overcome the challenges associated with mm-wave microstrip antenna optimization, ultimately leading to more efficient and effective antenna designs.
While researchers are actively addressing various challenges associated with mm-wave microstrip antennas, their approaches often result in increased complexity, larger antenna sizes due to the addition of parasitic elements or superstrates, and a focus on optimizing a single parameter of the antenna patch. In contrast, this optimization process aims to achieve simultaneous improvements in directivity, bandwidth, and multiband performance. By considering multiple performance factors and utilizing an autonomous optimization tool, this dissertation contributes to the advancement of mm-wave antenna technology. The proposed approach enables the antenna to operate across different frequency ranges, concentrate radiation in specific directions, and enhance overall performance while maintaining a simple antenna structure. These advancements have significant implications for various fields and applications utilizing mm-wave technology.

1.3 Objectives

1.3.1 General objective

- To model, optimize, and synthesize mm-wave microstrip patch antenna for wireless communication by applying a binary-coded genetic algorithm that will operate at required multiple frequency bands with improved performances.

1.3.2 Specific objectives

- To model and optimize a microstrip patch antenna for a mm-wave wireless application.
- To implement a genetic algorithm for microstrip antenna optimization to improve

dual-band and multi-band operation in allocated mm-wave bands.

- To investigate a mm-wave dual-band and multi-band microstrip patch antenna using a genetic algorithm with improved directivity.
- To enhance the bandwidths of mm-wave dual-band and multi-band microstrip patch antenna while keeping improved directivity in each operating band using a genetic algorithm.

1.4 Methodology

This dissertation adheres to the following methodologies to attain its objectives. To obtain adequate antenna performances on the specified frequencies, the reference model is examined using parametric analysis. Next, divide the patch area of the reference model into smaller cells and set up the optimization procedure of the genetic algorithm. Lastly, employ a binary-coded genetic algorithm from MATLAB in combination with HFSS to synthesize enhanced antenna performances based on the designed fitness function. Then, analyze the best-fit antenna in terms of measurable antenna parameters. Due to the lack of mm-wave communication lab facilities at AAiT, this paper solely gives simulation findings.

1.5 Thesis Contribution

The main contribution of this work is the development of a multiband microstrip patch antenna designed for wireless applications, specifically targeting the mm-wave frequencies. The dissertation project focuses on enhancing both the directivity and bandwidth of dual-band microstrip antennas operating in the millimeter-wave spectrum. It also addresses the challenge of improving the directivity of tri-band antennas while ensuring suitable impedance bandwidth. Furthermore, the research preferred bandwidth enhancements when the number of operating frequency bands is increased, such as in quad-band and penta-band microstrip antennas, as these additional bands contribute to the overall bandwidth of the antenna. The utilization of a genetic algorithm in this dissertation is a crucial element in improving the directivity and bandwidth of microstrip antennas. By utilizing this optimization technique, the research makes significant observations and achieves noteworthy contributions that have substantial implications for various wireless applications. The dissertation extensively elaborates on the specific contributions of this study in subsequent sections, providing comprehensive details and valuable insights into the advancements achieved.

Model and optimize a microstrip patch antenna for mm-wave wireless application:

The development of novel techniques or procedures to create enhanced performances and a well-designed microstrip antenna with the associated feeding line network at mm-wave is one of the major contributions of the study. There was an introduction of a unique patch antenna shape. Each newly synthesized and improved microstrip antenna model was subsequently validated using HFSS simulation. A study was done on the characteristics and features of the modeled antenna, including gain, directivity, far-field radiation pattern, reflection coefficient, return loss, VSWR, surface current distribution, and bandwidth. The physical characteristics of microstrip antennas, including their shapes and sizes, the impacts of various substrates, and the effects of human body models at various distances, were also investigated in the dissertation.

Implement genetic algorithm for microstrip antenna optimization to improve multi-band operation in allocated mm-wave bands

Implementing a genetic algorithm for antenna optimization was done as part of this thesis effort. A mathematical description of the optimization problems in terms of fitness functions was articulated to find the ideal solutions. A complete MATLAB code was written in a binary-coded genetic algorithm for microstrip patch antenna optimization. To improve the effectiveness of the genetic algorithm, crossover, mutation, and selection operators have been modified for antenna optimization. Then after, integration of the modified algorithm with the antenna model for optimization was also challenging. The approach and cost functions were developed for extensive antenna optimization. The results of simulations on large-scale multi-band, directivity, and bandwidth antenna challenges are reviewed in terms of efficiency, radiation pattern, return loss, and impedance matching vs. frequency.

Investigate high directive mm-wave multi-band microstrip patch antenna using binary coded genetic algorithm

The investigation of a high-directional multi-band microstrip antenna at mm-wave frequency is another significant contribution of this research. According to [29], the dissertation enhanced a dual-band microstrip antenna for wireless applications at 28.0 GHz and 46.6 GHz with better directivity from a single element. The peak directivity achieved was 8.4 dB and 9.0 dB at the resonance frequency. Another dual-band study that resonates at 28.0 GHz and 31.1 GHz with a peak directivity of 8.6 dB and 10.9 dB were carried out, respectively by circular cell patch geometry optimization, as shown in [30]. The dissertation also used a genetic algorithm to develop a triple-band microstrip antenna with improved directivity that resonated at 28.0 GHz, 40.0 GHz, and 47.0 GHz and had a maximum directivity improvement of 12.15 dB [31].

Enhance bandwidths of mm-wave multiband microstrip patch antenna while keeping high directivity in each operating band using genetic algorithm

The patch geometry optimization used in the dissertation examined a multiband microstrip antenna's bandwidth while keeping the rest of the antenna's performance good. As a result, [32] synthesized and demonstrated a dual-band antenna at 39.1 GHz and 50.2 GHz with a total of 4.9 GHz bandwidth. The proposed antenna was achieved a peak gain of 7.6 dB and 7.3 dB at resonance frequency. In reference [33], a patch antenna for quad-band wireless applications was optimized. The engineered antenna has a total improved bandwidth of 11.5 GHz and resonates at 28.3 GHz, 38.1 GHz, 46.6 GHz, and 60.0 GHz. Finally, using a genetic algorithm, a penta-band wearable microstrip antenna was optimized to attain 15.11 GHz of total bandwidth, as stated in [34]. The engineered antenna achieved multi-band operation at 27.8 GHz, 30.3 GHz, 40.1 GHz, 47.2 GHz, and 56.7 GHz. The study was also conducted on low-cost flexible fabric with different substrates.

The details of these contributions are published in reputed journals and presented at international conferences. The optimized antennas and simulation results are explained in detail in the subsequent chapters of this dissertation.

1.6 Thesis structure

Chapter 1 is the introduction section of the thesis. The objectives of the dissertation, the methodology, a full explanation of the research challenges, and an overview of mm-wave wireless communication technology are all included. The research contribution is also looked at, along with the dissertation's limitations and constraints.

In **Chapter 2**, a thorough overview of microstrip antennas is presented, including background information, feeding methods, design-related mathematical formulations, benefits, and drawbacks. The comprehensive review of performance enhancement strategies includes ways for improving directivity, gain, and bandwidth. Multi-band synthesizing methods were also reviewed for the mm-wave spectrum. The performance of multi-band microstrip antennas was discussed, along with methods for improvement. Finally, strategies for optimizing the performance of multi-band microstrip antennas were presented.

Chapter 3 explains the general implementation procedure of genetic algorithm for antenna optimization specifically a binary-coded genetic algorithm. It addressed how to optimize microstrip patch antennas in mm-wave frequency using a binary-coded genetic algorithm, as well as optimization settings, optimization parameters, and implementation methods. It introduced the fitness function formulation for various antenna problems, including multi-band antennas with improved directivity and bandwidth. Additionally, MATLAB and HFSS software integration is discussed in this chapter as it relates to the

implementation of realized genetic algorithm optimization via an iterative method. In **Chapter 4**, a pre-modeled single-band reference microstrip antenna is optimized using a binary-coded genetic algorithm to create a dual-band antenna with better directivity and bandwidth. This chapter contains three enhanced dual-band microstrip antennas, two of which are intended to increase directivity and the third to increase bandwidth.
Chapter 5 discusses the optimization of multi-band microstrip antenna using binary-coded genetic algorithm for directivity and bandwidth improvement. The approach was used to change the shape of the patch surface to cover additional frequency bands with a modified patch geometry optimization configuration. Three enhanced patch antennas were proposed in this chapter for various wireless applications. The first is an improved directivity tri-band mm-wave microstrip antenna, while the other two are broader bandwidth quad-band and penta-band antennas. Each study problem's cost function formulation was modified, and iterations were made to develop solutions with a higher degree of quality. The chapter also explores the impact of the human body model on antenna performance at various distances from the model as well as the effect of substrate dielectric strength and tangent loss on the proposed antenna.
Finally, **Chapter 6** summarizes the investigation's findings and provides comments on how this research will go forward. Future research will focus on improving the mm-wave microstrip antenna's performance, improving the effectiveness of the genetic algorithm optimization technique, and expanding the study to terahertz frequencies.

Chapter 2

A Comprehensive Survey on Microstrip Antenna

2.1 Introduction

In wireless communication, an antenna serves as an interface between electric currents flowing through metal conductors and radio waves traveling over space. It acts as a transmitter or receiver [35]. Using coils of wire connected to galvanometers, antennas were first employed to detect electromagnetic radiation when Michael Faraday tested the coupling of electricity and magnetism at the start of the 1830s [36]. Heinrich Hertz ignites an electrical spark in the gap of a dipole antenna in 1886. For the first time, Marconi sent a signal across a sizable distance in 1901 using a 200 m wire carried by a kite [37]. Following that, various researchers enhanced antenna technology, including Yagi-Uda in the 1920s, the horn antenna in the 1930s, the antenna array concept in the 1940s, the parabolic reflector antenna in the 1950s, patch antenna concepts in the 1970s, and PIFA in the 1980s [38, 39]. Antenna researchers now focus on the use of customized materials and shapes to increase performance and adaptability. Printable and small antennas for personal wireless communication devices are also being developed. Further, other initiatives are underway to mathematically model antennas to forecast their attributes before they are built and tested.

Multi-function wireless technologies have demanded significantly in recent years. It insisted on using newly developed multi-band antenna technology that operates across multiple frequency bands [40]. Simultaneously, antennas, as a vital component of a wireless system, must always be effectively designed and implemented. However, developing this technology is challenging, especially for portable mm-wave wireless devices. In the future mm-wave wireless communication, the antenna component is predicted to provide high directive, broad bandwidth, and multi-band operation to fit customer demand.

Researchers have tried to optimize and improve several topologies of multi-band antennas for existing wireless services such as LTE, GPS, GSM, PCS, DCS, UMTS, WLAN, and Wi-MAX bands, as well as recently recognized mm-wave spectrums. The most popular technique to obtain multi-band service is to put several antennas for each active band on a device [41]. However, the use of many antennas is restricted by cost and volume considerations as well as electromagnetic coupling between antennas hindering their performance. Another well-organized multi-band service option is to optimize and improve

a single antenna to operate at multiple frequency bands at the same time. As a result, various studies in the literature describe potential multi-band antenna approaches such as bending, folding, meandering, switching, and wrapping of the main radiator [42]. Depending on the application, each method has distinct advantages. However, the primary limitations of these approaches are their compactness and antenna performance.
Microstrip antennas are gaining popularity as a feasible solution to this challenge. When deployed on a flat or non-planar surface, these antennas have various advantages, including low profile, lightweight, low cost, ease of construction, and mechanical resilience [43]. The antenna's low profile allows it to be adapted for a range of applications such as radio locating, satellite communication, space research, radio astronomy, and mobile communication [44]. Despite these appealing features, microstrip antennas have certain downsides, including limited bandwidth, poor directionality, low gain, and operating at a specific frequency.
This review will explain the shortcomings and strengths of the various multi-band antenna techniques, microstrip antenna details, and performance enhancement mechanisms of microstrip antenna including the directivity improvement, bandwidth enhancement, and gain meliorations methods presented in the literature. It primarily describes the strategies, optimization algorithms, and procedures used to improve the multi-band performance of the antenna. The survey also highlighted research gaps and difficulties in various portrayed comparisons.

2.2 Microstrip Antenna

Following the second world war, new antenna design approaches emerged as microwave circuits stretched operational frequencies to shorter wavelengths. In between, fundamental antenna technologies such as dipoles, horns, fractals, spiral, wire, monopoles, and microstrip patch antennas were introduced. G.A. Deschamps originally introduced the notion of microstrip radiators in 1953. However, it became practical following additional development by Robert E. Munson and other researchers in 1970 [45]. After the invention of printed circuit board (PCB) technology, the antenna became more commercialized by utilizing a low-loss accessible substrate. Despite certain drawbacks, the microstrip patch antenna is likely the most successful and groundbreaking antenna technology since it offers various significant advantages over other types of antenna [46].
The substrate, radiating patch, and ground plane are the three fundamental layers of a microstrip antenna [47]. It can be built as a metallic patch on top of the dielectric substrate, with a ground plane beneath the dielectric layer, as illustrated in Figure 2.1. In the design of a microstrip antenna, the radiating patch can have a variety of geometries. However, rectangular and circular shapes are the most frequent due to their simplicity

of analysis and fabrication, as well as their appealing radiation properties, particularly low cross-polarization radiation [48].

The substrate is a dielectric substance designed for better electrical and mechanical stability in radiating patches. It can also assist in the generation of displacement current, which generates a magnetic field that changes over time. Due to Friday's law, then the magnetic field results in a time-varying electric field and propagating electromagnetic field. Therefore, a substrate can improve an antenna's capacity to radiate. For the optimum microstrip antenna design, substrate dielectric strengths should be between $2.2 \leq \varepsilon_r \leq 12$ [49]. Thick substrates with low dielectric constants are optimal for excellent antenna performance since they offer high efficiency, greater bandwidth, and loosely bound fields for radiation into space, but at the price of larger antenna size [50]. For microwave circuitry, thin substrates with large dielectric constants are preferable because they allow for smaller antenna sizes and strongly woven fields to reduce unwanted radiation and coupling. However, they are less efficient and have relatively narrow bandwidths due to their higher losses.

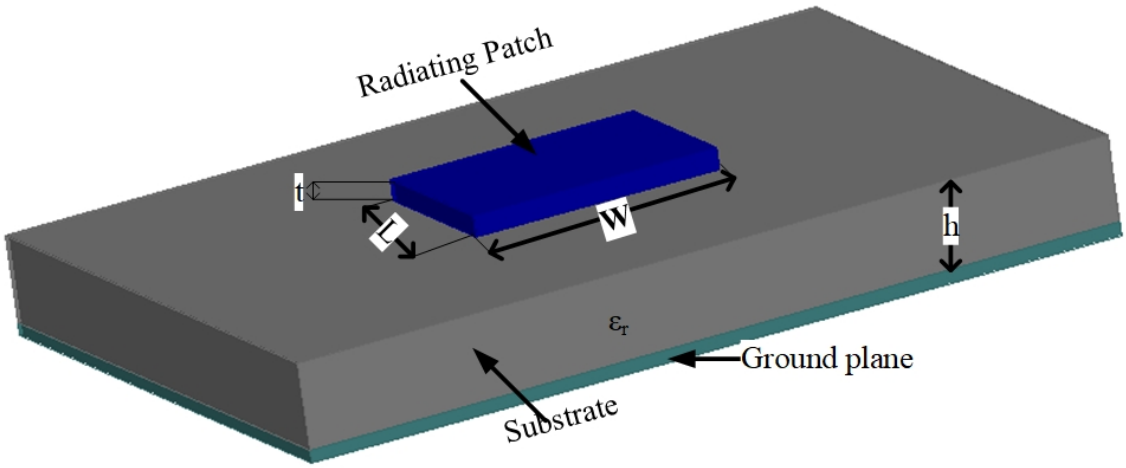

Figure 2.1: Structure of rectangular microstrip patch antenna

Typically, the feeding lines and radiating patch are photo-etched onto the dielectric substrate [51]. There are two types of feeding systems for microstrip patch antennas: contacting and non-contacting. The RF power is delivered directly to the radiating patch using a connecting device such as a microstrip line or coax cable in the contracting approach. In the non-contacting strategy, electromagnetic coupling using either the proximity coupling technique or the aperture coupling approach is used to transmit power between the feed line and the radiating patch. It is possible to model and analyze the microstrip antenna mathematically using defined methods based on its structure and geometry, as explained below.

2.2.1 Method of analysis

The three most widely used methodologies for modeling and analyzing microstrip antennas are the full wave model, the cavity model, and the transmission-line model. The simplest model is the transmission-line one, which provides good physical understanding but is less precise [52]. The cavity model is more accurate than the transmission line model with higher complexity, whereas the full wave model is the most complex and exact.

2.2.1.1 Transmission Line Model

The transmission line model mimics the microstrip patch antenna by using two slots and a low-impedance transmission line of length L to divide them. Although it yields less precision than other approaches, it is still sufficient to initiate the antenna design [53]. It begins the approximation by taking into account the substrate thickness, which is significantly much greater than the conductor thickness, and the conductor thickness has no impact on the computation. Therefore, the defined design parameter solely depends on the substrate's width (W), length (L), height (h), predicted resonance frequency (f_r), and dielectric constant (ε_r), as shown in Figure 2.2.

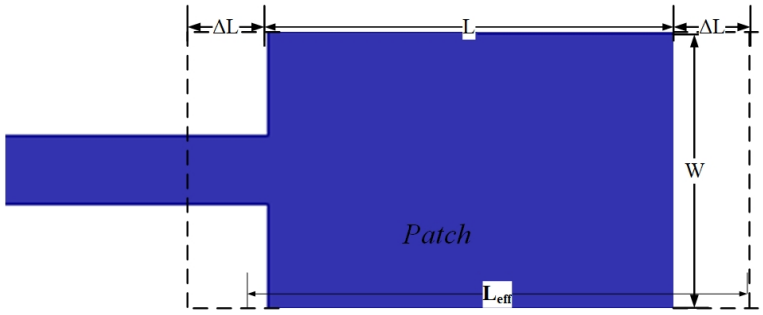

Figure 2.2: Physical and effective length of a microstrip antenna

The dimensions of the rectangular patch antenna presented in Figure 2.2 are calculated based on the following procedure for efficient radiation [20].

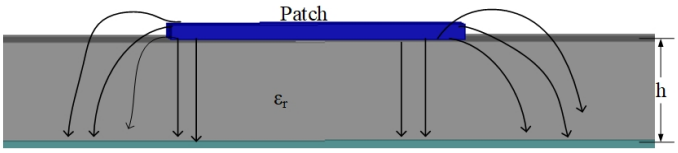

Figure 2.3: Electric field lines from the radiating patch

1. A practical patch's width, W, may be estimated using the formula presented in

equation (2.1), where c is the speed of light in a vacuum.

$$W = \frac{c}{2f_r}\sqrt{\frac{2}{\varepsilon_r + 1}} \tag{2.1}$$

2. Figure 2.3 shows that the fringing field from the patch to the ground plane is not only confined inside across the dielectric but also diffused to the surrounding air. Therefore, the effective dielectric constant (ε_{reff}), which is somewhat lower than the dielectric constant of the actual substrate ($1 < \varepsilon_{reff} < \varepsilon_r$), is utilized for the field analysis. When $\varepsilon_r \gg 1$ is present, ε_{reff} is closer to the substrate's actual value of the dielectric constant ε_r. The derivation of the effective dielectric constant (ε_{reff}) is as follows:

$$\varepsilon_{reff} = \frac{\varepsilon_r + 1}{2} + \frac{\varepsilon_r - 1}{2}\left(\frac{1}{\sqrt{1 + \frac{12h}{W}}}\right) \tag{2.2}$$

3. The fringing effect causes the physical length of the patch to appear shorter than its actual length, as seen in Figure 2.2. Therefore, the effective length of the patch is $2 \times \Delta L$ longer than the actual physical length. The actual physical length of the patch is determined by using the formulae presented in equations (2.3).

$$L_{eff} = \frac{c}{2f\sqrt{\varepsilon_{reff}}} \tag{2.3}$$

4. Patch's actual length is estimated using

$$L{=}L_{eff}{-}2\Delta L \tag{2.4}$$

5. The formula presented in reference [54] is a very well-liked approximation for calculating the extension of the patch's length ΔL.

$$\Delta L = 0.412h\frac{(\varepsilon_{reff} + 0.3)(\frac{W}{h} + 0.264)}{(\varepsilon_{reff} - 0.3)(\frac{W}{h} + 0.8)} \tag{2.5}$$

6. The ground plane should ideally be thought of as an infinitely large component of the microstrip antenna. However, in practice, this is challenging to implement on compact and space-constrained devices. Therefore, it is preferred that the dimensions of the ground plane are not less than $L_g{=}\ 6h{+}L$ and $W_g{=}\ 6h{+}W$.

7. The feeding method used in this dissertation is a microstrip line feed. A thorough explanation of the design, optimization and analysis of the microstrip line feed system is given in the impedance matching section.

2.2.1.2 Cavity Model

According to the cavity model, the space between the microstrip patch and ground plane is a resonant cavity enclosed by magnetic walls along the conductor's edge and the ceiling and floor of electric conductors, as illustrated in Figure 2.4 [38, 55].

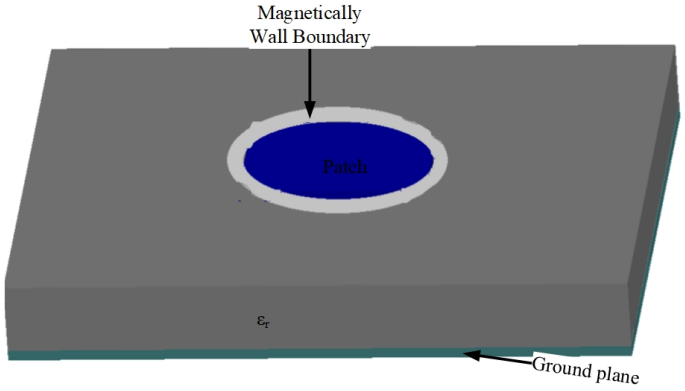

Figure 2.4: magnetically wall model of microstrip antenna

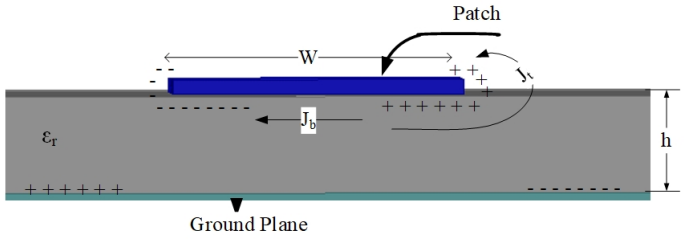

Figure 2.5: Charge distribution and current density on microstrip antenna

Take a look at the microstrip antenna in Figure 2.5. The charge distribution is established on the top and bottom planes of the microstrip antenna after it is connected to the source. Attracting and repulsive between charges is a governing mechanism of the distribution of charges. The attractive interaction between the opposite charges on the patch and ground plane creates a current density (J_b) inside the dielectric [56]. The tendency of the similar charges to repel one another also generates current density (J_t) around the patch.

Since the current flow around the edge reduces as h/W drops, it is possible to ignore it when $W \gg h$ and the attractive mechanism predominates [57]. This happens because charges will concentrate inside the dielectric underneath the patch. This would make it possible to simulate the four side boundaries as ideal magnetic conducting surfaces, which would ideally not affect the distribution of the electric field underneath the patch or the magnetic field. The side walls are treated as ideal magnetic conducting walls due to this accurate approximation of the cavity model.

When modeling cavities, the following observations are available [58, 59]:

- The region encircled by the hollow contains just the three field components E_z, H_x, and H_y.
- When $h \gg \lambda$, the inner region's field does not change with z-coordinates for any frequency.
- At no point in the microstrip patch does the electric current have a component that is normal to the edge of the patch.

The microstrip with the fringing field may be examined pretty effectively using this approach. According to Maxwell's equations for a free source cavity space, the homogeneous wave equations (2.6) and (2.7) , which the electric vector potential must meet.

$$\nabla^2 E + k^2 \overrightarrow{E} = -j\omega\mu_0 \overrightarrow{J} \tag{2.6}$$

Particularly, the field in the z-direction is given as:

$$\nabla^2 E_z + k^2 E_z = -j\omega\mu_0 \overrightarrow{J}\check{z} \tag{2.7}$$

where

$$k^2 = \omega^2\mu\varepsilon \tag{2.8}$$

$\overrightarrow{J}$= Electric current density fed by the feed line to the patch and $\check{z}$ is the unit vector normal to the plane of patch.
Consider that the thickness of the substrate, or h, is quite thin when compared to the dimensions W and L; as a result, the z-axis field is constant, and E_x= E_y= 0. Additionally, it was assumed that the equivalent ideal electric and magnetic wall had no tangential fields. Thus, for the top and bottom conductors, $\hat{n}\mathrm{x}\overrightarrow{E} = 0$, and for the wall, $\hat{n}\mathrm{x}\overrightarrow{H} = 0$ the wave equation's potential solutions, and then use the following boundary values .
$E_x(0 < x_0 < L, 0 < y_0 < W, z_0 = 0) = E_x(0 < x_0 < L, 0 < y_0 < W, z_0 = h) = 0$
$H_x(0 < x_0 < L, y_0 = 0, 0 < z_0 < h) = H_x(0 < x_0 < L, y_0 = W, 0 < z_0 < h) = 0$
$H_y(x_0 = 0, 0 < y_0 < W, 0 < z_0 < h) = H_y(x_0 = L, 0 < y_0 < W, 0 < z_0 < h) = 0$
The computed result be summarized as:

$$E_z = -j\frac{k_x^2 + k_y^2}{\omega\mu\varepsilon} k_{mn} \cos\left(k_x x'\right) \cos\left(k_y y'\right) \tag{2.9}$$

$$H_x = -\frac{k_y}{\mu} k_{mn} \cos\left(k_x x'\right) \sin\left(k_y y'\right) \tag{2.10}$$

$$H_y = \frac{k_x}{\mu} k_{mn} \sin\left(k_x x'\right) \cos\left(k_y y'\right) \tag{2.11}$$

Where k_{mn} represents the amplitude coefficients of each mn mode, The wave numbers $kx,\ ky$ equal to:

$$k_x = \frac{m\pi}{L} \qquad m = 0, 1, 2, \ . \ .. \tag{2.12}$$

$$k_y = \frac{n\pi}{W} \qquad n = 0, 1, 2, \ . \ .. \tag{2.13}$$

The values of m and n represent the number of half-cycle field variations along the x and y directions , respectively.

$$k_x^2 + k_y^2 = \left(\frac{m\pi}{L}\right)^2 + \left(\frac{n\pi}{W}\right)^2 = k^2 = \omega^2 \mu\varepsilon \tag{2.14}$$

The resonant frequencies of the cavity are determined from the equation as follows

$$f_r^{mn} = \frac{1}{2\pi\sqrt{\mu\varepsilon}} \sqrt{\left(\frac{m\pi}{L}\right)^2 + \left(\frac{n\pi}{W}\right)^2} \tag{2.15}$$

2.2.1.3 Full wave analysis

The full-wave models can handle single elements, finite and infinite arrays, stacked components, arbitrarily shaped elements, and coupling. They are also exceedingly accurate and adaptable. Nevertheless, they are the most complicated models and typically provide less physical insight. Full wave analysis is used by the commercial electromagnetic simulation software currently available on the market [60]. Even though they have a simple shape, microstrip antennas are extremely challenging to evaluate precisely. The method of moments (MoM) was the first numerical analytic technique to achieve computational efficiency that allowed for a realistic analysis of microstrip antennas on modern computers with sufficient memory and CPU power [61]. Now, design experts can employ numerical techniques like the finite difference time domain (FDTD) method and the finite element method (FEM), which consume a lot more memory than MoM solutions.

A. Method of Moments (MoM)

Volume-polarized currents in the dielectric material are used to describe fields in the dielectric slab. The microstrip radiating patch is also modeled by surface current distribution [62, 63]. An integral equation is established for the unexplained currents on the feed lines, patches, and their representations in the ground plane. The integral equations are transformed into computer-quickly solvable algebraic problems. This approach provides a more precise answer because it considers the fringing fields that extend beyond

the two-dimensional patch's physical boundaries.

B. Finite Difference Time Domain (FDTD)

The FDTD approach is ideally adapted for modeling the many structural inhomogeneities avail in microstrip patch antenna layouts, making it ideal for these devices [64]. Additionally, a single simulation is used to forecast the behavior of patch antennas across a large spectrum. FDTD grids space and time to compute electric and magnetic field solutions. Based on three Cartesian coordinates, the spatial discretization is assumed to be the same. Each grid cell contains material properties. An appropriate excitation function propagates across the structure and excites the cells holding the sources. The desired location is chosen to determine the fields' discretized time variations. It is possible to compute the voltage between the two points using a line integral of the electric field [65]. A loop integral of the conductor's magnetic field is used to calculate the current, and the Fourier transform produces a frequency response.

C. Finite Element Method (FEM)

Any volume or planer configuration in FEM is split up into a variety of finite surface or volume elements, often known as finite elements [66]. In order to solve the wave equation, the discretized units can be any well-defined geometry that is appropriate for the integration of a certain base function over the entire patch. In the HFSS field computational technique at the third chapter of this dissertation, the detailed analysis of FEM will be explained.

2.3 Performance Metrics

The survey in this part introduces the background information on selective performance measurement parameters of microstrip antennas that are essential for this dissertation. The references provide further information on the mathematical derivation of the microstrip antenna metric parameters.

2.3.1 Radiation pattern

Antenna parameters like the radiation pattern describe how the radiation properties look graphically and mathematically as they relate to spatial coordinates. A typical patch antenna's pattern is wide and has low radiation power based on the equations (2.16)-(2.18). The magnetic field H is parallel to the strip edge of the patch and the electric field E is perpendicular to the patch and ground plane [54].

$$P_{rad} = \frac{1}{2} Re \left[\iint_s E \times H^* \cdot ds \right] \tag{2.16}$$

$$= \frac{1}{2\eta} \iint \left(|E_\theta|^2 \times |E_\vartheta|^2 \right) r^2 \sin\theta d\theta d\vartheta \tag{2.17}$$

$$\vdots$$

$$P_{rad} = \frac{|V_0|^2}{2\pi\eta_0} \int_0^\pi \left[\frac{\sin\left(\frac{k_0 w}{2} \cos\theta\right)}{\cos\theta} \right] \sin^3\theta \; d\theta \tag{2.18}$$

Where, V_0 the voltage across the slot, w is the width of the path, k_o is the wave number, η is intrinsic impedance.

2.3.2 Directivity and Gain

Directivity is a unit used to describe how well an antenna can focus in a specific direction. As a result, the antenna's radiation intensity increases in that direction. Mathematically, directivity is the ratio of 4π time's radiation intensity to the total radiated power, as presented equation (2.19).

$$\mathrm{D} = \frac{4\pi U(\theta,\vartheta)}{\mathrm{P_{rad}}} \tag{2.19}$$

Where radiation intensity is U(θ,ϑ). The approximate patch size and conductance for a rectangular antenna are shown below, as presented in references [38, 47, 54].

$$\mathrm{D} = \frac{4(\mathrm{k_0 w})^2}{\pi\eta \mathrm{G_{rad}}} \tag{2.20}$$

Where k_o is the wave number, η is intrinsic impedance, w is the width and the radiation conductance of the patch is represented by G_{rad}

Gain of an antenna:

As stated in its definition, gain of the antenna is "the ratio of the intensity in a given direction to the radiation intensity that would be achieved if the power absorbed by the antenna were emitted isotropically" [53]. It is closely tied to its directivity; it is a measurement that considers the antenna's effectiveness as well as its directional capabilities and may be obtained by:

$$\mathrm{G} = \mathrm{eD} \tag{2.21}$$

Where e represents the antenna's radiation efficiency. Due to the range of efficiency being from 0 to 1, antenna gain is never higher than directivity.

2.3.3 Efficiency

Efficiency for a microstrip patch antenna is calculated by dividing the power radiated from the element by the power received as input. The conductor loss, dielectric loss, cross-polarized loss, reflected power (Voltage Standing Wave Ratio, VSWR), and power lost in any loads in the antenna element are the factors that determine the efficiency of the antenna. Most literature on antennas include references to this study are used the following generic formulation of radiation efficiency [37, 45, 52]:

$$e = \frac{P_{rad}}{P_{rec}} \tag{2.22}$$

P_{rad} is power radiated by the antenna and P_{rec} is power received by the antenna.
In other words, the quality factors of an antenna may be used to represent an antenna's efficiency.

$$e = \frac{Q_t}{Q_{rad}} \tag{2.23}$$

Where, Q_t (a total quality factor)

$$\frac{1}{Q_t} = \frac{1}{Q_{rad}} + \frac{1}{Q_c} + \frac{1}{Q_d} + \frac{1}{Q_{sw}} \tag{2.24}$$

$Q_c = h\sqrt{\pi f \sigma \mu}$, is a quality factor due to conduction loss, (σ conductivity of conductor)
$Q_d = \frac{1}{\tan\delta}$, is due to dielectric loss ($\tan\delta$ loss tangent of a substrate)
$Q_{rad} = \frac{2\omega\varepsilon_r}{hG_t/l}$, is quality factor due to radiation losses (G_t/l total conductance per unit length)
The total efficiency of antenna is the ratio of radiated power to the input power.

$$e_t = \frac{P_{rad}}{P_{in}} \tag{2.25}$$

2.3.4 Return loss and Bandwidth

Return loss is a crucial characteristic to consider while evaluating an antenna. It is associated with maximum power transfer theory and impedance matching. It also evaluates how well an antenna transmits power from a generator to an antenna. The power incident at the antenna pin divided by the power reflected from the antenna (P_{ref}) is what determines the amount of return loss (RL), here is the mathematical formula in dB:

$$RL = 10\log\left(\frac{P_{in}}{P_{ref}}\right) \tag{2.26}$$

For good power transfer, the ratio $\frac{P_{in}}{P_{ref}}$ is high and always positive.
Return loss (dB) could also be expressed in another way using the reflection coefficient as stated in equation (2.26 and 2.27) [67, 68].

$$RL = 10\log_{10}\left|\frac{1}{\rho}\right|^2 = -20\log_{10}|\rho| \tag{2.27}$$

Where ρ, is the complex reflection coefficient at the input of the antenna. Its value is in the range of $0 \leq |\rho| \leq 1$ and can be mathematically computed via equation (2.28).

$$\rho = \frac{V_{ref}}{V_{inc}} = \frac{Z_{in} - Z_0}{Z_{in} + Z_0} \tag{2.28}$$

where Z_{in} is the input impedance of the antenna or the load impedance for the transmission line, Z_0 is characteristics impedance of transmission line, V_{ref} is reflected voltage, and V_{inc} incident voltage.
Voltage Standing Wave Ratio (VSWR), which is the ratio of the highest voltage to the minimum voltage in the standing voltage wave, is the other crucial parameter after knowing the value of the reflection coefficient, computed based on equation (2.29).

$$VSWR = \frac{V_{max}}{V_{min}} = \frac{1 + |\rho|}{1 - |\rho|} \tag{2.29}$$

S-parameters are used to characterize the input-output link between terminals in an electrical system. S_{11} is the most frequently cited S-parameter in relation to antennas. S_{11}, sometimes referred to as the reflection coefficient measures the amount of power reflected from the antenna. An antenna's operating frequency range with the least amount of loss is known as its bandwidth, and it may be estimated from the S_{11} curve. Although some researcher can use S_{11} values of less than -6 dB to estimate antenna bandwidth, the most popular and appropriate method is to use the frequency range where S_{11} values are less than -10 dB [60].

2.3.5 Input impedance

The conjugate of the antenna input impedance and the characteristics impedance of the transmission line should be matched in order to have a maximum radiated power at the patch.

$$Z_0 = {Z_{in}}^* \tag{2.30}$$

The goal of the antenna designer is to fit the antenna to the 50Ω transmission line characteristics, which are typically used in RF applications [69]. Therefore, to determine the width and length of the transmission line that can be fitted to the given antenna topology,

the majority of experts use the transmission line model analysis. Building transition lines that are useful to aid the matching may occasionally be necessary because it is not always possible to find a direct match. Take a look at Figure 2.6, which illustrates a patch antenna with a parallel counterpart of admittance Y [54].

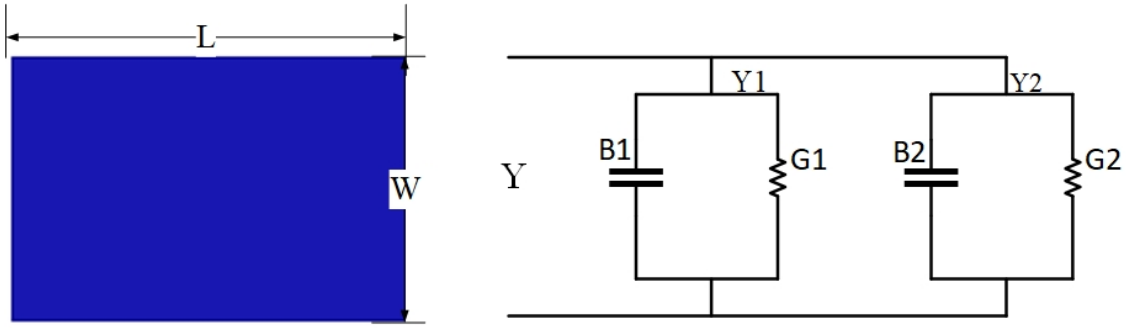

Figure 2.6: The radiating patch surface and the equivalent transmission line model

$$Y = \frac{1}{Z_{in}} = G + jB \tag{2.31}$$

$$Y_1 = Y_2 \tag{2.32}$$

That means $G1 = G2,\ B1 = B2$ where the conductance $G1$ can be expressed as

$$G1 = \frac{2P_{rad}}{|V_0|^2} \tag{2.33}$$

Since the total input admittance is real, the resonant input impedance is also real, or

$$Y_{in} = Y_2 + Y_2^* = 2G \tag{2.34}$$

and

$$Z_{in} = \frac{1}{Y_{in}} = R_{in} = \frac{1}{2G} \tag{2.35}$$

Equations (2.31)-(2.35) show that the resonance input resistance of the microstrip patch antenna primarily depends on the patch's width (W), which decreases as W increases, rather than the substrate's dielectric constant (ε_r) or its height (h). This is acceptable as long as the ratio of W/L is under 2, as the aperture efficiency of a single patch starts to decline when W/L exceeds 2.

2.3.5.1 Microstrip Line Feeding and impedance matching

This dissertation preferred to employ a microstrip line, one of the four microstrip antenna feeding technologies, since it is so simple to construct, design, and evaluate [70]. Figure 2.7 depicts a patch antenna feed by a microstrip line. The equation (2.36) below, as

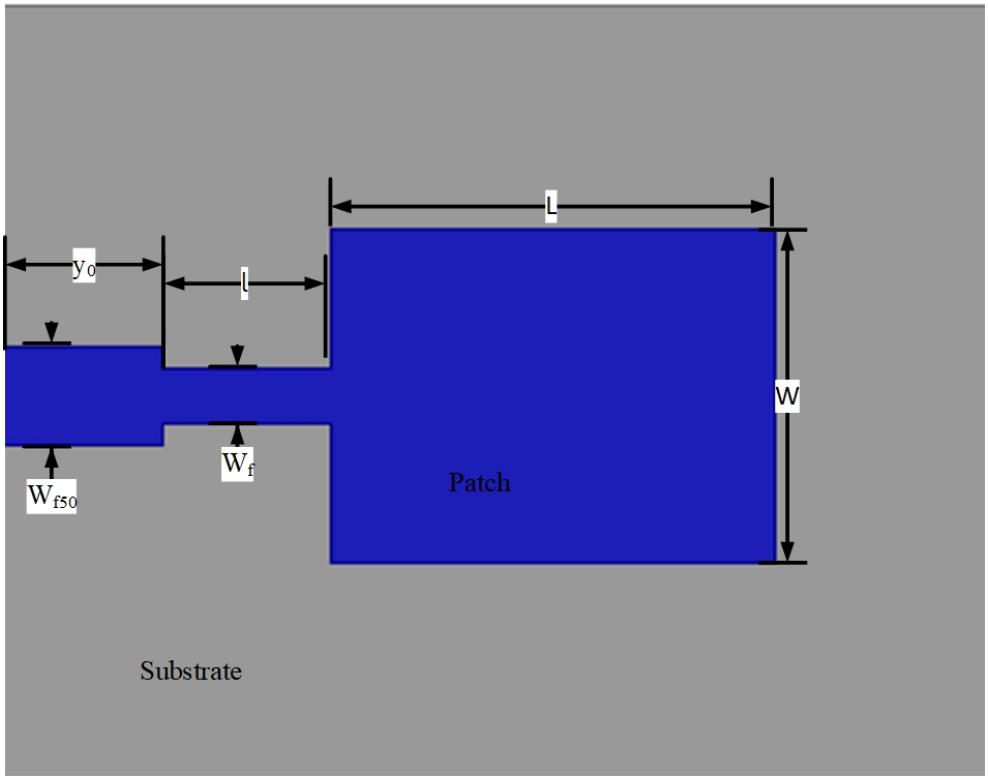

Figure 2.7: Rectangular microstrip antenna with transitional impedance matching line

mentioned in [71], can be used to determine the width of the most 50Ω transmission line.

$$Z_0 = \frac{120\pi}{\sqrt{\varepsilon_{reff}}(1.393 + \frac{w_{f50}}{h} + \frac{2}{3}\ln(\frac{w_{f50}}{h} + 1.444))} = 50\Omega \tag{2.36}$$

The below transition strategies can be used for matching. The transition region should have the following characteristic impedance:

$$Z_{Total} = \sqrt{50 + Z_{ina}} \tag{2.37}$$

Where Z_{ina} is antenna's input impedance, approximated as

$$Z_{ina} = 90\frac{{\varepsilon_r}^2}{\varepsilon_r - 1}\left(\frac{L}{W}\right)^2 \tag{2.38}$$

The width of the transition line is calculated from:

$$Z_{Total} = \frac{60}{\sqrt{\varepsilon_r}} ln\left(\frac{8h}{W_f} + \frac{W_f}{4h}\right) \tag{2.39}$$

The length of the transition line is quarter the wavelength:

$$l = \frac{\lambda}{4} = \frac{\lambda_0}{4\sqrt{\varepsilon_{reff1}}} \tag{2.40}$$

Where

$$\varepsilon_{reff1} \approx \frac{\varepsilon_r + 1}{2} + \frac{\varepsilon_r - 1}{2\sqrt{1 + 12h/w_f}} \tag{2.41}$$

Where ε_{reff1} is effective dielectric constant of transition line, W_f, l, w_{f50}, h, L, W are all illustrated in Figure 2.7.

2.4 Performance Improvement Techniques

Microstrip antennas are compatible with MMIC designs, low profile, conformable to planar and non-planar surfaces, simple and affordable to manufacture using modern printed-circuit technology, mechanically robust when mounted on rigid surfaces, and very versatile in terms of resonant frequency, polarization, pattern, and impedance when the specific patch shape and mode are selected. In addition to the benefits of low profile and simple integration with other electronic circuits, the antenna would be desirable for many mm-wave wireless applications if it is operated at many bands with improved directivity and good bandwidth.

Despite these appealing benefits, microstrip antennas have several drawbacks, such as low gain, low efficiency, low power handling, poor polarization purity, poor scan performance, spurious feed radiation, and very narrow bandwidth. Research reveals that some of these limitations can be overcome by utilizing various techniques, such as slotted patches, thick substrates, substrates with low effective permittivity, incorporating multiple resonances, and improving impedance matching [44, 55]. There is a rising need for multiband, wide-band, miniaturized, and economically viable antennas as a result of the previous decade's advancements in communication technology. There is a considerable need for a single microstrip patch antenna that performs adequately at several resonance frequencies [72]. As a result, many processes and optimization techniques have been put forth in the literature to enhance certain characteristics of the microstrip patch antenna. The following are some of the approaches that are addressed in this dissertation.

2.4.1 Gain and Directivity Improvement Methods

High gain and directional antennas are becoming more and more popular as users expect communication that is quick, reliable, and minimizes path loss. The gain and directivity of a microstrip antenna can be increased in a variety of methods, including impedance matching [73], fractal shaping [72], feeding strategies [41], and etching a slot in the radiating patch [74]. Directivity apparently increased by reducing out-of-phase current in

TM_{odd-0} mode of microstrip patch antenna [75]. In this thesis, several gains and directivity enhancement methods are theoretically examined and contrasted to determine which is best for enhancing the performance of microstrip antennas, as described below and presented in Table 2.1.

Antenna Array

One of the most common and popular practices to boost the directivity and gain of the microstrip patch antennas are array technologies [76–78]. In an antenna array, individual antenna components are constructively coupled to work as a single antenna to improve far-field performance. However, the complexity of the feeding networks, mutual coupling effects, and array sizes are the cons of the antenna array in the majority of portable wireless applications. As a result, researchers are looking into alternative methods on a single antenna rather than an antenna array to attain good far-field gain and directivity demand.

Metamaterial

A recent technique to increase directivity and gain is to surround the proposed antenna with metamaterial resonating structures [79], ladder-like directors [80], and polarization rotation metasurface [81]. When the substrate's refractive index is higher than that of the additional structures, the added metamaterial structures function as a director. The gain and directivity of an antenna are increased by these directors because they reradiate in the same direction as the antenna. The overall effectiveness of the antenna is described in multiple works with metamaterial loading [82, 83]. For WLAN applications, a high directivity and gain antenna is reported based on a zero index metamaterial structure [84]. For gain increase, a microstrip patch antenna array filled with Metamaterial SRR is presented in [85].

Shorting Pins

Researcher reported in reference [86] employed shorting pin to enhance directivity and gain of microstrip antenna. A square patch radiator measuring 60 $\times$ 60 mm^2 is symmetrically equipped with two sets of metallic pins to produce 9.4 dB of directivity at 1.59 GHz [87]. Shunting inductive loading, in which the ground is connected to the patch structure using shorting pins, results in an increase in patch area and leads to improvement in directivity, gain, and bandwidth [88]. Incorporating shorting pins into the design increases current density and improves surface uniformity. The ground and patch both have current flowing in the same direction, which causes radiation to be superimposed. The shorting pin not only augments performance but also assists in reducing cross-polarization magnitude. As a result, the antenna's gain, directivity, and bandwidth are boosted.

Superstrate

By superstrate loading on top of the patch and utilizing a high permittivity raggedy substrate to create an in-phase electric field on top [89] and partly reflecting surfaces [90],

this technique was employed to boost the directivity and gain. At 10.9 GHz, a Cavity Resonator Antenna with metamaterial superstrate of 65 x 65 mm^2 was claimed to increase directivity to 12.5 dB [91]. Multiple dielectric superstrates were reported in the literature to enhance directivity and gain [92]. Altering the radius of holes drilled into the superstrate to reduce its permittivity, the phase of radiation can be controlled. Such antennas are referred to as high-profile antennas since the superstrate size determines how much gain and directivity are enhanced.

Substrate Removal and Using EBG

Surface waves and dielectric losses are reduced by partial removal of the substrate or by employing electromagnetic band gap (EBG) or photonic band gap (PBG) structures. A combination of EBG and Split Ring Resonator (SRR) surface approaches was used to improve the gain of a compact microstrip antenna operating at dual-band frequency. At 5.4 GHz, the proposed antenna obtained 7.39 dB with a total efficiency of 64.7% [93]. On a 235 x 270 mm2 substrate, a mesh-like EBG structure was substantially eliminated to obtain 12.2 dB directivity and 11.8 dB gain [94]. The reduction in losses increases the gain of the microstrip antenna.

Reflectors

The survey also touches on the common practice of enhancing gain and directivity by including artificial magnetic conductors (AMCs), metallic reflectors, and FSS below the patch [95]. A two layer FSS having a size of 30 x 60 mm^2 was reported to enhance the gain of a patch 8.1 dB [96]. Another antenna was reported in reference [97] by employing a 13 x 13 FSS unit cell with the size of 55 x 55 mm^2 to achieve a directivity of 13.6 dB at 10.8 GHz. These structures serve as a reflector and are positioned optimally beneath the patch antenna to produce in-phase radiation that contributes to the main radiation and increases the gain and directivity in the bore-sight direction.

2.4.2 Bandwidth Enhancement

As wireless technology develops and demands higher data rates, broadband antennas become more and more essential. Considering the conventional narrow bandwidth of microstrip antennas, techniques for increasing antenna bandwidth are vital [98]. Some of the existing methods for boosting the bandwidth of microstrip antennas are briefly covered in this study and performances achieved by the researcher are summarized in Table 2.2.

Slot Technique

Slots of various sizes and shapes formed on the radiation patch are vital to increasing the impedance bandwidth. Two symmetrically rectangular slots were used for the mm-wave microstrip antenna to enhance a bandwidth of 4.10 GHz at 28 GHz center frequency [99]. They affect the current distribution and current path length on the radiator. Accordingly,

Table 2.1: Comparison summary of gain and directivity enhancement techniques

Paper	Employed Method	Antenna size(mm^3)	Resonance frequency (GHz)	Achieved gain (dB)	Achieved directivity (dB)	Remark
[79]	Zero Index Metamaterial	90x90x4.54	8.59	7.4	7.65	3x3 metamaterial superstrate increases complexity and thickness
[49]	Near Zero Index Metamaterial	170x170x33.2	0.534	7.27	Not given	Large structure
[90]	Superstrate	100x100x35	5.8	6.8	Not given	A holey superstrate increases size
[91]	Superstrate	65x65x21.52	10.09	12.1	12.5	5 x 5 DASR superstrate
[87]	Shorting Pins	60x60x0.8	1.59	10.3	10.7	4 symmetrically aligned pins at the corner of the path
[94]	Partial Substrate Removal	235x270x1.5	3.2	11.8	12.2	mushroom-like circular EBG complicated
[93]	Partial Substrate Removal	98x109.4x3	2.4 5.4	7.39	9.29	Mushroom-Like EBG and SRR surface, complicated
[96]	Reflectors	30x60x19.8	9.1	8.1	Not given	Two layer FSS and Too much slots create spurious resonance
[97]	Reflectors	55x55x18.5	10.8	Not given	13.6	13 × 13 array unit cells (FSS)

the slots can increase the bandwidth of the antenna. An improved bandwidth is produced

by properly designing the slot sizes and geometries on the radiating patch [100]. However, the radiation efficiency and gain of the corresponding antenna decrease by slots [101].

Adding Parasitic Patch

In staking and co-planer configurations, parasitic patch techniques are used to improve the bandwidth of the microstrip antenna [102]. The addition of two parasitic components to an 11.85 x 8.87 mm^2 patch antenna increased the bandwidth by up to 12 % [103]. In addition, the parasitic method can achieve better impedance matching and higher radiation efficiency with the cost of a large size [104].

Thick and Low Dielectric Substrate

Some crucial properties, including bandwidth, efficiency, and radiation pattern of a patch antenna, are enhanced by selecting the suitable dielectric material for the substrate. The efficiency and bandwidth may be increased by raising the substrate's height [105]. The patch antenna's bandwidth was increased by 12.6 % at 2.4 GHz resonance frequency using a thick substrate and low dielectric strength approaches [106]. However, when the height increases, surface waves are introduced, which degrades the effectiveness of the antenna. From substrate materials, the air has a lower permittivity that is able to produce an effective radiation pattern with minimal return loss when utilized as a substrate. This creates a possibility of a higher amount of input power converted to radiated power over the range of frequency [107]. This shows air gap is a useful factor in enhancing the bandwidth and directivity of the microstrip patch antenna [108].

Multiple Feeding

Multiple feeding refers to exciting an antenna at various radiating patch locations. The technique is utilized to stop some current modes from being excited, which can impair the polarization characteristics and reduce the antenna's impedance and gain performance [109, 110]. Along with numerous resonance frequency actions, it also enhances impedance matching and increases radiation efficiency, all of which lead to bandwidth expansion [111].

Defective Ground Structures In recent years, the idea of "defective ground structures" has emerged. These structures are created by simply carving a defect of any shape on the ground plane [112]. The insertion of these structures in the ground plane alters the current distribution. A patch antenna's performance at 10 GHz was enhanced using a mix of DGS and EBG techniques [113]. Additionally, DGS configuration aids in modifying the inductance and capacitance of transmission lines [114, 115]. The ground defect may continually change from a simple to a more complicated shape to attain the desired performance.

Table 2.2: Summary of bandwidth improvement techniques with their achievement

Paper	Employed Method	Antenna size (mm^3)	Resonance frequency(GHz)	Achieved bandwidth % $S_{11} \leq -10dB$	Obtained gain (dB)
[100]	Slots on ground plane	80x80x1.6	2.4	22.5%	2.185
[99]	Rectangular Slots on radiator	5.5x4.35x1.6	28.0	14.6%	5.32
[104]	Multiple Parasitic Patches	36x39x1.6	6.0	17.5%	5.4
[106]	Thick substrate and low dielectric	47.7x47.7x20	2.4	12.6%	Not given
[107]	Air substrate	10.68x9.06x2	28.0	7.1%	9.45
[112]	Defected Ground structure	57.8x64.6x0.76	10.5	20.5%	6.9
[113]	Defected Ground structure and EBG	36.67x40x1.52	10.0	7.7%	9.64

2.4.3 Multi-band Creation Techniques

Recently, a number of intriguing and cutting-edge ideas and methods have been created to accomplish multi-band antenna designs that can accommodate many wireless communication protocols. Many works were committed to suggesting new, advantageous pathways or strategies for multi-band antenna design [116–119]. Antennas with fractal shapes were used to produce multi-band frequencies [98,102]. In reference [84], the unique feature of metamaterial was used as a benefit to generate three distinct resonant bands from a single antenna. Furthermore, this technology has greatly simplified the device structure and satisfies the WLAN/WiMAX application requirements. In reference [120], a single PIFA was resonated at multiple frequencies by customizing the gridded ground plane. Size reduction and multi-band operation were both accomplished using such a gridded ground plane. For multi-band operation, some other re-configurable strategies are used, including the use of PIN diodes, MEMS switches, and varactor diodes [121–123]. These techniques allow the frequency bands to be electronically adjusted or tweaked to match the target band without altering the geometry or structure of the antenna. The

most utilized methods include slot antenna, loading a parasitic element, and using an optimization algorithm that has been studied.

2.4.3.1 Parasitic Element Method

By including the parasitic element, the multiple-frequency operation has been accomplished [124, 125]. The parasitic components absorb radiation from the primary radiator and then reradiate at a frequency that resonates with them. Each parasitic element must be well optimized in relation to the other antenna structure components using this strategy. Inverted L-shaped and T-shaped parasitic elements are used on microstrip patch antennas to provide multiband operation [126]. A double U-shaped parasitic element on a rectangular microstrip antenna for tri-band service was presented in [127]. Additionally, by including two parasitic components with a rectangular shape, tri-band PIFA antenna functioning was established [128]. These publications demonstrate the use of a single antenna for multiple frequency operations. But a parasitic component makes the device structure heavier and more massive. Additionally, the antennas' bandwidths are insufficient, making it challenging to suppress high-frequency harmonics. Table 2.3 describes the multiband operation with parasitic components presented in the chosen publication.

2.4.3.2 Slot Antenna Methods

Slot antenna approaches have offered several mm-wave multi-band antennas. By designing various slot configurations on the patch antenna, a multi-band operation may be accomplished using this technique. The slots control various current courses on the antenna construction, which results in several resonances. Given that the majority of studies on mm-wave multi-band antennas employ this technique, it would be wise to read additional literature on both single microstrip patch antennas and patch antenna arrays. That will make it easier to assess their success in developing mm-wave communication and plainly show where their research is lacking.

A multi-band patch antenna using a microstrip inset feed line and rectangular slits is proposed in [129]. The antenna operates in mm-wave bands resonating at 14.66GHz, 23.25GHz, and 28.9GHz. The antenna has an overall size of $17 \times 17mm^2$ printed on an FR-4 substrate material with a dielectric constant of 4.4. The simulated return loss was -37.81, -15.58, and -30.44dB at 14.66GHz, 23.25GHz, and 28.9GHz, respectively. The maximum directivity achieved over the three bands is 5.44dB with a narrow bandwidth. The other proposed antenna has a size of $20 \times 20mm^2$ and resonates at 11.65,13.96 and 17GHz with a return loss of -24.75, -42.06, and -30.48 dB, respectively in [130]. The different bands of operation has been generated by optimizing the position and size of the slit. This antenna provides a maximum directivity of 7.41dB, 7.99dB, and 7.3 dB and impedance bandwidth of 0.8GHz, 1.8GHz, and 0.6 GHz at the resonant frequency.

The 28GHz and 38GHz working bands of a dual-band U-shaped slotted microstrip patch

Table 2.3: Parasitic element method literature summary

No.	Papers	Multi-band tech-nique	Reson. freq. (GHz)	Research focus	Identified gaps
1	[124]	Strip-Parasitic ele-ments	2.4 3.5 4.0	Triple bands Independent adjustment of each frequency Bandwidth enhancement Better isolation vs smaller size	At higher frequency the pattern starts to undulate Cannot achieve omnidirec-tional goals and Null occurred High envelope corre-lation Low diversity gain
2	[126]	Inverted-L- and T-shaped para-sitic ele-ments	2.45 2.0175 3.5	Independently tuned resonant frequencies Good band-width in high band	Increase the antenna size High cross-polarization in two low frequency bands
3	[127]	Rectangular para-sitic ele-ments	2.1 2.6 3.5	Good Impedance bandwidth cov-ering the three applications	Low gain was achieved Difficult to get omni-directional radiation pattern Increase antenna size

antenna with a dimension of $8 \times 8.5mm^2$ are shown [131]. The maximum directivity provided by this antenna is 6.7dB and 7.92 dB at 28GHz and 38GHz, respectively. The antenna operates a return loss of -32 dB at 28 GHz and -40 dB at 38 GHz, respectively. In reference [132], the author attempts to achieve a multiband rectangular microstrip patch antenna using single-layer geometry by introducing a slot in the feeding line of the radiating patch in different positions and sizes. The antenna operates at five operational bands with center frequencies at 23.8 GHz, 39.4 GHz, 66.2 GHz, 81.9 GHz, and 93.9 GHz with a dimension of $8.6 \times 9.2mm^2$. The antenna provides bandwidth of 1.46 GHz, 2.56 GHz, 5.66 GHz, 7.93 GHz, and 11.3GHz with a minimum return loss of -31,51 dB, -30.36 dB, -38.78 dB, -27.99 dB, and -13.28 dB at each band respectively. The maximum directivities of the antenna at the operating frequencies are 6.18 dB, 6.52 dB, 7.37 dB, 7.48 dB, and 7.70 dB, respectively.

Microstrip patch antenna proposed with an elliptical slotted circular radiating patch over a Roger RT-5880 substrate with an overall size of $6 \times 6mm^2$ [133]. The proposed antenna

has propagated at 28 GHz with 1.3 GHz bandwidth at maximum directivity of 7.6 dB and 45 GHz with 1 GHz bandwidth at a maximum directivity of 7.2 dB. In reference [134], the author reported a multi-band antenna using a band-switching mechanism. The antenna resonates at 27.5 GHz with a bandwidth of 1.9 GHz, and at 39GHz with a bandwidth of 3.29 GHz in terms of S_{11}<-6dB. The antenna has an overall size of $4.2 \times 4.8mm^2$ and a peak directivity of -0.56 dB at 27.5GHz and 5.77 dB at 39 GHz. In reference [135], the author proposed a single antenna resonating at dual-band frequencies of 28 GHz and 37 GHz with a gain of -17.26 dB and -22.08 dB, respectively. A dual-band is also achieved by creating a slit antenna and adding shorting pins in the high magnetic field region of the antenna.

A Tri-band patch antenna using an inset feed with dimensions of $6.1949 \times 7.251mm^2$ and a thickness of 0.6mm was attempted in [136]. The antenna was resonant at the frequency of 23.9 GHz, 35.5 GHz, and 70.9 GHz with directivity of 4.435 dB, 3.6602 dB, and 5.6402 dB, respectively. The other dual-band printed slot antennas for the mm-wave mobile network communication were proposed in [137]. A circular radiating patch is positioned non-concentrically inside a circle that has been carved out of the ground plane and makes up the fundamental antenna design. According to the findings, the suggested antenna has dual-band operations at 28 and 38 GHz and band-notched operations at 33 GHz. It also has a directivity of 5.30 dB and 5.6 dB and estimated radiation efficiency of 93 % and 94 %, respectively.

Figure 2.8 summarizes the aforementioned literature to assess the mm-wave wireless communication standards against the antenna size and desired directivity based on the average peak directivity of each suggested single-patch microstrip antenna and its matching patch area size in terms of λ^2. The graph shows that the highest average directivity of a single patch antenna is only 7.56 dB, except the one reported in [75]. Thus, the directivity of patch antenna has always needed to be improved to a certain acceptable level for mm-wave wireless communication. Therefore, the majority of studies have recommended employing antenna arrays to create multi-band high gain and high directivity mm-wave microstrip antennas, although the array has a lot more drawbacks in terms of complexity and antenna size.

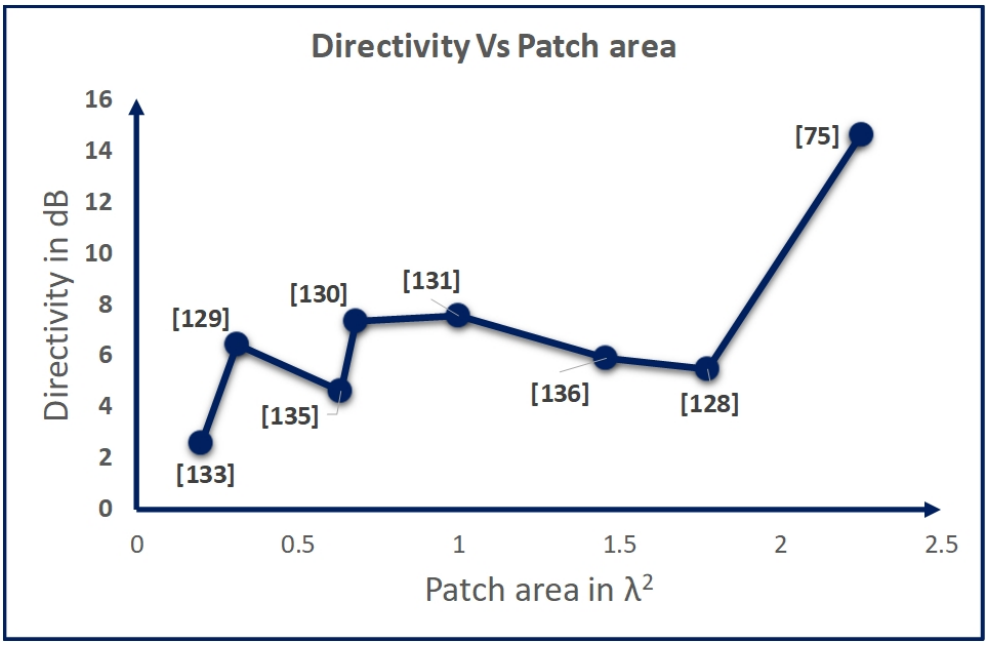

Figure 2.8: Summary of peak average directivity vs patch area (λ^2) of single patch element

2.5 Current State of the Art

The conventional techniques to boost the microstrip antenna's directivity, bandwidth, and resonant frequency have increased its complexity, dubious compactness, and performance-impairing issues. For instance, forming an array of antennas is a traditional way to boost directivity and gain [76–78]. However, antenna arrays require a complicated feeding network, which both increases mechanical complexity and results in spurious radiation that distorts the intended radiation pattern. To eliminate any undesirable radiation qualities and achieve the necessary high directive, multi-band, and broad bandwidth antenna for mm-wave antennas require carefully reconciled optimized dimensions and geometries [138]. Each of the proposed techniques models a microstrip antenna through several trial designs with the assistance of the designer's unique experiences. The full-wave evaluation computation process is always dawdling of time and squandering limited resources so scholars proposed several AI-based optimization strategies in the literature. In an established set of antenna parameters and settings, optimization techniques are iterative algorithms that seek to solve a user-defined cost function. The outcome is then utilized to identify a range of geometries and dimensions that meet the specified performance requirements. The state-of-the-art methods to optimize microstrip antennas are modeling several trial designs and picking the best out of a pool of tested solutions from the solution space being sought. Bio-inspired algorithms have been used and applied in the recent decade to tackle electromagnetic computing challenges [8]. These approaches are gaining popularity owing to their ability to manipulate antenna parameters to reach optimal performance [139, 140]. Many studies have been conducted to improve the

performance of microstrip antennas using bio-inspired algorithms such as genetic algorithms [141, 142], particle swarm optimization [143], differential evolution [144], invasive weed optimization [145], wind-driven optimization [146], ant colony optimization [147], simulated annealing algorithm [148], and tabu search algorithm [149]. Despite the fact that bio-inspired algorithms have significant challenges in articulating the actual objective functions that reflect the real problem and are computationally expensive, they are more accurate and faster in addressing various electromagnetic difficulties.

This dissertation adopted a genetic algorithm to overcome the limitations of a microstrip antenna and increase its performance in the mm-wave spectrum. The genetic algorithm offers various benefits over existing microstrip antenna optimization techniques, including a broader solution space, the ability to handle noisy functions efficiently, and the ability to solve complicated, multi-modal, and multi-objective problems [147, 150]. It can also readily find the global optimum or avoid being caught in local optima, employs just cost function evaluations, is easily changed for new challenges, and does not require knowledge or gradient information about the response surface [151]. It can handle huge and poorly understood search spaces and performs well for large-scale optimization issues. In addition, discontinuities on the response surface have little impact on overall optimization and performance [152]. The algorithm encountered difficulties in determining the optimum fitness function for the problems. The algorithm also becomes more complicated and time-consuming as the population and generation grow [153]. The genetic algorithm is still superior in examining challenges and improving performances concerning microstrip antennas.

In this dissertation, the challenges related to genetic algorithm (GA) optimization are tackled by employing a combination of commercially available software tools, namely HFSS and MATLAB. This integration allows for a comprehensive approach to address these challenges effectively. HFSS is utilized for detailed analysis of antenna performance, leveraging its capabilities in electromagnetic simulation. On the other hand, MATLAB is used for the efficient implementation of the genetic algorithm, taking advantage of its mathematical and optimization functionalities. By combining HFSS and MATLAB, the dissertation benefits from the unique strengths of each tool, resulting in a robust framework for optimizing mm-wave microstrip antennas.

2.6 Chapter Summary

The chapter went through further theoretical and computational information on microstrip antennas, as well as the precise performance measurement parameters and their derivations that are essential to this dissertation. The primary advantages and disadvantages of the antenna were examined. A thorough analysis of performance improvement

methods was offered, along with comparisons of each methodology supported by research work in the areas of bandwidth, gain and directivity, and multi-band.

Some of the shortcomings of conventional microstrip characteristics are resolved by utilizing one of the methods or combinations outlined in this chapter. However, there are still a limited number of usable strategies that face different problems, including the complexity of the structure and the absence of any relevant but unsolved issues. Thus, more extensive and appropriate consideration must be given to future developments in microstrip antennas. It has been found that it is challenging to design microstrip antennas for multi-band operations with wide impedance bandwidths, high directivity, and gain, which are crucial for mm-wave wireless communication to overcome high path loss and offer high data rates and multi-functional services.

The chapter also evaluated a technique that is less complicated but still effective in achieving goals and solving the challenges indicated in the problem statement. The state-of-the-art for establishing microstrip antennas for mm-wave applications is covered in the dissertation. The employment of a genetic algorithm is a potential strategy to improve the gain, efficiency, bandwidth, directivity, and multi-band characteristics with multiple radiating and scattering parameters in a straightforward iterative-based patch geometry adjustment. A single microstrip element may be improved using a genetic algorithm to produce a multiband, high-directive pattern with a broader bandwidth without the need for an array, a complicated feeding network, or the addition of a complex system.

Chapter 3

Genetic Algorithm Optimization for Microstrip Antenna Design

3.1 Introduction

All radio wave communication systems are inseparable from the antenna, and the choice and layout of the antennas have a direct impact on the overall system performance [37]. Developing an antenna with suitable performance reduces the design complexity and expense of the complete communication service's back-end while improving wireless system performance [154, 155]. Antenna optimization and design are influenced by several elements, including operating frequencies, size, radiation pattern, gain, polarization, and others [156]. The employment of autonomous algorithms in antenna optimization has grown significantly to solve the intricate and continuously developing wireless communication requirements on multi-band, high-directional, high gain, and broadband antenna operation. This chapter describes the overarching methodology to which this dissertation adheres to accomplish the predefined goals. Optimization approaches are utilized to overcome the limitations of microstrip antennas for mm-wave wireless communication with a less sophisticated structure. As mentioned in chapter two of this dissertation, genetic algorithms (GA) have been among the most prolific and valuable microstrip antenna optimization methods during the last two decades [150]. As a result, this chapter will present the reliability of the algorithm's optimization parameters, theorems related to the genetic algorithm, and implementation techniques for microstrip antenna optimization.

3.2 Genetic Algorithm Optimization

The idea of a genetic algorithm is based on Darwin's theory of evolution. It states that populations of individuals gradually develop by spreading traits to their offspring that allow them to thrive and reproduce [8]. The algorithm uses a global search technique to locate the precise and actual solutions. Bremermann was the first to create the algorithm in 1958. Holland, on the other hand, promoted the algorithm by introducing the Schema theorem in 1975 [157]. Several scientists have advanced the genetic algorithm and its application, including Goldberg in 1989, and others as reported in [158,159]. Throughout the decades of genetic algorithm advancement, several approaches such as adaptive [160],

fast messy [161], hybrid [162], independent sampling [163], real-coded, and binary-coded [164] genetic algorithms have been described in the literature to address a variety of challenges. In 1997, genetic algorithms were also utilized for antenna development, as reported in reference [165]. This dissertation employs a binary-coded genetic algorithm since it is convenient to represent the conduction and non-conduction features of the antenna.

3.2.1 Binary-Coded GA Terminologies

In a binary-coded GA, a gene is a binary bit with a value of '1' or '0', the chromosome is a string of bits that represents an individual, and an individual is a single candidate solution drawn from the solution space [166]. In the search space, a population is a collection of individuals at any particular time. When the population size clustered as a single generation becomes large, the algorithm has more search space. However, it requires much more computational cost, memory, and time [167].

3.2.2 Fitness Function

The fitness function takes a candidate solution as input and determines how to fit the individual in accordance with the overall targets. Developing an appropriate fitness function is critical in practical optimization situations. The fitness function is inarguably more complex to establish in the case of multi-criterion optimization and the fitness function's characteristics are not subject to any particular mathematical constraints. Prior to evaluating the objective function, the chromosome must first be decoded. The computed value of an objective function for a phenotype determines an individual's fitness in a genetic algorithm. Determining the fitness function in antenna optimization aims to solve problems with the number of operational bands, gain, directivity, and bandwidth of the antenna [168]. As a result, it might be difficult to describe and represent the particular problems of the antenna that the algorithm is trying to solve.

3.3 GA Operators and Procedures

An algorithm refers to a set of procedures for fixing problems. A genetic algorithm is a problem-solving approach that uses genetics as its paradigm [169]. It is a search technique that handles a large number of optimum and approximation solutions from the solution space. The first cluster of individuals or generations is generated at random. At each next stage, GA swaps out fewer fit members of the previous population with more fit individuals from the current population [170]. Utilizing the cost function, it is possible to determine each individual's fitness value. Then, fresh generations can be produced by mating the fit individuals. It means that the fittest individuals are chosen

and given increased chances of creating a new population. The method eventually reaches an optimal individual, which is probably a representation of the idealized solution to the problem, after several generations [171]. By depending on biologically inspired processes like selection, crossover, and mutation, a new population is created. The diagram in Figure 3.1 shows how these processes interact during the reproduction process.

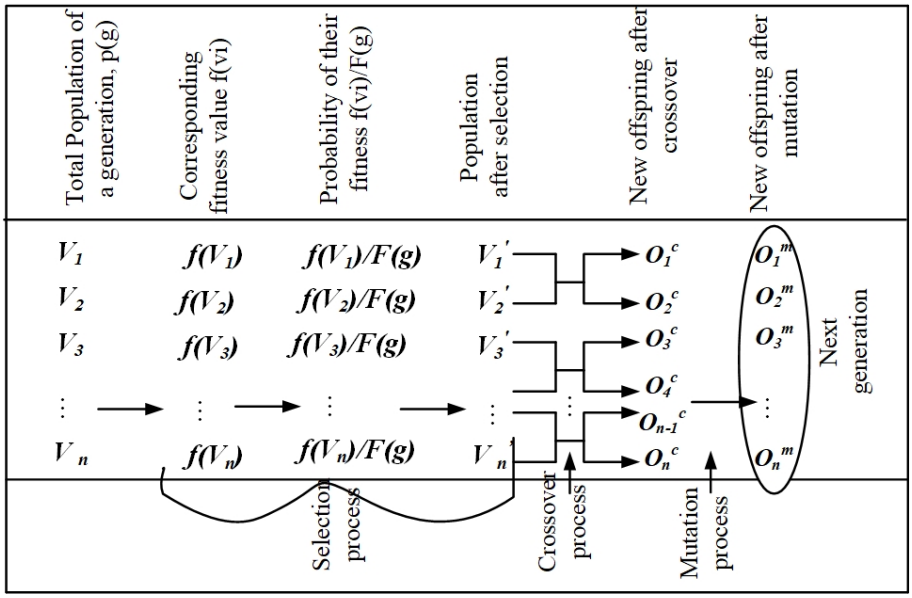

Figure 3.1: Process of reproducing next generation in genetic algorithm [171]

3.3.1 Selection

Selection is a process that arbitrarily selects chromosomes from a population based on their fitness value. It should be capable of comparing every individual in the group. A candidate has a better chance of being selected if their fitness value is higher. A value matching the fitness of the solution is allocated to each chromosome. As competent parents encourage individuals to seek more effective and appropriate solutions, parent picking is advantageous to the GA's convergence rate [172]. Premature convergence can occur when everyone is compelled to follow a single, incredibly successful solution. In light of this, GA may continue to succeed by fostering diversity. For proper convergence in GA operation, it is necessary to choose from a variety of approaches or algorithms. Roulette wheel, tournament, and rank techniques were all mentioned in the literature as selection mechanisms [173].

Roulette Wheel Selection

It is the concept of sequential search across a roulette wheel with slots; that are weighted according to the fitness values of the candidate. A goal metric is selected at random from the population's fitness. A physically fit individual will provide higher to the desired

value. It is critical that the individuals aren't ordered by fitness value, as it would significantly skew the selection. Roulette wheel selection is less challenging to execute but more disruptive. The variance in fitness value in the population determines the rate of progression.

Rank Selection

Rank Selection rates the population and then assigns fitness to each chromosome based on the ranking. It retains diversity, resulting in an effective search. In essence, possible parents are identified, and a competition is conducted to choose who will become the parent.

Tournament Selection

Tournament selection is an excellent approach for the refinement of GA search performance by applying selective pressure and adjusting population diversity. The victor of the competition is the one with the highest fitness level. Tournament competitions are conducted, and the top is subsequently introduced into the selection pool. The competition continues until the mating pool for producing new offspring is depleted. The breeding pool of the tournament winner has a better existing population fitness. The selection pressure created by the fitness disparity pushes GA to increase the fitness of the surviving genes [174]. This approach is more effective and produces the best result.

3.3.2 Crossover

Crossover is the process of creating a newborn from the contributions of two individuals who are considered as parents. Once the selection is complete, the generation is improved with more suitable individuals. In an effort to produce superior offspring, the crossover operator is applied to the mating pool. The genes of the parents are swapped during conception to produce offspring. When mating two distinct strings, the operator randomly chooses a cross-site, and after the cross-site, the placement values of the two strings are switched [171, 175]. The three most often employed crossover operators in antenna optimization are uniform crossover, multi-point crossover, and one-point crossover [176].

Single Point Crossover

The most common crossover operation in GA entails making a single cut at the proper locations on the two mating chromosomes, then exchanging the sections after the incision. In this instance, a random crossover point is picked along the length of the matched strings, and bits near the cross-sites are then switched. The combination of excellent parents can result in better offspring if the correct site is chosen, but if not, string quality will be significantly restricted.

Figure 3.2 depicts a single-point crossing and it illustrates a scenario where eight gene parents are involved in mating. In this particular case, a random cut is made at the end of the third gene. The crossover operation is then performed by exchanging genetic

information between the parents, specifically on the second portion of the random cut. As a result of this crossover, new offspring with a modified genotype are produced, as depicted in the diagram.

Two Point Crossover

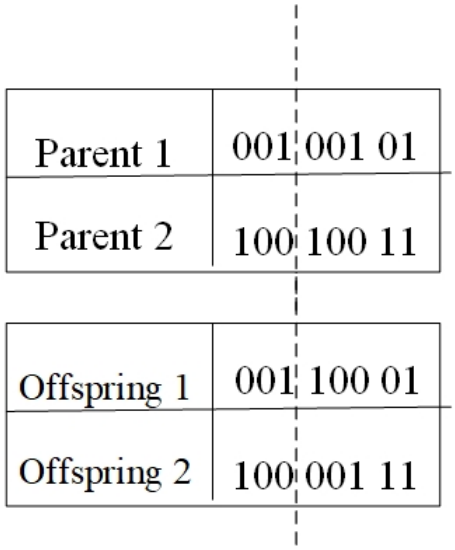

Figure 3.2: Example of single point crossover operation

In addition to single-point crossover, other crossover algorithms have been developed, sometimes incorporating multiple cut points. When using two-point crossover, the cross-bred parents choose two cross-sites and exchange information. The performance of the algorithm is decreased when the number of crossover points is increased since the building blocks of GA are more vulnerable to disruption. On the other hand, having more crossing points allows more investigation of the problem space.

Uniform Crossover

In a uniform crossover, each gene in the offspring is generated by copying the relevant gene from one or both parents using a randomly generated binary crossover mask having a similar length as the parent's chromosomes. When the crossover mask includes '1,' the child gene is copied from the first parent, otherwise it is copied from the second parent. A fresh crossover mask is generated at random for each pair of parents in order to ensure that each offspring inherits a diverse set of genes from both parents.

Crossover Probability

The crossover probability (Pc) is a metric that specifies how frequently crossover will occur. If there is no crossover (Pc=0%), the offspring are identical to their parents. If there is a crossover, portions of each parent's chromosomes are used to create the offspring. All children are produced through crossover if the crossover probability is 100%. Crossover is done with the notion that the newborn chromosomes would be better

since they will have beneficial portions of the old chromosomes.

3.3.3 Mutation

A modest random probability of gene mutation can occur after a particular new offspring has been created. Mutation keeps the algorithm from being stuck at a local minimum or avoids early convergence [175, 177]. A mutation is also responsible for restoring lost genetic material and randomly disrupting genetic information. It introduces new genetic structures into the population and preserves variety by changing parts of an individual's features at random. There exists a wide variety of mutational forms. In binary-coded GA, the simple mutation method can be achieved by flipping the value of each gene according to its mutation probability (Pm). Inferred from this is the possibility of flipping part of the string's bits from 0 to 1 or vice versa. Figure 3.3 depicts a basic flowchart that summarizes the iteration of essential GA operations.

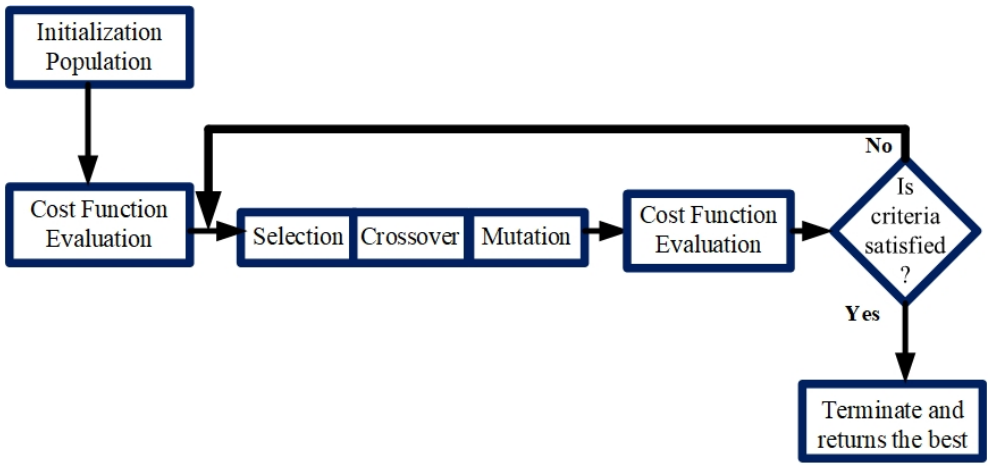

Figure 3.3: Genetic algorithm flowchart

3.4 The Schema Theorem

Holland's scheme theorem underpins GA's search heuristics and a base for GA optimization. Templates for defining a subset of chromosomes with comparable regions are specified as schemas. According to the Schema Theorem, "short, low-order schemata with above-average fitness grow in frequency exponentially in succeeding generations" [178]. It was noticed that only a decent schema will be passed on to future generations, while those with fitness below the average will decline rapidly and eventually die. Holland developed an expression that forecasts the number of copies of a certain schema in the future generation after selection, crossover, and mutation. To prove the schema theorem, it is better to demonstrate the relationship between the relative selection frequency of

a schema in the current generation (M(H, g)) and its relative selection frequency in the next generation (M(H, g+1)). The following derivations are based on the books presented in [171], [178], [179].
The population's overall fitness value in a particular generation is calculated as

$$F(g) = \sum_{i=1}^{Npop} f(vi) \tag{3.1}$$

where N_{pop} is number of population and f(vi) is the fitness value each individual (Vi)
And probability of choosing an individual based on its cost value is

$$Pi = \frac{f(vi)}{F(g)} \tag{3.2}$$

The schema theorem offers a complete map of how individuals are selected to be parents for the following generation depending on their fitness value.
Let f(H,g) be the average cost of all strings in the population that meet the schema H.

$$f(H,g) = \frac{\sum_{i=1}^{p} f(ui)}{P} \tag{3.3}$$

Where P is the total number of individuals in the population matched by a schema H at a given generation g.
The average likelihood that individuals matched by schemata H will be chosen.

$$P_{av} = \frac{f(H,g)}{F(g)} \tag{3.4}$$

Now investigating the probability of survival of all schemata $H(H_1, H_2, \ldots .H_N$ bits)

$$M(H, g+1) = M(H, g) \times N_{pop} \times P_{av} \tag{3.5}$$

$$= M(H, g) \times N_{pop} \times \frac{f(H, g)}{F(g)} \tag{3.6}$$

$$= M(H, g) \times \frac{f(H, g)}{F(g)/N_{pop}} \tag{3.7}$$

$$= M(H, g) \times \frac{f(H, g)}{\overline{F(g)}} \tag{3.8}$$

$$\overline{F(g)} = \frac{F(g)}{N_{pop}} \tag{3.9}$$

Where
It is the average fitness value of the population. Then, it can be re-write as

$$M\left(H, g+1\right) = M\left(H, g\right) \times \frac{\overline{F(g)} + f\left(H, g\right) - \overline{F(g)}}{\overline{F(g)}} \tag{3.10}$$

Now let,

$$\in (g) = \frac{f\left(H, g\right) - \overline{F(g)}}{\overline{F(g)}} \tag{3.11}$$

$$M\left(H, g+1\right) = M\left(H, g\right) \times \ (1+ \in (g)) \tag{3.12}$$

If $\in (g)$ >0 from the generation : $M\left(H, g+1\right)$ is increasing and if $\in (g)$ <0 from the generation : $M\left(H, g+1\right)$ is decreasing.
It implies that any schemata will acquire an increasing number of strings in the following generation, but that below-average schemata will die off as generation g grows.
When considering crossover, the theorem considers the probability of destruction of a schema.

$$P_d\left(H\right) \leq \frac{\delta(H)}{L-1}) \tag{3.13}$$

And the probability of survival

$$P_S\left(H\right) \geq 1 - \frac{\delta(H)}{L-1} \tag{3.14}$$

The schema growth equation with this consideration will modified as

$$M\left(H, g+1\right) \geq M\left(H, g\right) \times \frac{f\left(H, g\right)}{\overline{F\left(g\right)}}(1 - \frac{\delta(H)}{L-1}) \tag{3.15}$$

When we consider a single bit flipping mutation
Probability of a single bit survival is (no mutation takes place) $1 - pm$, where pm is the probability of mutation.

$$P_H\left(H\right) = \left(1 - pm\right)^{O(H)} \tag{3.16}$$

Finally, when mutation and crossover considers the schemata growth equation is developed as

$$M\left(H, g+1\right) \geq M\left(H, g\right) \times \frac{f\left(H, g\right)}{\overline{F\left(g\right)}}(1 - \frac{\delta(H)}{L-1})(1 - pm)^{O(H)} \tag{3.17}$$

3.5 GA for Microstrip Antenna Optimization

In a typical antenna design, the antenna's structure is developed from functional prototypes, and the antenna can only be optimized in terms of the dimensions of its structural characteristics, such as length, width, spacing, and so forth. By employing this size optimization strategy, it is challenging to locate an appropriate antenna shape over a wide range. On the other hand, GA is an effective optimization approach that has been utilized in the wide area of electromagnetics problems [116]. Literature review shows that GA has been used to enhance the performance of microstrip patch antennas in multiband operation, broad-band services, and making them more directive. GA can be utilized for optimization of microstrip antenna as pointing the best place of shorting pins in patch antenna [180], finding the best position of feeding especially in coaxial feed microstrip patch antenna [181], optimizing the size and location of predefined slots and slits on different parts of patch antenna [182], and optimizing dimension of the patch antenna to meet the required criteria [151].

GA readily captures such antenna difficulties by discretizing a large patch area into tiny components, and the continuous arrangement of these elements may be approximated as the original form and surface size [183]. In the binary-coded GA situation, the discretized antenna surface features are assigned a value of '0' or '1' depending on their conducting and non-conducting properties. Where '0' indicates that a cell is a non-conducting unit and '1' indicates a conducting cell on the surface, as illustrated in Figure 3.4. It applies binary coding to the area covered by the range of antenna size. Increasing the number of grids can enhance computation accuracy, but it will also result in an exponential increase in calculation time.

By applying binary-coded GA to selectively remove or add smaller radiating cells from/on the patch, and at the end, non-intuitive shapes or geometry of the patch antenna can be produced. The presence or absence of the patch on each cell is represented by '1' and '0' in each GA chromosome [138]. When two cells are touching at the corner there is a creation of infinitesimal points of connection. This may pose a connection problem in manufacturing the microstrip patch due to the tolerances of the fabrication [184]. To overcome this problem, this dissertation uses the overlaps between adjacent cells to avoid cells contacting each other by infinitesimal points and to ensure electrical contact in such patterns in the fabricated antenna.

In the patch geometry optimization based on GA, multiple objectives need to be considered, and the corresponding fitness function is similar to a multimodal problem. This dissertation is going to improve the multi-band operation, the directivity of multi-band, bandwidth of the patch antenna, the fitness is designed not only an improvement of the reflection coefficient of the antenna but also includes other additional antenna parameters enhancement based on the objective of the design.

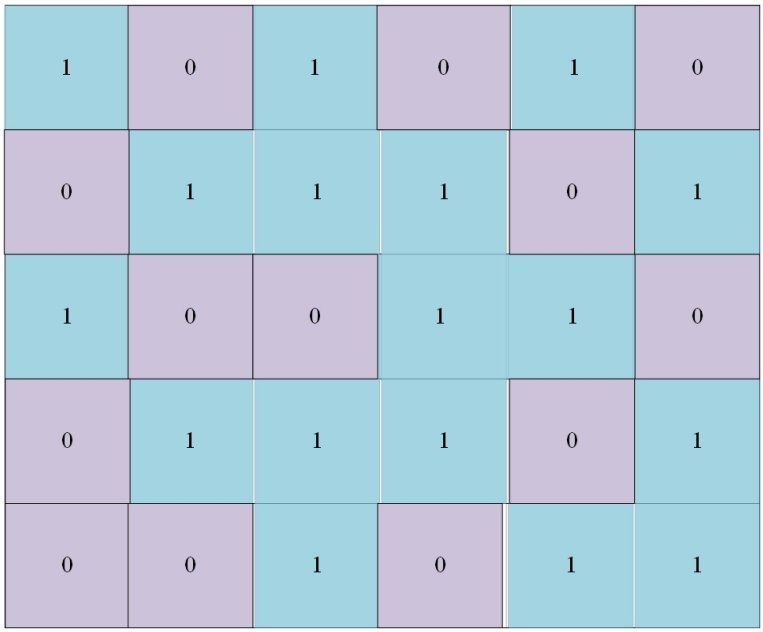

Figure 3.4: Gridded rectangular patch surface

3.6 Interfacing Ansys HFSS and MATLAB

One commercially accessible electromagnetic simulator is the Ansys High-frequency structure simulator (HFSS). MATLAB, on the other hand, is used to code any type of mathematical problem and analysis depending on the approach defined by the analyst. As a result, two very efficient software are merged in this dissertation to create an efficient solution. Before delving into the integration, the HFSS computational system is briefly explained below.

3.6.1 HFSS computation methods

The finite element approach is one of the most efficient full-wave numerical modeling techniques used by HFSS (FEM). This approach divides the antenna construction into several smaller subsections known as finite elements (tetrahedral in HFSS) [185]. Once the fields within the finite element are solved, these fields are integrated to fulfill Maxwell's equations across inter-element boundaries by creating a field solution for the entire, original structure. Equation (3.18) is used by HFSS to solve for the electric field E under excitation and boundary conditions:

$$\nabla \times \left(\frac{1}{\mu_r} \nabla \times E \right) - {k_0}^2 \varepsilon_r E = 0 \tag{3.18}$$

Where

$${k_0}^2 = \omega^2 \varepsilon_0 \mu_0 \tag{3.19}$$

HFSS determines the magnetic field H using equation
(3.20),

$$H = \frac{1}{\omega\mu}\nabla \times E \tag{3.20}$$

The constitutive relationships between the electric and magnetic fields are used to obtain the remaining electromagnetic quantities. The above field equations are employed to construct a finite element matrix. The next step is to use tetrahedral elements to divide the structure into a finite element mesh. Lastly, defining a test function W_n for each tetrahedron, resulting in thousands of fundamental functions [186]. The field equation presented in equation (3.18) is multiplied by a test function (W_n) and integrated by volume, as shown in equation (2.21)-(2.24).

$$\int_v w_n . \left(\nabla \times \left(\frac{1}{\mu_r}\nabla \times E\right) - {k_0}^2 \varepsilon_r E\right) dv = 0 \tag{3.21}$$

This procedure yields thousands of equations for n=1, 2, ..., N. Manipulating the N equations, using Green's theorem and the divergence theorem yields:

$$\int_v \left[(\nabla \times w_n) . \nabla \times \left(\frac{1}{\mu_r}\nabla \times E\right) - {k_0}^2 \varepsilon_r w_n . E\right] dv = \int_s (boundary\ terms)\ \ ds \tag{3.22}$$

If electric field E is given as

$$E = \sum_m^N X_m w_n, \quad n = 1, 2 \ldots\ldots M \tag{3.23}$$

The general equation is rewritten as below

$$\sum x_m \int_v \left[(\nabla \times w_n) . \nabla \times \left(\frac{1}{\mu_r}\nabla \times w_m\right) - {k_0}^2 \varepsilon_r w_n . w_m\right] dv = \int_s (boundary\ terms)\ \ ds \tag{3.24}$$

This can be simplified as

$$\sum X_m A_{n,m} = b_n, \ \ n = 1, 2 \ldots . N \tag{3.25}$$

$$Ax = b \tag{3.26}$$

Where A is the N × N matrix, which includes boundary conditions, the port excitation, voltage, current sources, and incident waves applied. The only unknown matrix in the above equation is x; nevertheless, once the value of x is solved, the value of E becomes known. The above approach reveals that the HFSS solution process is easy and relatively simple. HFSS's field solution technique, on the other hand, is iterative.

3.6.2 Implementing GA

The full procedure of GA starts from gene creation on the surface of the patch antenna, which is called cells. This dissertation employed patch area division to create the genes. Then the string of genes produce a proposed individual antenna or a chromosome in GA. A collection of individuals at a time creates a generation (population). Accordingly, the patch area is divided into $n \times m$ cells. The conducting or non-conducting property of each cell is defined using binary encoding. If a cell is conducting, then the corresponding gene is assigned 1, and if a cell is non-conducting, it is assigned 0. Then the optimization and implementation steps in this dissertation are summarized as follows:

Step 1: It is necessary to establish GA parameters such as chromosomal size, population size, and the total number of generations utilized for antenna shape optimization.

Step 2: A fitness function must be built to accomplish a specific objective based on issue criteria such as high directivity, multi-band operation, and increased bandwidth. It can be done by extracting individual antenna performance from HFSS and exported to MATLAB.

Step 3: The first generation of individuals is generated at random to provide a starting point for the optimization process in MATLAB. Each individual antenna detail was coded into a Visual Basic Script file (VBS file) and then called in HFSS software for the computation of all necessary antenna parameters in the required frequency band.

Step 4: The main function of the optimizer in MATLAB was then called with each candidate antenna attribute and performance determined in HFSS. The algorithm starts to evaluate the fitness value of each individual based on the defined cost function. All findings from the fitness value of each individual will be an input for GA operators. The fitness values are executed from the fitness function. A MATLAB and HFSS interfacing is presented in Figure 3.5.

Step 5: At this stage, GA operators began to put up their best effort to reproduce the

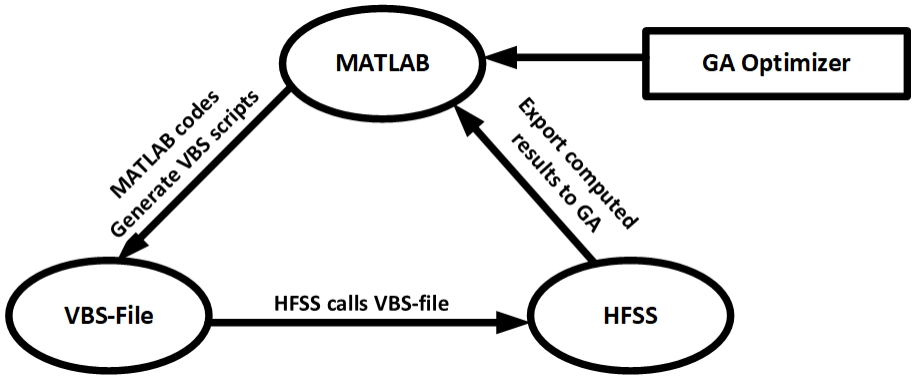

Figure 3.5: Iterative implementation GA using HFSS and MATLAB

following generation. The selection operator is used based on one of the recommended selection mechanisms to pick the fittest individual to serve as parents.

Step 6: Once the parent individuals have been identified based on the selection operator, a crossover operation is carried out between the parents to generate offspring of the next generation.
Step 7: Further, a mutation operator was used on the newborns to diversify the population and ensure the search for globally optimal solutions. Following mutation, a new generation is formed in the same number of individuals as the original population.
Step 8: The fitness values of the offspring again computing. The offspring and individuals of the previous generation again sort according to their fitness values.
Step 9: Up until the termination requirements are met, steps 3 through 8 will be repeated. When the fitness value stays the same, the iteration will end following the intended criterion, which may be the maximum number of generations. More information on the GA processes and implementation methodologies in this dissertation is provided in the flow chart in Figure 3.6.

3.7 Chapter Summary

This chapter presents the general flowing methodology of the dissertation to resolve the multi-band, high directive, and widen the bandwidth of mm-wave microstrip antenna, which is about binary-coded genetic algorithm. The idea of the schema theorem was introduced, which is a fundamental principle of new offspring production in a genetic algorithm. The operators such as selection, crossover, and mutation are responsible for the creation of new candidate solutions in antenna optimization. In addition, the chapter's discussion includes the general procedure of implementing a genetic algorithm for microstrip antenna, the combination operation of HFSS and MATLAB software, and the overall flowchart of the genetic algorithm. The idea of gene/ small cells was introduced in the chapter. After having the whole procedure in this chapter, it is easy to synthesize the multiple band antennae with improved detail performance will be discussed in the subsequent chapters.

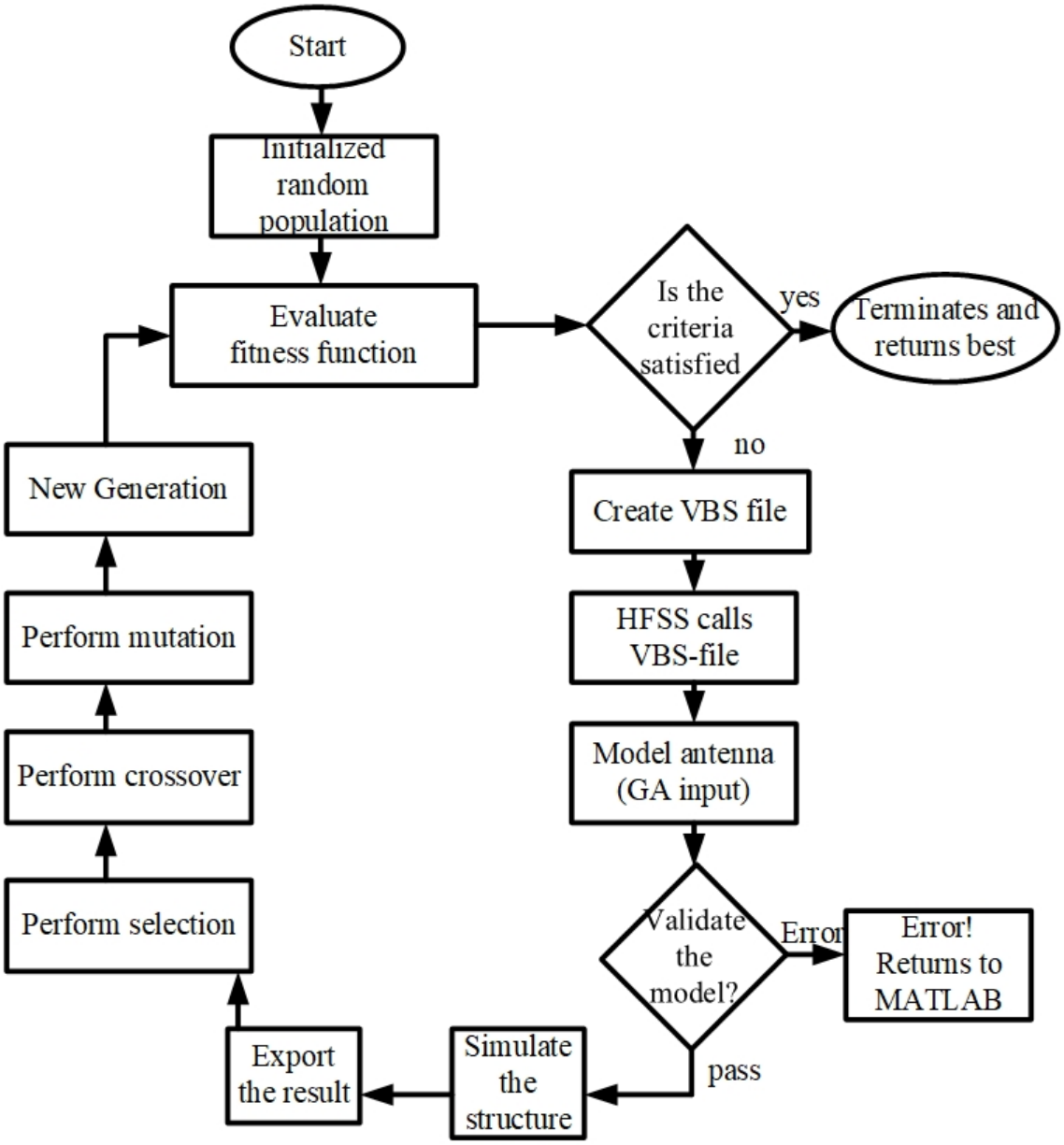

Figure 3.6: The proposed Genetic Algorithm optimization flowchart

Chapter 4

Synthesis of Dual-band Microstrip Antenna based on GA

4.1 Introduction

In the dynamic field of wireless communication, an increase in the number of required services from a single device opens up a new avenue for research into a new multi-band antenna technology. For optimal exploitation of the available resource at the band, the mm-wave spectrum necessitates a high-directive, broad-bandwidth antenna. It is not a simple effort to design and synthesize a dual-band microstrip antenna particularly for mm-wave wireless communication, as there are several performance-improving aspects. As a result, developing a high directional, broad bandwidth, dual-band patch antenna in the mm-wave spectrum is a difficult challenge.

A number of techniques to advance a patch antenna for dual-band service were reported in the literature. Dual-band antenna were designed based on artificial magnetic conductor [187]. Moreover, C and O slot structures also were presented [188]. A dual-band elliptically slotted circular radiating patch antenna resonating at 28 GHz and 45 GHz is proposed [133]. Another investigation on dual-band antenna designed using branch fractal bionic antenna [189], and employing bow tie structure [190] was described. Dual-band optimization of patch antenna using genetic algorithm in microwave frequency is presented [142]. This chapter also presents three dual-band patch antennas for mm-wave frequency using a binary-coded genetic algorithm optimization with improved directivity and bandwidth.

4.2 Dual-band with Improved Directivity

High-directional antenna technology may be one of the most important aspects in overcoming some of the propagation issues of mm-wave communication, boosting spectrum efficiency, and enabling larger data rates for wireless broadband services. A number of techniques to improve the dual-band directivity of patch antenna were reported in the literature. Among them, slot antenna methods [131, 191], fractal shaped geometry were presented in [74, 192], and frequency selective surface (FSS) were reported in [193, 194]. Most commonly, the directivity of an antenna can also be improved by implementing

an antenna array [195, 196]. Besides the above, directivity improvement was also done using TModd-0 modes, as reported in [75]. Adding a superstrate zero-index metamaterial [197, 198] and genetic algorithm (GA) also presented [141, 199]. GA is preferable since it does not need a complex feeding network and has no detrimental impact on antenna size [61]. This dissertation proposes two methods for enhancing the directivity of a dual-band patch antenna using a binary-coded genetics algorithm. The surface of the patch is split into small rectangular cells as one choice and circular cells as the other.

4.2.1 Employing Small-rectangular Cells

Antenna Configuration

A rectangular microstrip radiating patch is designed on the top of $\lambda \times \lambda$ substrate with patch dimension of L_{xp}= 3.6 mm (0.34λ) and W_{yp}= 5.0 mm (0.47λ) and made of thin copper having thickness (0.0003266 $\lambda \gg \lambda$; where λ the free space wavelength at 28 GHz). In the proposed design, the Roger RT/duriod 5880 (tm) substrate is used with a dielectric constant of 2.2, a tangent loss of 0.0009, and thickness 0.028 λ (0.3 mm) is employed on finite ground plane $L_{xg} \times W_{yg}$ size as shown in Figure 4.1. Table 4.1 also summarizes all dimensions of the reference microstrip patch antenna.

Table 4.1: summary of dimensions of reference microstrip patch antenna

Parameter	**L**$_{xp}$	**W**$_{yp}$	**h**	**L**$_{xg}$	**W**$_{yg}$	**W**$_{f}$	**L_feed**
Dimension (mm)	3.6	5.0	0.3	10.7	10.7	0.7	3.5

GA Optimization Setup

In order to optimize the patch geometry using a genetic algorithm, the patch area is divided into 64 genes or cells (8 x 8) as shown in Figure 4.2.

The fitness function is designed based on maximizing the directivity (D (f) in dB) and negative of reflection coefficient (S_{11} (f) in dB) in two desired bands, as presents in Equation 4.1. Optimizing the difference involves increasing the directivity towards more positive and decreasing the reflection coefficient towards more negative in the specifically optimised band, which is the main goal of this antenna optimization. To eliminate the algorithm's narrow band convergence, the fitness function sets any reflection coefficients smaller than -10 dB to -10 dB, as shown in Equation 4.2.

$$Fittness\ function = \sum_{f} [D\,(f) - S_{11}(f)] \tag{4.1}$$

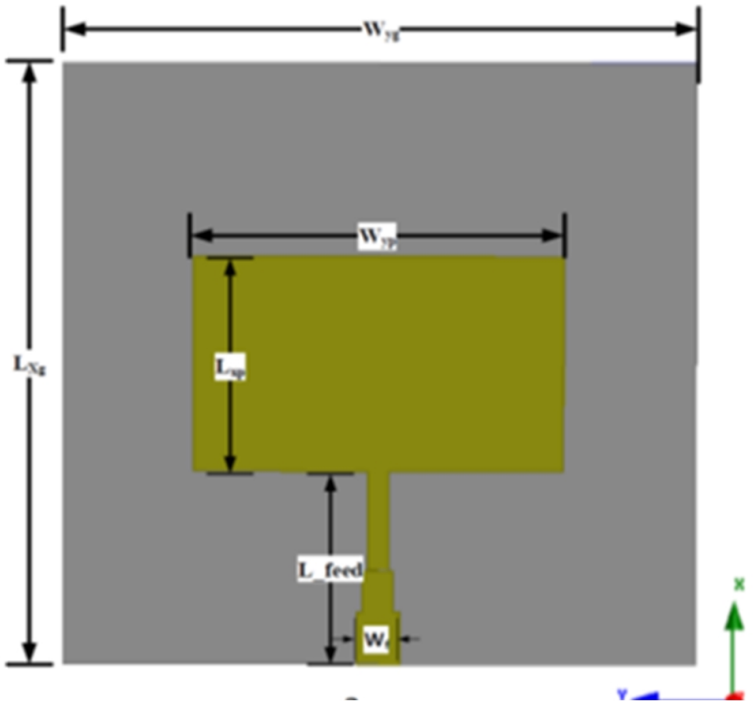

Figure 4.1: Single patch antenna top view at 28.0 GHz on finite substrate

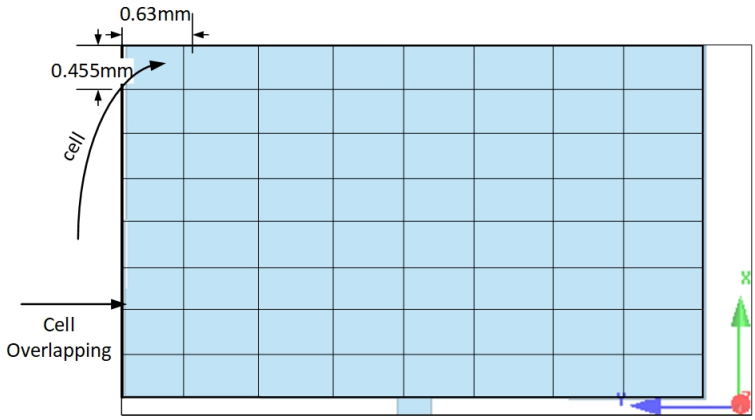

Figure 4.2: 8 x 8 division of the reference microstrip patch surface

$$S_{11}(f) = \begin{cases} S_{11}, & if\ S_{11} > -10 \text{ dB} \\ -10dB, & if \quad S_{11} \leq -10 \text{ dB} \end{cases} \tag{4.2}$$

The population size clustered as a generation is set to 20 individuals and each individual is represented by 64 genes. A single point crossover with a 70 % probability and a 0.02 mutate rate has been used to create a diversity of the population in each generation. The tournament selection mechanism has been applied to select individual parents that are fit to reproduce offspring for the next new generation.

The strategies for optimization are based on the principles and phases described in Chapter 3. GA optimizes the patch geometry by deactivating certain cells from the patch's surface due to the cells' non-conductive properties, as implemented by the binary-coded

genetic algorithm. The algorithm underwent 100 generations, during which it continuously reviewed the fitness function. It consistently employed a greedy approach to search for the best antenna design that maximizes directivity and minimizes reflection coefficient within the specified frequency bands, as determined by the fitness function, The best-fit individual is shown in Figure 4.3.

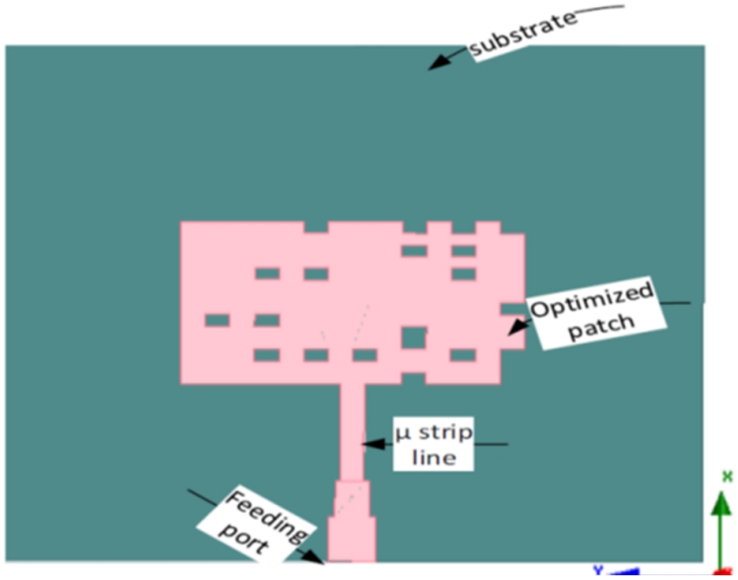

Figure 4.3: Genetically optimized proposed patch geometry

Results and Discussion

The proposed reference antenna and optimized antennas were simulated using HFSS software. The simulated results show that the proposed reference antenna is resonated only on a single frequency at 28.0 GHz with S_{11}= -17.2 dB and with S_{11} < -10 dB bandwidth (BW) of 2.1 % as shown in Figure 4.4.

The directivity of reference antenna was examined at θ=0^0 and $\phi = 90^0$ as 6.8 dB which is expected from a single conventional microstrip patch antenna in broadside direction. Figure 4.5 shows the radiation pattern of this antenna.

Genetically engineered microstrip antenna shown in Figure 4.3 was simulated in a similar platform that proves improvement in directivity and resonance at dual-band.

As Figure 4.6 illustrates the reflection coefficient of optimized antenna becoming dip at two frequencies 28.0 GHz and 46.6 GHz with BW=1.8 % and BW=1.5 %, respectively. Furthermore, a broadside direction directivity of 8.4dB at 28.0GHz, θ=0^0 and $\phi = 90^0$ is demonstrated at Figure 4.7-a and higher directivity also verified at 46.6 GHz, θ=0^0 and $\phi = 90^0$ which is 9.0 dB in broadside direction as shown in Figure 4.6(b). Besides the above directivity improvement, the antenna is also too compact. The overall performance of the antenna is summarized in the Table 4.2

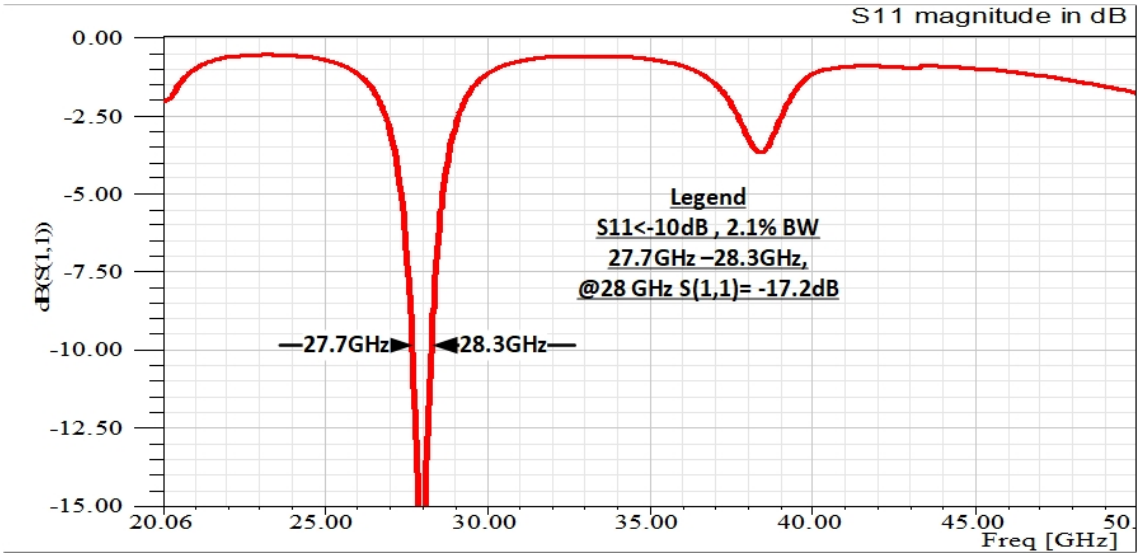

Figure 4.4: Simulated results of reference antenna magnitude of S11 resonating at 28.0 GHz

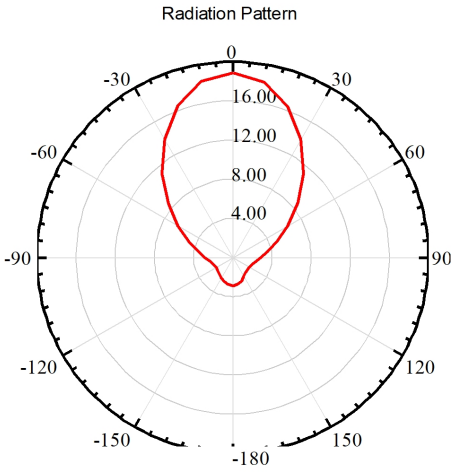

Figure 4.5: Radiation pattern plot of reference antenna at 28.0 GHz

Table 4.2: Summary of performance of proposed and reference antenna

	Overall Size of antenna (mm^3)	Resonant frequency(GHz)	BW(%, S_{11} ≤-10 dB)	Directivity
Reference patch	10.7x 10.7x0.3	28.0	2.1%	6.8 dB
GAO Patch	10.7x10.7x0.3	28.0 46.6	1.8% 1.5%	8.4 dB 9.0 dB

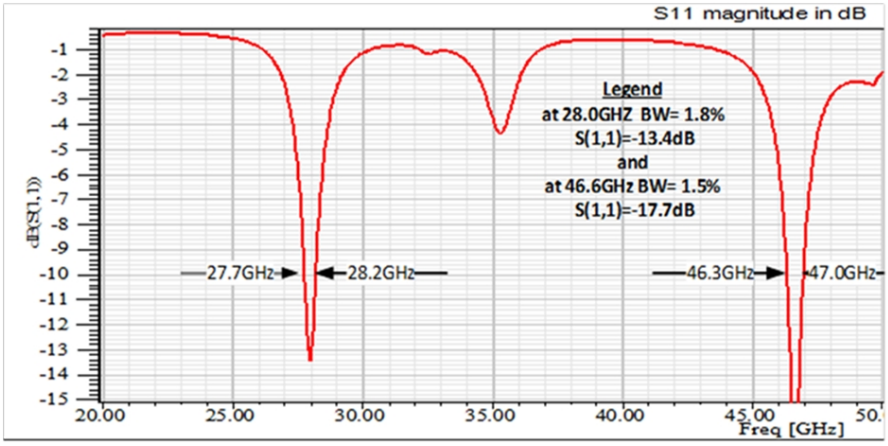

Figure 4.6: S_{11} result of genetically optimized patch antenna

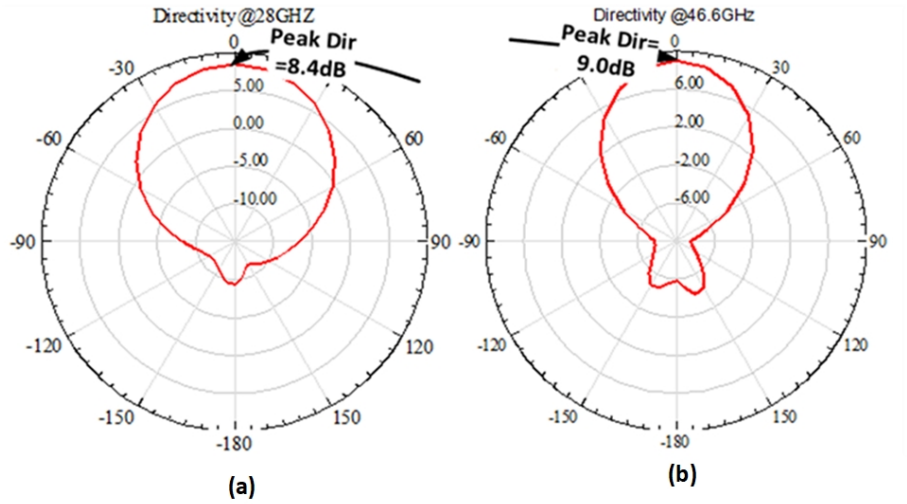

Figure 4.7: Directivity of genetically optimized patch antenna (a) at 28.0 GHz and (b) directivity at 46.6 GHz

4.2.2 Employing Circular Cells

Antenna Modeling

The dimension of the radiating patch is L_{xp}=3.36 mm and W_{yp}= 5.26 mm where the patch is made of thin copper having thickness of 0.00032 $\lambda \ll \lambda$ (λ is free space wavelength at 28 GHz) located on the top side of a thin non-conducting substrate with the size of $\lambda \times \lambda$. In the proposed design, the Roger RT/duriod 5880 (tm) substrate with a dielectric constant of 2.2, a tangent loss of 0.0009, and a thickness of substrate is 0.3 mm was employed on a finite ground plane with the size of $L_{xg} \times W_{yg}$. The dimensions of the microstrip patch antenna shown in Figure 4.8, which is proposed for the genetic algorithm, are summarized in Table 4.3.

Table 4.3: Proposed antenna dimension summary

Parameter	L_{xp}	W_{yp}	h	L_{xg}	W_{yg}	L_{feed}	W_f
Dimensions(mm)	3.36	5.26	0.30	10.7	10.7	3.52	0.74

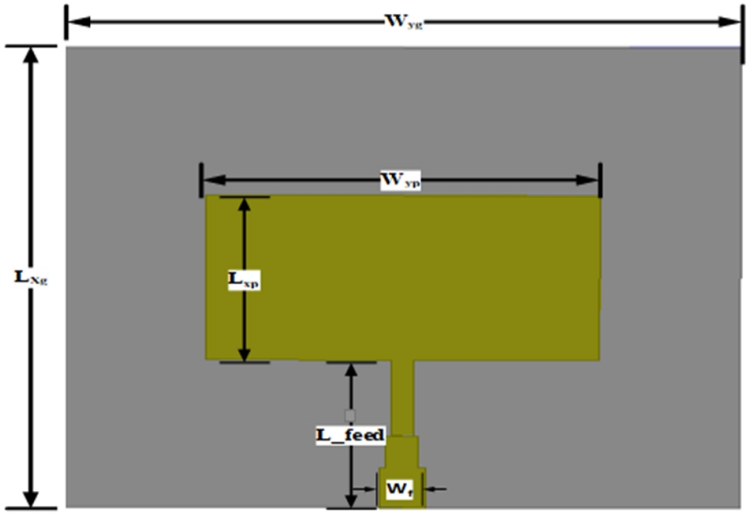

(a)

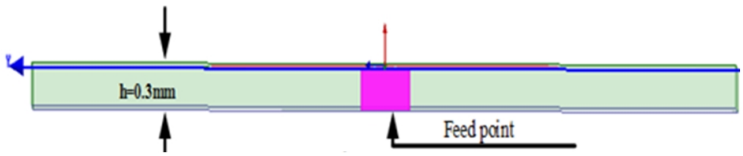

(b)

Figure 4.8: Reference patch antenna element operating at 28.0 GHz printed on a substrate (a) top view and (b) side view.

GA Optimization Setup

In order to optimize the patch geometry, an array 10 x 10 of random and non-uniform small circular cells is positioned on the patch surface as shown in Figure 4.9. The probability of the diameter of the cell to be 0.35 mm is 0.8 and 0.27mm is 0.2. This helps to create varieties of circular geometries on the patch surface. These cells are subtracted from the rectangular patch if and only if they are non-conducting. The conducting and non-conducting cell is defined by a binary coding algorithm as discussed in chapter three of this dissertation. According to the GA principle, the initial generation is generated at random, and the subsequent generations are reproduced in this research work by using tournament selection, single-point crossover, and random single-bit operation. In this dissertation, binary '0' represents the patch's non-conductive surface, and binary '1' represents the conducting cells, which exist in both random and reproduced individuals. Thus in this research task, the fitness function is defined to maximize the directivity D (f) and negative of reflection coefficient S_{11} (f) in the two bands (27.5 GHz-29.5 GHz

and 31 GHz-31.5 GHz) of frequencies.

$$Fitness\ function = \sum_{f} [D\,(f) - \ \ S_{11}(f) \tag{4.3}$$

$$S_{11}\,(f) = \begin{cases} S_{11}, & if\ S_{11} > -10\ \text{dB} \\ -10\ \text{dB}, & if \quad S_{11} \leq -10\ \text{dB} \end{cases}$$

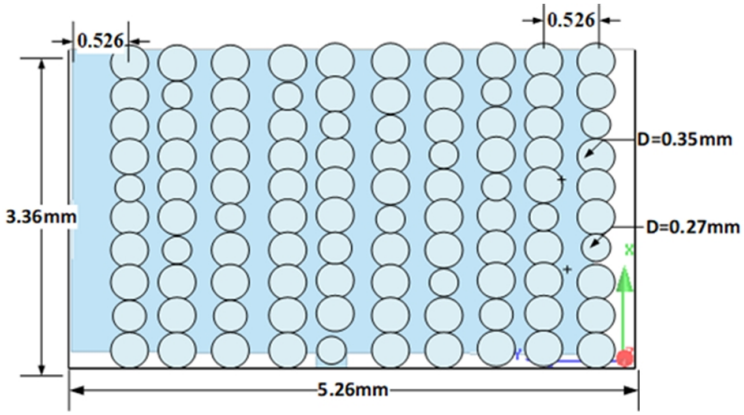

Figure 4.9: Placement of 100 circular cells on rectangular patch surface

The population size clustered as a generation is set to 20 individuals and each individual is represented by 100 genes. A single point crossover with a 70 % probability and a 0.02 mutate rate has been used to create a diversity of the population in each generation. The tournament selection mechanism has been applied to select individual parents that are fit to reproduce offspring for the next new generation. The simulation is carried out until 150 generations. The simulation convergences after 130 iterations as shown in Figure 4.10 and the best-fit individual is shown in Figure 4.11.

Results and discussion

The proposed genetically engineered patch antenna shown in Figure 4.11 was simulated using HFSS. The result proves that the directivity of the antenna was improved and it resonates at two frequencies. As Figure 4.12 illustrates the reflection coefficient of the reference antenna resonates at 28.0 GHz only with S_{11} =-17.9 dB whereas genetically optimized antenna resonates at two frequencies of 28.0 GHz and 31.1 GHz with BW=2.9 % and BW=1 % respectively. At both ranges of frequencies (27.6 - 28.4 GHz and 31.0 – 31.3 GHz); VSWR is less than 2. Furthermore, in Figure 4.13 directivity improvement in both operating bands was verified. A broadside direction directivity of 8.6 dB at 28.0 GHz, is demonstrated in Figure 4.13-a, and a directivity of 10.9 dB was verified at 31.1 GHz along broadside direction Figure 4.13-b.

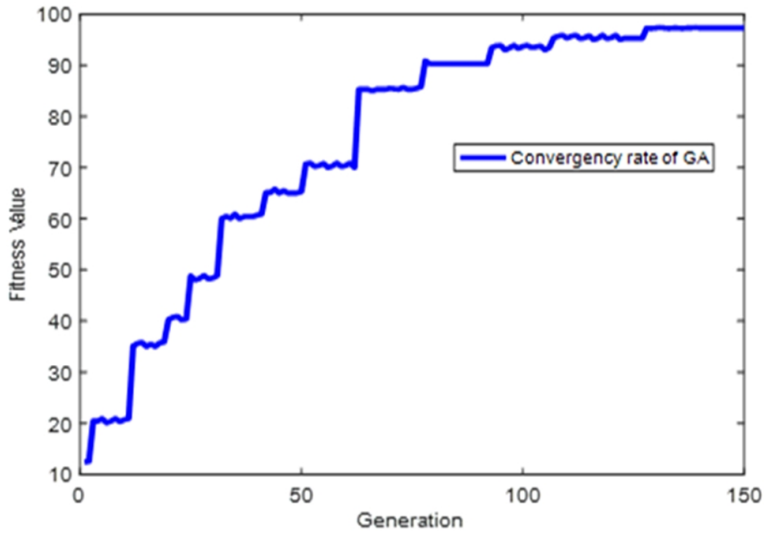

Figure 4.10: average fitness value of a generation vs number of generation

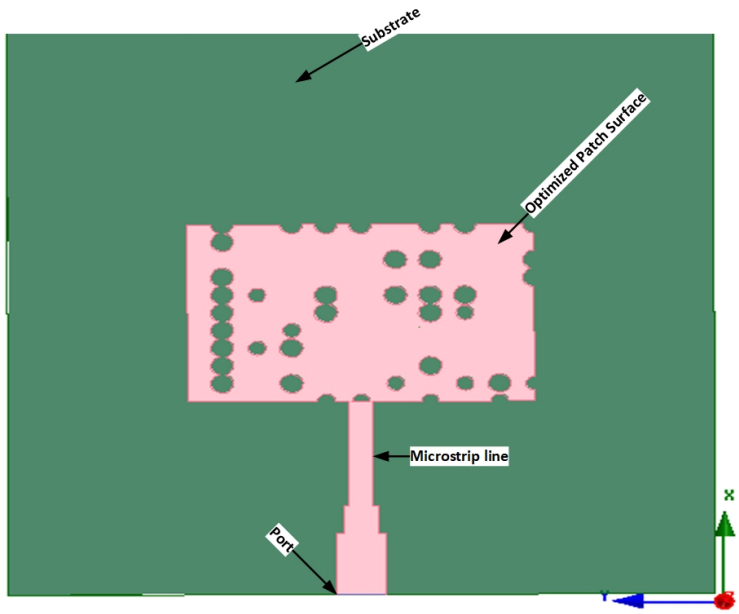

Figure 4.11: genetically optimized microstrip radiating patch geometry

The surface current distribution of the reference antenna at 28 GHz is presented in Figure 4.14-a. The surface current distributions of the genetically optimized antenna at 28 GHz and 31.1 GHz are shown in Figure 4.14-b and Figure 4.14-c, respectively.

4.2.3 Comparison with Related Works

The radiating patch area division in patch geometry optimization was portrayed in both random circular cells and smaller rectangular cells. The better directivity from circular cells is owing to the increased number of genes and generations used in optimization,

Table 4.4: Overall performance of genetically optimized proposed antenna

	Overall Size of antenna (mm3)	Resonant frequency	Bandwidth (%, S11<-10dB)	Directivity
Reference patch antenna	10.7x10.7x0.3	28.0 GHz	2.1%	6.8 dB
Genetically optimized patch antenna	10.7x10.7x0.3	28.0 GHz 31.1 GHz	2.9% 1%	8.6 dB 10.9 dB

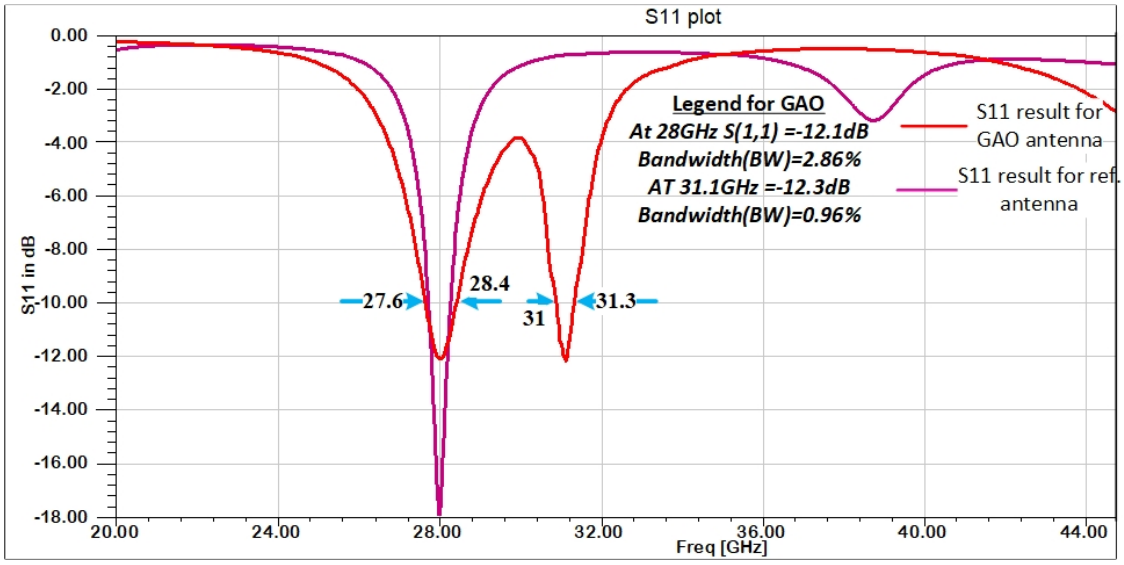

Figure 4.12: Simulated S11 of the GAO dual-band patch antenna resonates at 28.0 GHz and 31.1 GHz

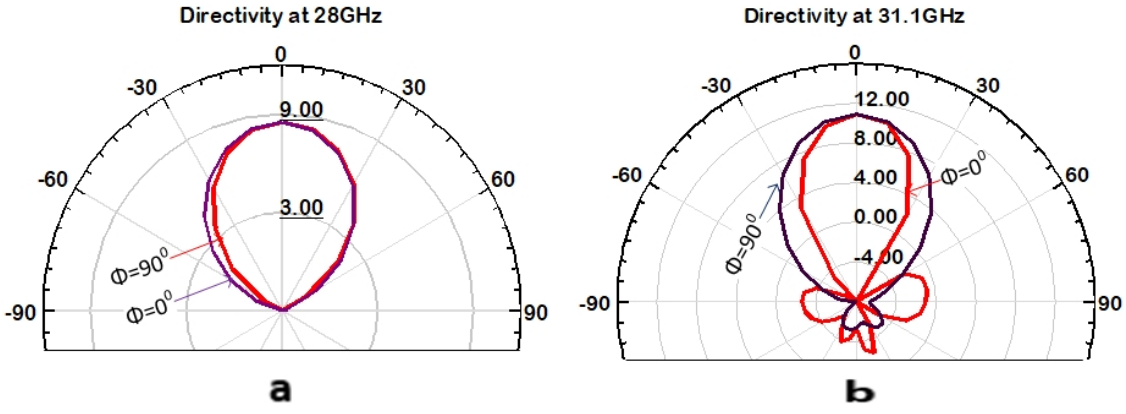

Figure 4.13: Directivity of genetically optimized patch antenna a) at 28.0 GHz b) at 31.1 GHz

although it required more computation time. However, as shown in Figure 4.9, the radiating patch is not entirely covered by the gene of the generation in the circular cell division method, so optimization cannot cover the whole patch area. In this sense,

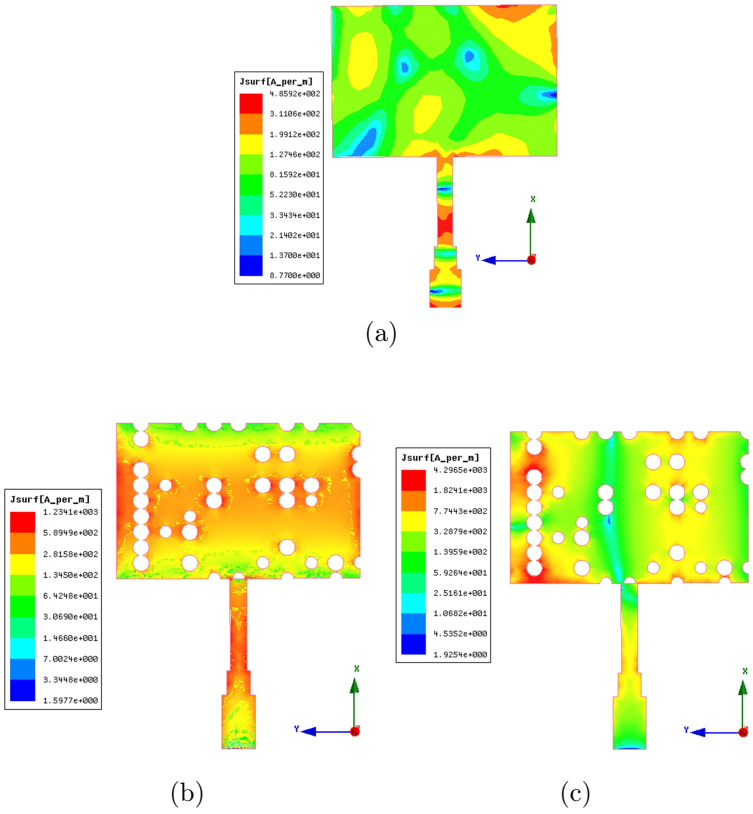

Figure 4.14: Surface Current distribution: a) reference antenna at 28 GHz, b) GAO antenna at 28 GHz, and c) GAO antenna at 31.1 GHz

rectangular cells are preferable for assessing the entire surface of the patch during genetic algorithm optimization.

Table 4.5 compares the directivity of the proposed dual-band antenna with relevant research in the literature. According to the fractal geometry techniques used, the peak directivity is 7.09 dB with a double superstrate from a single antenna element. The suggested antennas in this dissertation, on the other hand, attained a peak directivity (1.4-3.9 dB) greater than the peak in [192]. The 8 patch element array obtained in [196] likewise had less directivity than the works presented in this dissertation.

Table 4.5: Comparison of proposed works with related simulated results

Papers	Employed method	Area of patch ($\lambda 2$)	Dual-Resonance freq. (GHZ)	Directivity (dB)	Bandwidth (MHz)	Remark and (Drawback)
[192]	Fractal geometry	0.39 x 0.51	10.89 15.92	7.09 6.56	0.67 1.07	Double substrate
[191]	Slot antenna method	0.72 x 0.72	27.3 39.75	5.42 6.25	- -	Complex structure
[194]	Frequency selective surface	0.59 x 0.59	28 39	5.68 6.93	0.8 0.8	FSS adds size
[197]	Zero-index metamaterial	1.2 x 0.9	2.4 3.5	2.8 3.8	- -	Superstrate adds size
[196]	Patch array	3.73 x 1.47	29.5 38	8.4 9.3	1.32 1.36	8-element array
This work-1	Rectangular cell GA	0.33 x 0.47	28.0 46.6	8.4 9.0	0.5 0.7	GAO
This work-2	Circular cell GA	0.31 x 0.49	28.0 31.1	8.6 10.9	0.8 0.3	GAO

4.3 Dual-band Antenna with Enhanced Bandwidth

Large bandwidth antennas are necessary for dense users to connect at once in wireless communication and achieve a high data rate. To overcome mm-wave propagation obstacles and satisfy the needs of wireless communication, it is essential to consider dual-band antennas with strong bandwidth and directivity capabilities. In the literature, many ways for advancing a patch antenna for bandwidth enhancement of dual-band operation were published. A dual-band U-shaped slotted microstrip patch antenna that resonates at 28 GHz and 38 GHz with bandwidth improvement is presented [131]. Dual-band antenna is also modeled using varieties of optimization algorithms such as auto-context broad learning system [200], deep Gaussian process model [201], and genetic algorithm [202]. In reference [203] the author presented a dual-band single antenna using a band switching mechanism and the antenna resonates at 27.5 GHz and 39 GHz. A slot patch antenna was presented for dual-band service at 28 GHz and 38 GHz [204]. In [142], a dual-band optimization of a patch antenna in microwave frequency using a genetic algorithm is described. This particular study proposes dual-band patch antenna optimization for the mm-wave frequency with enhanced antenna bandwidth using a binary-coded genetic algorithm.

4.3.1 Antenna Modeling

A rectangular microstrip patch antenna with a dielectric constant of 2.2, tangent loss of 0.0009, and thickness of 0.5 mm is proposed and designed on a 10x10mm^2 Roger RT/duriod 5880 (tm) substrate. The initial dimension of a reference model, a rectangular microstrip antenna was calculated using the standard formula presented in chapter two of this dissertation. However, the estimated dimensions do not have adequate antenna performance at a specified center frequency and band. Therefore, parametric analysis was used to determine the actual length and width of the radiating patch. Accordingly, the length of the patch was varied in the four stages from 5.2 to 5.8 mm, while the width of the patch was adjusted in 0.2 mm increments from 6.2 to 6.8 mm. When the antenna is desired to resonate at 39 GHz center frequency, the optimal length is 5.6 mm and the width is 6.6 mm. A 50-ohm microstrip feed line having a length of 2.6 mm and width of 0.75 mm is connected to the patch. The antenna's dimensions of the reference model are shown in Figure 4.15, which is ready for patch geometry optimization with a binary-coded genetic algorithm.

4.3.2 GA Optimization Setup

In order to optimize the patch geometry, the patch surface is segmented into 10 x 10 tiny random and uniform rectangular cells to optimize the patch shape, as illustrated in Figure 4.16. A binary coding scheme defines the cell's conducting and non-conducting features as presented in chapter three of this dissertation. The goal of this optimization is to look into improving the operating bandwidth with dual-band resonance. As a result, the fitness function is developed by increasing the sum of the operating bandwidth of the antenna and the sum of the negative reflection coefficient at theses operating bands. The purpose of maximizing the cost function is to provide bandwidth enhancement while maintaining appropriate radiation qualities, as illustrated in equation (4.4)-(4.7).

$$Fitness\ fucntion = \frac{1}{N}\sum_{i=1}^{N}(Bw_T - \ S_{11}(f_i)) \tag{4.4}$$

Where Bw_T is the total bandwidth of the antenna in GHz and $S_{11}(f_i)$ is the reflection coefficient of the antenna in dB.

$$Bw_T = Bw_1 + Bw_2 \tag{4.5}$$

$$Bw_1 = f_{\mathrm{H1}} - f_{\mathrm{L1}} \tag{4.6}$$

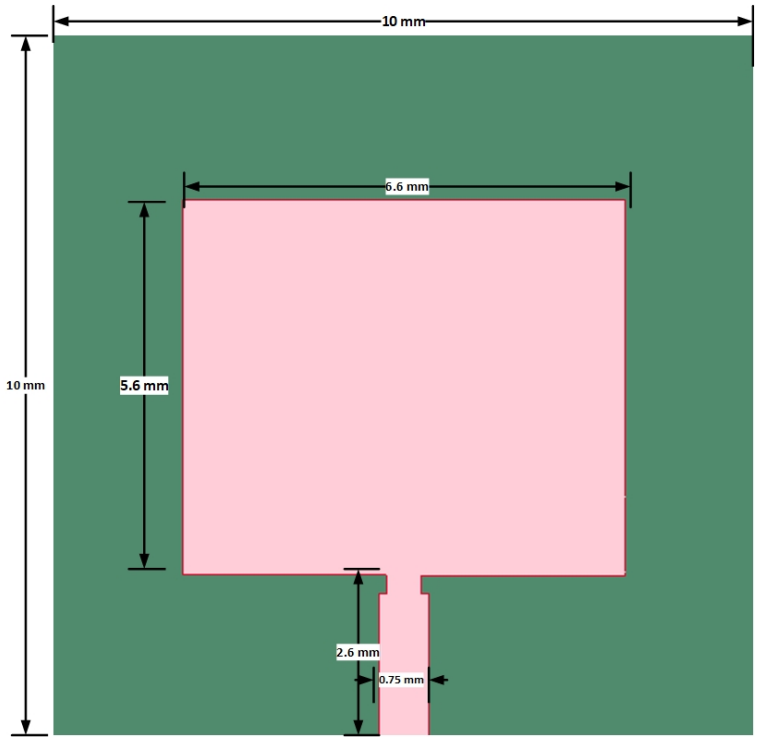

(a)

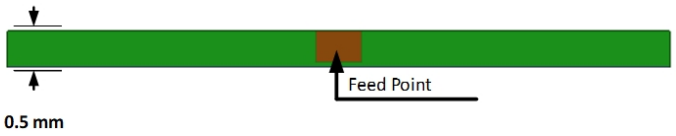

(b)

Figure 4.15: patch antenna element operating at 39.0GHz printed on a substrate (a) top view and (b) side view.

$$Bw_2 = f_{\mathrm{H2}} - f_{\mathrm{L2}} \tag{4.7}$$

$$Bw_T = \begin{cases} 5 \text{ GHz} & \text{if } Bw_T \geq 5 \text{ GHz} \\ Bw_T & \text{if } Bw_T \leq 5 \text{ GHz} \end{cases} \tag{4.8}$$

Where $S_{11}(f_i)$ is designed as.

$$S_{11}(f_i) = \begin{cases} S_{11}(f_i) & if \quad S_{11}(f_i) \geq -10 \text{ dB} \\ -10 \text{ dB} & if \quad S_{11}(f_i) \leq -10 \text{ dB} \end{cases} \tag{4.9}$$

where

N: the number of sample frequencies in the band, fi: the sample frequency at each 100MHz interval, $S_{11}(fi)$: the reflection coefficient of the antenna, Bw_T: total operating bandwidth of antenna, Bw_1 : bandwidth of antenna at the first operating band, Bw_2 : bandwidth of antenna at the second operating band, f_H1: higher operating frequency in a first band, f_H2: higher operating frequency in a second band, f_L1: Lower operating

frequency in a first band, f_L2: Lower operating frequency in a second band.

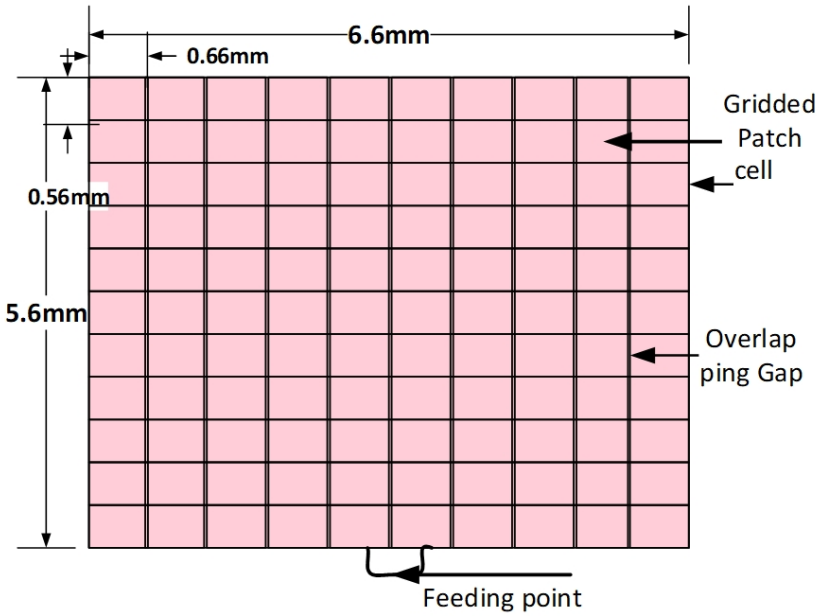

Figure 4.16: Placement of 100 rectangular cells on the patch surface

The genetic algorithm optimization setup has been arranged and summarized in Table 4.6.

The solution space has a capacity of $2^{100} = 1.3 \text{ x} 10^{30}$ individuals in it. If the computing

Table 4.6: Summary of optimization setup

No.	Parameter	Value
1	Population Size	30
2	Number of gene (represent an individual)	100
3	Number of Generation	125
4	Crossover Type	Single point
5	Crossover probability	0.7
6	Mutation	Single bit
7	Mutate rate	0.02

time of each individual design is 1 second, the overall computation time to find the best-fitting individual will be 1.2 x 10^{24} years. However, owing to applying the genetic algorithm, the best-fit individuals are picked in around 44.86 hours by utilizing a core I7, 8 GB RAM, and a 2.7 GHz processing speed computer. The simulation converged after

48 iterations as shown in Figure 4.17 and the iteration continued until 125 iterations to see the consistency of the convergence. Lastly, the best-fitted individual is presented in Figure 4.18.

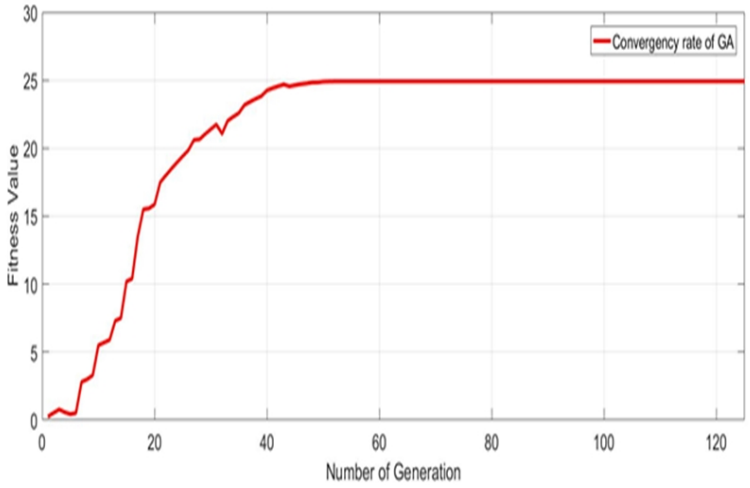

Figure 4.17: average fitness-value vs number of generation

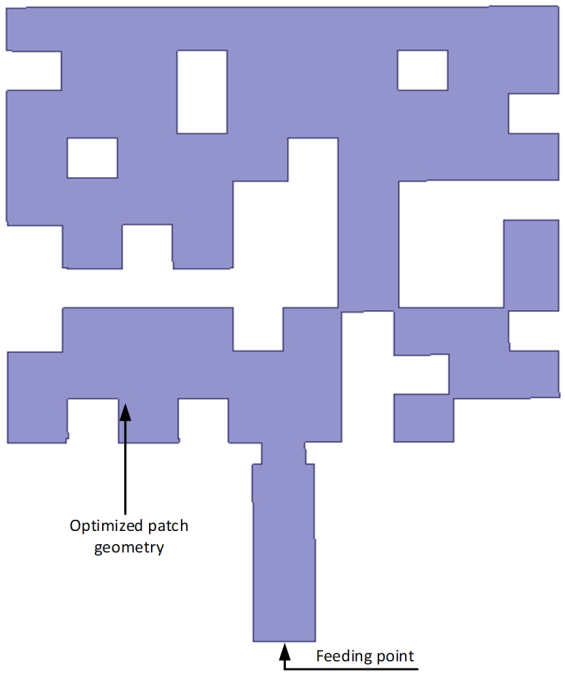

Figure 4.18: Genetically optimized radiating patch geometry (fittest individual candidate)

4.3.3 Results and Discussion

ANSYS HFSS was used to simulate the reference and the genetically modified antennas. The reference antenna resonated at a 39 GHz single frequency band and had a covered impedance bandwidth of 1.2 GHz. The baseline antenna operates in a single band and has a covering impedance bandwidth of 1.2 GHz at 39 GHz. The reference model's peak S_{11} value at 39 GHz is -17.6 dB, where the antenna's greatest actual gain is 5.4 dB. The suggested genetically engineered antenna, nevertheless, operates at two separate frequencies: 39.1 GHz and 50.2 GHz. The outcomes demonstrated that the antenna's bandwidth has increased in both bands. The antenna's directivity and gain are also sufficient for mm-wave wireless applications. The antenna resonates at 39.1 GHz and 50.2 GHz, as shown in Figure 4.19, with a peak value of return loss S_{11} =-12.6 dB and $S_{11} = -26.0dB$, respectively. When $S_{11} < -10dB$ is taken into account, bandwidth improvement in the two resonant bands is visible. At 39.1 GHz center frequency, the antenna has a fractional bandwidth of 4.1 % or 1.6 GHz and 6.6 % or 3.3 GHz at 50.2 GHz. VSWR is less than 2 in both operational bands (38.5 GHz – 40.1 GHz) and (49.0 GHz - 52.3 GHz).

Furthermore, directivity enhancement in both working bands was seen in Figure 4.20.

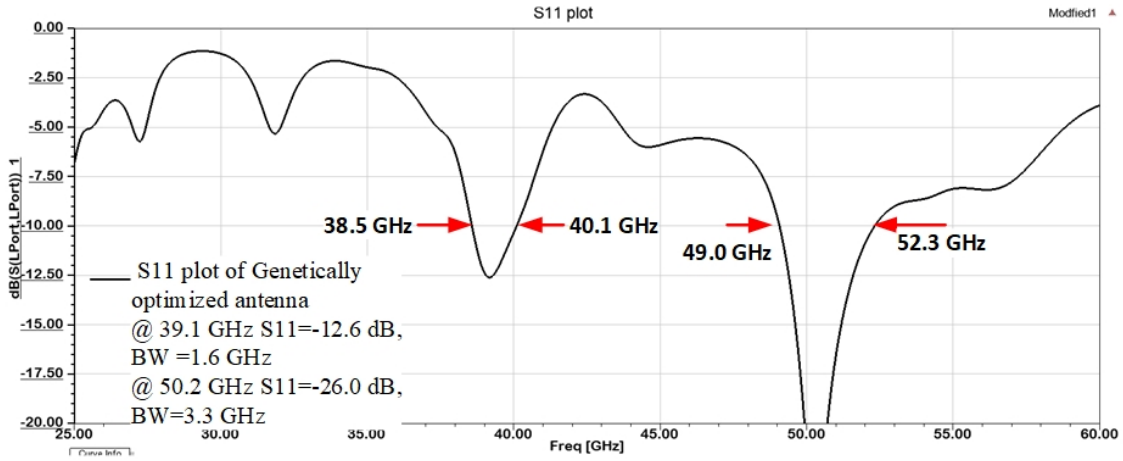

Figure 4.19: Simulated S_{11} of the GAO dual-band patch antenna resonates at 39.1 GHz and 50.2 GHz

At 39.1 GHz, broadside direction peak directivity was 7.9 dB, while at 50.2 GHz, directivity was 7.4 dB.

The 3D gain plot of antenna is presented in Figure 4.21 at two operating frequencies. At 39.1 GHz, the max gain of the optimized antenna is 7.6 dB, and 7.3 dB at 50.2 GHz. The radiation pattern of the antenna is projected in broadside direction in both frequency bands as plotted in Figure 4.22. The pattern plot includes both the E-plane and the H-plane.

The antenna has an overall efficiency of 89.3% at 39.1 GHz and 98.8% at 50.2 GHz as

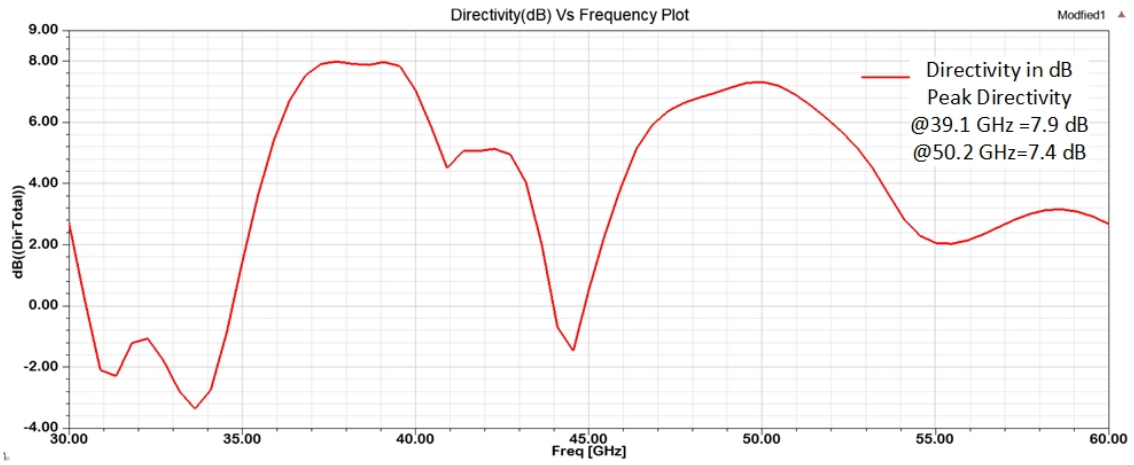

Figure 4.20: Directivity versus frequency plot of genetically optimized antenna ϕ='90^0' and θ='0^0'

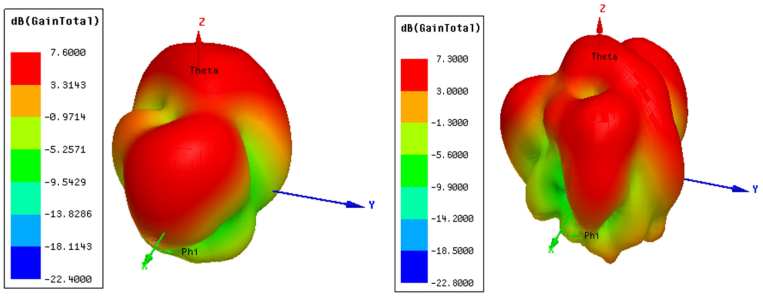

(a) (b)

Figure 4.21: 3D gain plot of the optimized antenna (a) at 39.1 GHz and (b) at 50.2 GHz

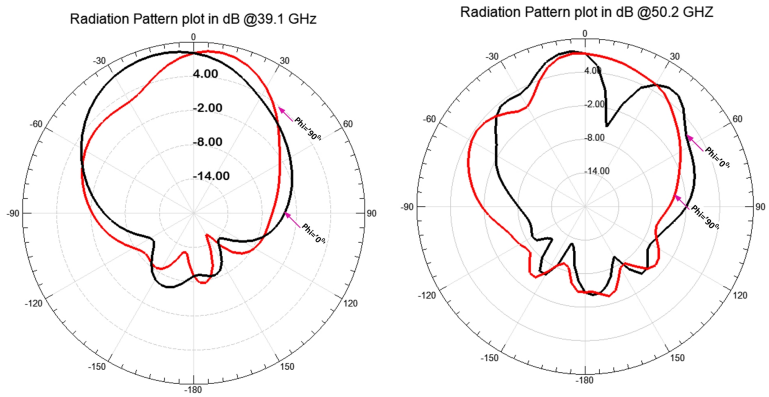

(a) (b)

Figure 4.22: E-plane and H-plane 2D radiation pattern cut of the optimized antenna (a) at 39.1 GHz and (b) at 50.2 GHz

presented in Figure 4.23.

As indicated in Table 4.7, the antenna performance parameter was compared to several relevant works. The band switching approach in [203] is used to acquire a comparable bandwidth. The antenna's bandwidth, on the other hand, is examined when S_{11}<-6 dB

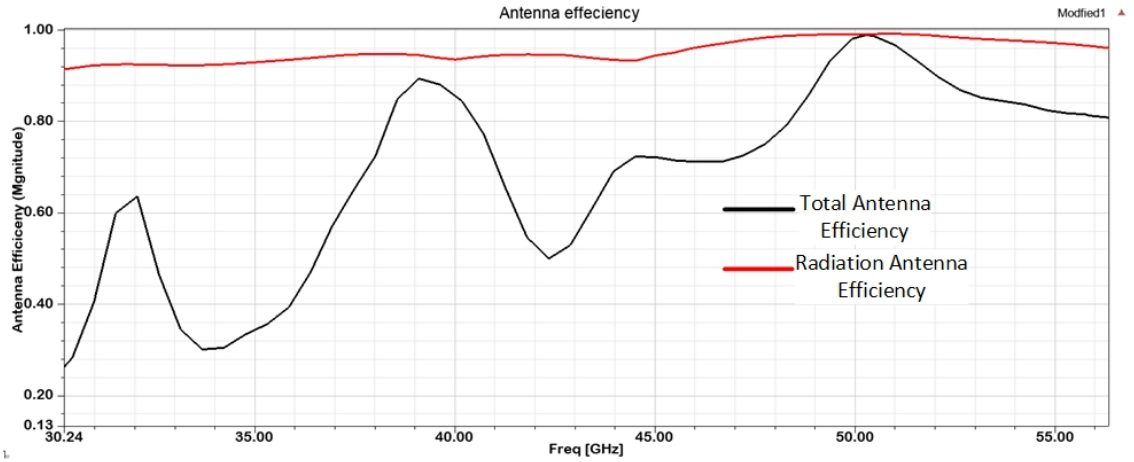

Figure 4.23: total and radiation efficiency of engineered antenna

at the same time the antenna has poor directivity in comparison to this study. Additionally, this study achieves a gain of 7.6 dB, which is 2.5 dB greater than the maximum gain reported in the literature. When compared to previous relevant studies, the originality of this work can be seen in the bandwidth improvement, gain enhancement, and directivity improvement of a single antenna with dual-band frequency operation by employing a binary-coded genetic algorithm optimization. Where the antenna performance parameters were compared this reveals the uniqueness of this work. It also demonstrates that the antenna is adequate for mm-wave wireless communication.

Table 4.7: Performance comparison of this work and related works

Paper	Patch area (λ^2)	Reson. freq.(GHz)	Bandwidth (S_{11}<-10dB)	Directivity(dB)	Gain (dB)	Employed Techniques
[131]	0.74x0.79	28 38	0.3 0.5	6.7 7.9	- -	U-shaped slot
[190]	0.26x0.14	28 60	0.4 3.1	- -	3.5 4.6	Bow-tie array
[205] *	0.56x0.56	28 45	1.3 1.0	7.6 7.2	- -	Elliptical slot
[203]	0.38x0.44	27.5 39	**1.9**** **3.29**	0.56 5.77		Band switch
[204]	0.93x0.93	28 38	1 3	- -	4.73 5.13	Slot method
This work	0.73x0.86	39.1 50.2	1.6 3.3	7.9 7.3	7.6 7.1	Genetic Algorithm

** Bandwidth is measured when s_{11} <-6dB is considered

* Results are based on prototype measurements

The current distribution on the surface of the engineered antenna is presented in Figure 4.24 at 39.1 GHz and 50.2 GHz resonance bands. On the edges of cells and around the junction points between the feed line and the optimized patch, a greater degree of current dispersion is visible.

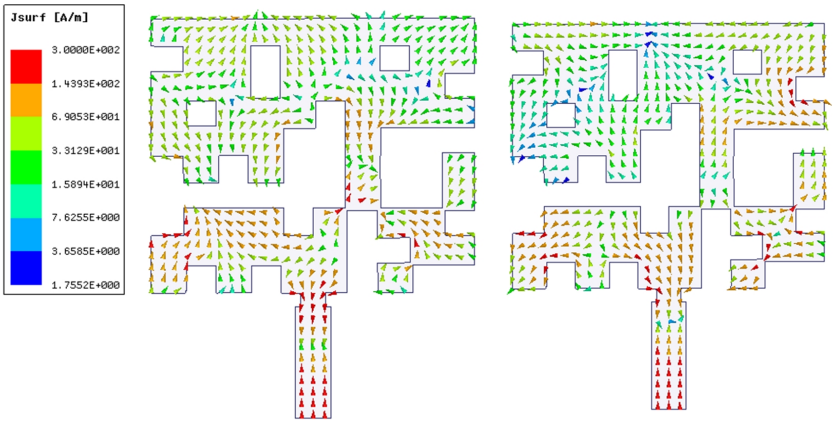

(a) (b)

Figure 4.24: Surface Current distribution of genetically optimized antenna (a) at 39.1 GHz and (b) 50.2 GHz

4.4 Chapter Summary

This chapter proposes three dual-band microstrip mm-wave antennas with enhanced directivity and bandwidth using a binary-coded genetic algorithm. The proposed genetically optimized antennas are simulated in HFSS and compared to the reference antennas, related works in literature, and each other. Fortunately, in this situation, the circular cell method performs better directivity than the rectangular cell distribution. However, the circular cells did not cover the entire surface of the patch (refer to Figure 4.9) for the whole execution.

Directive antennas are vital to solve some propagation challenges of mm-wave signals. At the same time, dual-band antennas for mm-wave applications are becoming a good glance for research due to the increasing demand for multi-functional services. This dissertation presents two microstrip antennas for dual-band services with improved directivity using genetic algorithm optimization. The results presented in this chapter explore that the optimized antennas are operated in two distinct bands. A proposed circular cells patch geometry optimization was used to improve the directivity to 8.6 dB and 10.9dB at 28.0 GHz and 31.1 GHz, respectively. The proposed rectangular cell patch antenna also resonates at 28.0 GHz with 8.4 dB directivity and 46.6 GHz with 9.0dB directivity. In

general, the genetic algorithm has been used successfully to improve the directivity of dual-band mm-wave microstrip patch antenna.

This chapter has also examined the usage of a genetic algorithm to boost bandwidth as well as the dual-band features of a microstrip antenna for mm-wave wireless communication. The antenna is optimized to resonate at 39.1 GHz and 50.2 GHz. At 39.1 GHz, the improved antenna obtained 1.6 GHz bandwidth and 7.6 dB gain, while at 50.2 GHz, the optimized antenna reached 3.3 GHz bandwidth and 7.4 dB gain. This study can also be compared to other relevant studies and the proposed mm-wave reference antenna. The antenna performs admirably in terms of bandwidth, gain, return loss, radiation pattern, and efficiency, making it a viable option for mm-wave wireless applications.

Having gained expertise with dual-band enhancements such as increased directivity and bandwidth, the following chapter will expand the work into various multi-band possibilities for a variety of mm-wave applications.

Chapter 5

Synthesis of Multi-band Microstrip Antenna with Improved Directivity and Bandwidth based on GA

5.1 Introduction

Recent advancements in wireless integrated technologies have made it possible to combine several distinct apps that operate on many channels into a single device. As a result, having multi-band antennas that can support many wireless signal protocols is turning into a crucial design need. Due to the demands and difficulties of 2G/3G/4G/5G coexistence, multi-band antennas have caught the attention of many operators for usage in their networks, and antenna firms are obliged to develop multi-band antennas to meet customers' needs.

Many studies in the literature were intended to enhance the antenna's multi-functionality and directivity while maintaining its bandwidth. Multi-stacking or multi-shorting pins, multi-feed, fractal-shaped, parasitic loading, and meta-material loading are only a few of the techniques [130, 131, 133]. These methods are complicated and complex to build, ineffective, and difficult to install for portable devices. Therefore, finding a suitable multi-band approach for numerous operating devices remains a vital research area, especially in mm-wave wireless communication.

This chapter discusses three unique multi-band antennas developed using binary-coded genetic algorithms. The directivity of a tri-band antenna was increased, and the bandwidth augmentation quad-band antenna was examined. The penta-band antenna is intended for wearable applications with increased bandwidth, and it has been tested on a variety of substrates. The chapter covers reference antenna design specifications, optimization procedures, simulated results, and descriptions of genetically altered antennas. A comparison of the proposed works with relevant works in the literature has been given for each individual proposed antenna.

5.2 Tri-band Antenna with Directivity Improvement

The optimization and synthesis of a tri-band antenna by employing a binary-coded genetic algorithm will be explained in this section. A tri-band antenna, which uses a single antenna to operate at three different frequencies, has several applications. These include satellite, military, maritime, mobile communication, sensing, and imaging applications. However, it is challenging to achieve high-performance and low-profile triple-band antennas using conventional designing techniques. Thus it is necessary to investigate a revolutionary methodology beyond the usual antenna designing mechanism. Innumerable mechanisms have been reported in the literature to develop tri-band mm-wave microstrip patch antennas. Particle swarm optimization was used to obtain ideal patch size and slot positions on the patch surface, resulting in triple frequency resonance [156, 206]. To achieve tri-band operation, genetic algorithm optimization was also implemented by different approaches [139], [183], [207]. Alternative techniques such as slot, slit, or a loading stub on one of the patch antenna structures viz. radiating patch, substrate, or ground plane were employed to enhance tri-band functionalities of antenna [129,136,140]. Specifically, this research focuses on mm-wave wireless communications. The signals in this spectrum are agonizing atmospheric fascination and high path loss, thus the outline of the mm-wave antenna with additional high directivity concerns to minimize the impact of them [137]. The majority of studies related to directivity improvement of microstrip patch antenna are linked to patch arrays [208, 209]. However, the antenna's performance is hampered by the intricate array feeding network, the antenna size, and mutual coupling. As a result, researchers suggested a variety of methodologies and optimization strategies for improving antenna directivity and expanding triple functionality while avoiding the convoluted feeding network [141, 190, 210]. In order to avoid an array of antennas, numerous methods to improve the directivity of multiband microstrip antennas can be found in the literature, such as frequency selective surface (FSS) [96, 97], fractal inspired antennas [74, 211], and zero-index metamaterial [102] are all increasing the complexity and size of antenna. The better approach this literature has got is a genetic algorithm optimization technique [150], [212]. The proposed tri-band antenna has been synthesized to resonate at the center frequencies of mm-wave wireless applications at 28 GHz, 40 GHz, and 47 GHz with directivity improvement. The design and optimization procedures are described in the following subsequent sections.

5.2.1 Antenna Modeling

In this particular study, a rectangular patch microstrip antenna with microstrip line feeding has been considered. In the reference antenna design, the finite ground plane is made of copper having a dimension of L_s x W_s was employed. The selected substrate

material is FR4- epoxy with a thickness of 0.6 mm, dielectric constant of 4.4, and loss tangent of 0.02 in the size of the ground plane due to its availability and affordability. The research has been started with a conventional microstrip patch antenna design which resonates at a center frequency of 28 GHz. The maiden sub-optimal dimensions of the microstrip antenna were computed using the governing standard design formulae presented in chapter two. A proportional modification has been done on dimensions to obtain an adequate antenna performance at a proposed center frequency using parametric analysis. The analysis was carried out to determine reference antennas' optimal dimension by a possible decrease of reflection coefficient at the resonating frequency (28 GHz). The engagement of a specific antenna variable is investigated at a time, while all other parameters are maintained at sub-optimal values in the computation. The length of the patch dimension was varied from 3.8 mm to 4.6 mm in five stages, while the width of the patch was varied from 6.2 mm to 7.0 mm with a 0.2 mm gap to get the ideal value of 4.4 mm length (L_p) and 6.6 mm width (W_p).

The rectangular patch antenna is fed by a characteristics impedance of 50 Ω microstrip line feeder with a total feed length of 3.3 mm and a width of 0.7 mm. The feed-line width is constructed in three segments for input impedance matching, and the starting width of the feeding line is 0.7 mm. Figure 5.1 shows the final model of a proposed reference rectangular microstrip patch antenna that is ready for patch shape optimization, and Table 5.1 summarizes the optimal dimensions of antenna parameters.

Since the aim of this research is to develop a tri-band patch antenna with enhanced

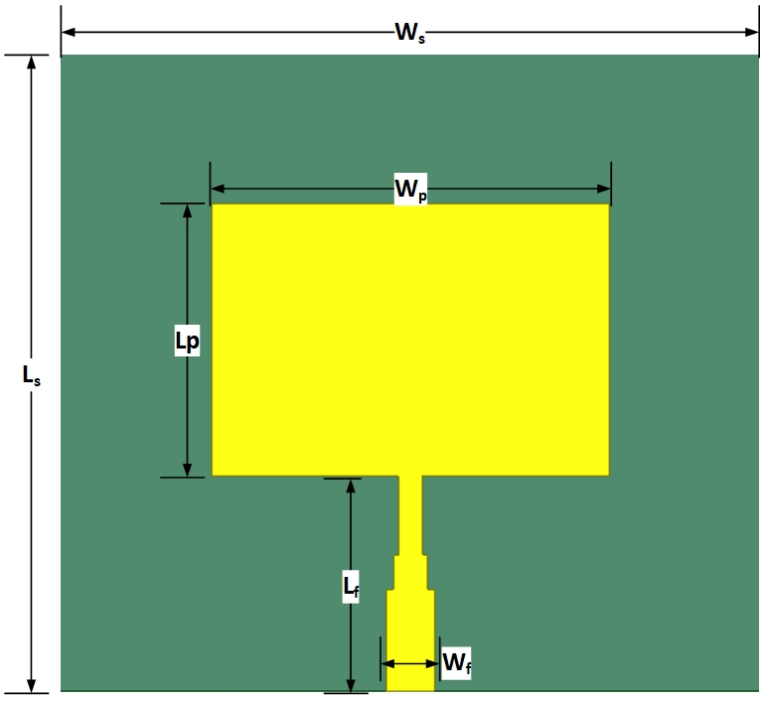

Figure 5.1: The front and perspective view of reference microstrip patch antenna on finite ground plane

Table 5.1: Summary of dimensions for the referenced antenna model

Parameter	substrate			Patch		Feed line	
	Length (L)	Width (W)	Thickness (h)	Length (L_p)	Width (W_p)	Length (L_f)	Width (W_f)
Value (mm)	8.2	10.2	0.6	4.4	6.6	3.3	0.7

directivity, genetic algorithm optimization is applied on the patch surface in order to create various current paths that will assist the antenna in attaining multiple resonating mm-wave frequencies.

5.2.2 GA Optimization Setup

To perform a binary coded genetic algorithm optimization, the reference antenna's patch surface is partitioned into 10 x 10 uniform small rectangular cells. As indicated in Figure 5.2, each chromosome in the population is represented by 100 genes. The first generation was twisted at random, and subsequent generations are made up of more fit individuals depending on the cost function's scrutiny. In order to avoid infinitesimal points contacting each other at the corner of a cell as presented in Figure 5.2-a, overlapping was done by shifting cell dimensions as illustrated in Figure 5.2-b. The size of a rectangular cell is 0.44 mm x 0.66 mm and the overall pattern of the gridded patch surface is presented in Figure 5.2-c.

The main goals of this optimization are to improve the broadside directivity and achieve the best possible reflection coefficient of the antenna at three pre-defined frequencies. As a result, the fitness function is defined as increasing the negative sum of the reflection coefficient $S_{11}(f_i)$ and maximizing the directivity $D(f_i)$ over the desired frequency range, as presented in equation (5.1).

$$Fitness\ Function = \frac{1}{N}\sum_{j=1}^{M}\sum_{i=1}^{N}[D(f_i) - S_{11}(f_i)] \tag{5.1}$$

Where

N: total number of sampling points at each band,

M: Desired number of the operating band , in this case, three

f_i: the sampling frequency, the sampling period was taken as 100 MHz

$D(f_i)$: directivity of the antenna at sample frequency in dB

$S_{11}(f_i)$: reflection coefficient at sample frequency in dB

Taking $S_{11}(f_i)$ =-10 dB if its value is less than -10 dB avoids the narrow impedance

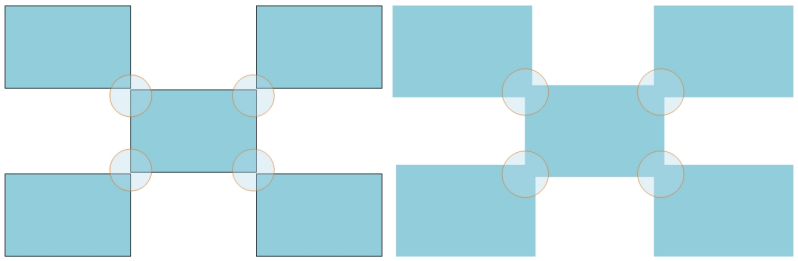

(a) (b)

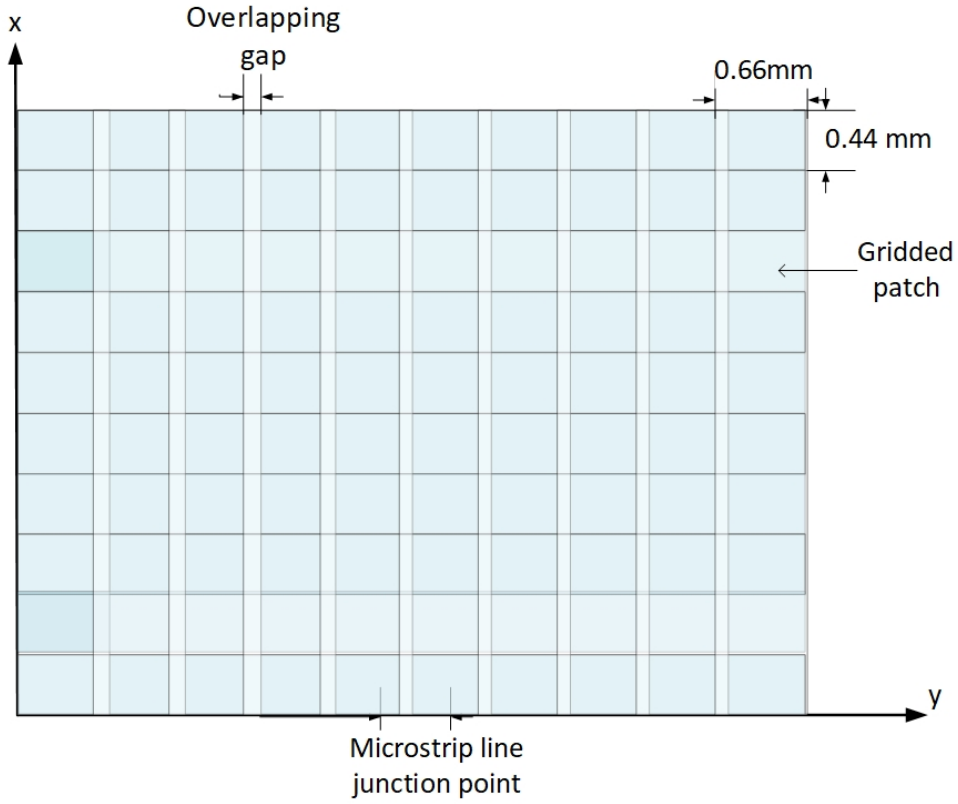

(c)

Figure 5.2: (a) Conventional building blocks with infinitesimal connections. (b) Proposed overlapping outline, (c) cell distribution on the patch surface

bandwidth at the center frequency.

$$S_{11}(f_i) = \begin{cases} S_{11}(f_i) & if \quad S_{11}(f_i) > -10 \text{ dB} \\ -10 \text{ dB} & if \quad S_{11}(f_i) \leq -10 \text{ dB} \end{cases} \tag{5.2}$$

This dissertation focuses on the objectives of the research work vs the algorithm's time of convergence while setting up optimization parameters in GA. When the algorithm utilizes a high number of generations, an extensive population, and chromosomal size, the exploration potential of GA in the solution space rises; nevertheless, it requires more computing time and resources. The summary of optimization parameters for this research task is presented in Table 5.2.

Table 5.2: Summary of genetic algorithm optimization setup

No.	Optimization parameter	Values	Remarks
1	Number of cell/genes in a chromosomes	100	10 X 10
2	population size	30	Individuals
3	Maximum number of generations	200	
4	Crossover type	Single point	
5	Probability of crossover	0.7	
6	Mutation	Single bit	
7	Mutation rate	0.2	
8	Selection Type	Tournament selection	

5.2.3 Results and Discussion

As previously highlighted, each patch geometry is represented by 100 genes, resulting in 2^{100}= 1.27 x 10^{30} potential solutions according to the binary coded genetic algorithm. Each individual candidate is modeled and simulated in HFSS with the finite element method. The individuals are run through a fast sweep computation from 25 GHz to 50 GHz with a 100 MHz sampling frequency and the far field radiation sphere setup of 0^0-360^0 for both θ and ϕ components in a 10^0 step size. If each simulation takes 1 second to compute, the total computing time to address the whole solution space is 4.02 x 10^{22} years. However, thanks to the genetic algorithm, it was able to search for the fittest individual from the solution space in 6.25 days using a Core-I7 computer with 8 GB RAM and a processor speed of 2.7 GHz.

On each iteration, the patch cell's (gene in a chromosome) 'on' and 'off' states were maintained. The algorithm evaluates the fitness function and runs its process indefinitely until a new radiating patch model meets the termination conditions. The algorithm's fitness value increases dynamically until convergence is obtained at the 160^{th} generation, as illustrated in Figure 5.3-a. The optimization procedure is carried out until the 200^{th} generation in order to demonstrate the consistency of the fitness value over the next 40 generations. Finally, after 200 generations, the best-fitting individual antenna is returned, as shown in Figure 5.3-b.

The simulated results of both the optimized and reference antennas are given and compared after optimization is completed. Figure 5.1 shows a reference rectangular microstrip patch antenna that was simulated and found to resonate at 28 GHz, resulting in a single frequency resonance with a 1.7 % bandwidth, as seen in Figure 5.4. The directivity of this antenna is 6.8 dB, which is adequate for a traditional rectangular

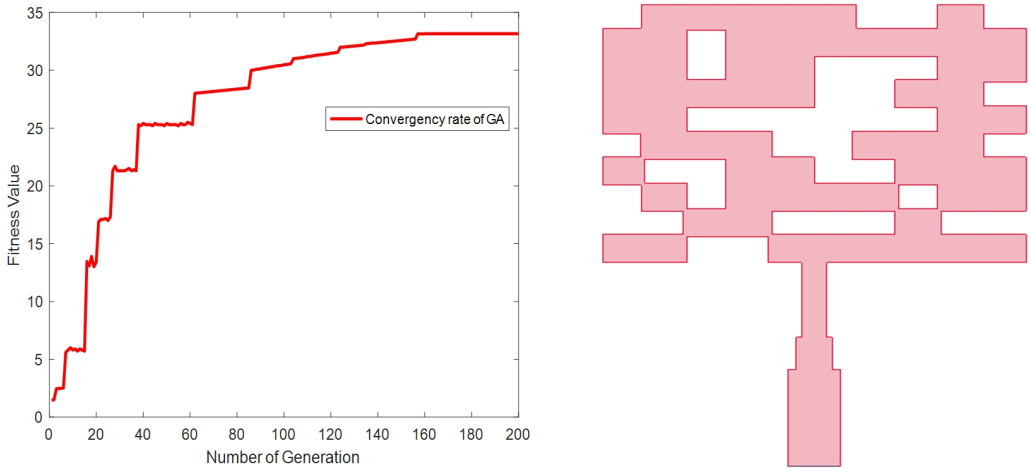

(a) (b)

Figure 5.3: (a) convergence rate of genetic algorithm and (b) The best fitted individual patch antenna structure

microstrip antenna. However, this is insufficient for mm-wave wireless communication. Therefore, optimization was applied to hoist directivity and tri-band operation.

The simulated results depicted that the genetically engineered antenna operates at three

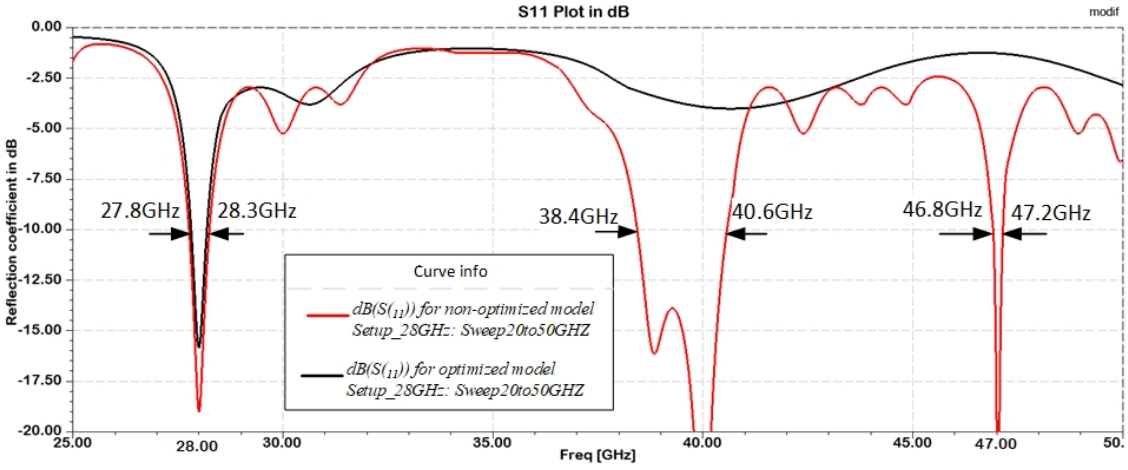

Figure 5.4: Simulated S11 results of both reference model and genetically optimized antenna

distinct frequency bands: 27.8 GHz-28.3 GHz, 38.4 GHz -40.6 GHz, and 46.8 GHz -47.2 GHz, as shown in Figure 5.4. The antenna resonates at a center frequency of 28 GHz with peak S_{11} value of -18.8 dB, at 40 GHz with peak S_{11} of -48.1 dB, and at 47 GHz with peak S_{11} of -26.89 dB. When considering $S_{11} \leq -10$dB, the bandwidth augmentation of the antenna has been visualized when compared to the reference model and previously stated antennas. It is delineated that the impedance bandwidth is realized 500 MHz at 28 GHz, 2.2 GHz at 40 GHz, and 400 MHz at 47 GHz. Table 5.3 shows that the proposed antenna outperformed the reference antennas in terms of reflection coefficient across all

operational bands. In working bands, the optimized antenna has a reflection coefficient that is roughly 1.23 - 3.14 times lower than the reference antenna. The lesser the value of the return loss, the better the outcome.

The input impedance should be close to 50 Ω according to the specifications of this

Table 5.3: Performance of the reference and optimized antennas

	Resonating frequency (GHz)	S_{11} (dB)	Bandwidth (MHz)	Fractional Bandwidth (%)	Directivity (dB)	Radiation Efficiency (%)
Reference antenna	28	-15.3	480	1.7	6.8	80.8
Genetically optimized antenna	28 40 47	-18.8 -48.1 -26.9	500 2200 400	1.8 5.5 0.85	7.7 12.1 8.2	73.1 71.6 75.2

optimizer. The input impedance of the genetically optimized antenna is 49.69 + j11.29 Ω, 50.23 + j0.41 Ω, and 48.5- j3.85 Ω at 28 GHz, 40 GHz, and 47 GHz, respectively. This shows how the antenna's input impedance matching level has improved. The conventional microstrip antenna in the reference model has an input impedance of 44.36-j14.29 Ω at 28 GHz resonant frequency. The antenna's impedance matching is enhanced to this level because the method is utilized to study a lower level of the reflection coefficient. Furthermore, the antenna's directivity is improved when compared to a conventional antenna. When the maximum peak directivity larger than 10 dB is considered, it is observed that the techniques presented in [129] provide a better directivity in the literature for a single antenna, however, this paper presents 12.15 dB using genetic optimization. As shown in Figure 5.5, which is the directivity versus frequency cut at $\phi = 90^0$ and $\theta = 0^0$, the optimized antenna has a peak broadside directivity of 7.7 dB at 28 GHz, 12.1 dB at 40 GHz, and 8.2 dB at 47 GHz. In an mm-wave multi- functional wireless network directivity improvement of the antenna is essential to resist the propagation attenuation in the link. In all three operational bands, the proposed antenna produced a broadside radiation pattern, as shown in Figure 5.6. The pattern in the figure was cut when $\phi = 90^0$ at three distinct resonant frequencies with all theta values. As a result, the optimized antenna has the upper hand in all three operating bands.

Figure 5.7 shows that a proposed tri-band antenna has a radiation efficiency of 62.2 % at 28 GHz, 45.1 % at 40 GHz, and 61.9 % at 47 GHz. However, radiation efficiency can be improved by employing low-loss dielectric material [212]. For instance, radiation efficiency is enhanced to 90.3 % at 28 GHz, 93.5 % at 40 GHz and 89.7 % at 47 GHz when $tan\delta = 0.002$ is considered. As a result of this, mm-wave antennas are not recommended to use lossy substrate material, as it highly hinders their efficiency.

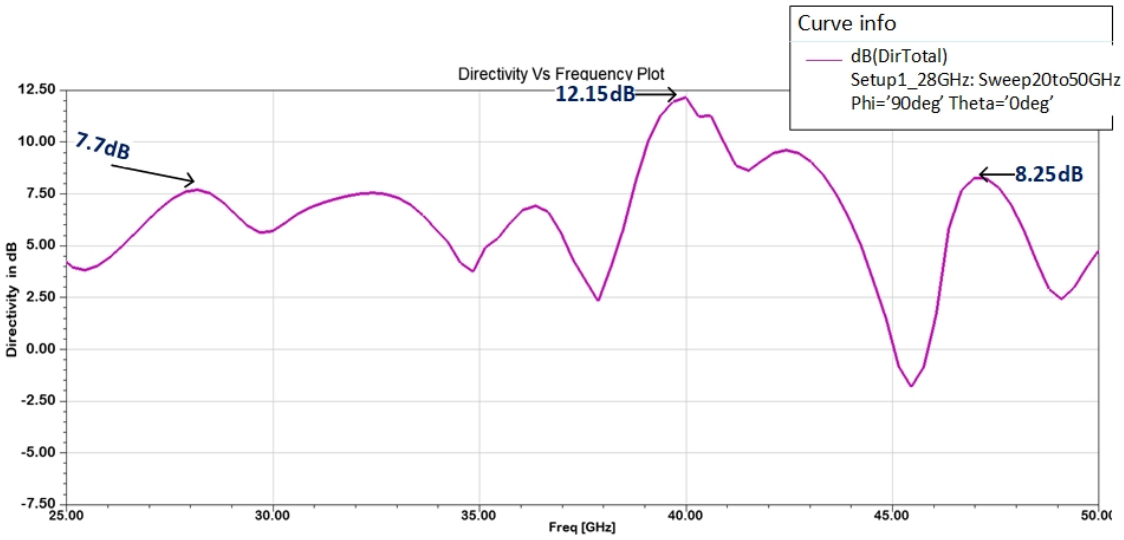

Figure 5.5: Directivity in dB Versus frequency plot at ϕ=90^0 and θ=0^0

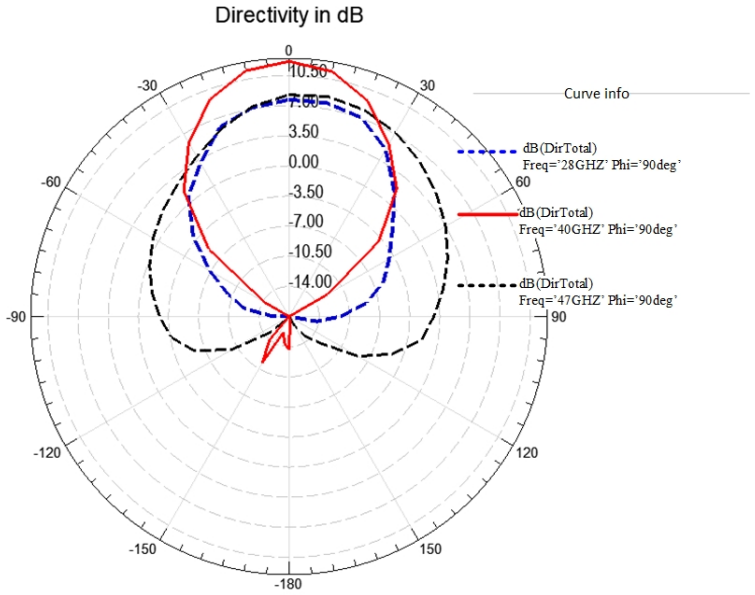

Figure 5.6: Polar plot of directivity in dB at three resonant frequencies when ϕ=90^0

The antenna also has a gain melioration of 5.6 dB, 8.7 dB, and 6.1 dB at 28 GHz, 40 GHz, and 47 GHz respectively. The realized gain of the genetically engineered antenna at each resonance frequency is presented in Figure 5.8 in the polar plot. As seen from the figure, the pattern has a comparable beam width for both $\phi = 0^0$ and $\phi = 90^0$. The pattern also reveals a null propagation at $\theta = 180^0$ for the two operational bands 28 GHz and 47 GHz. However, at 40 GHz when $\phi = 90^0$, a little back lobe appears. At 47 GHz, the antenna's wider beam width is detectable, but the narrow beam width is also visible at 40 GHz. From the far field radiation parameters, it can be seen that the genetically optimized antenna significantly outperforms the reference antenna in terms of the number of operation bands, directivity and gain.

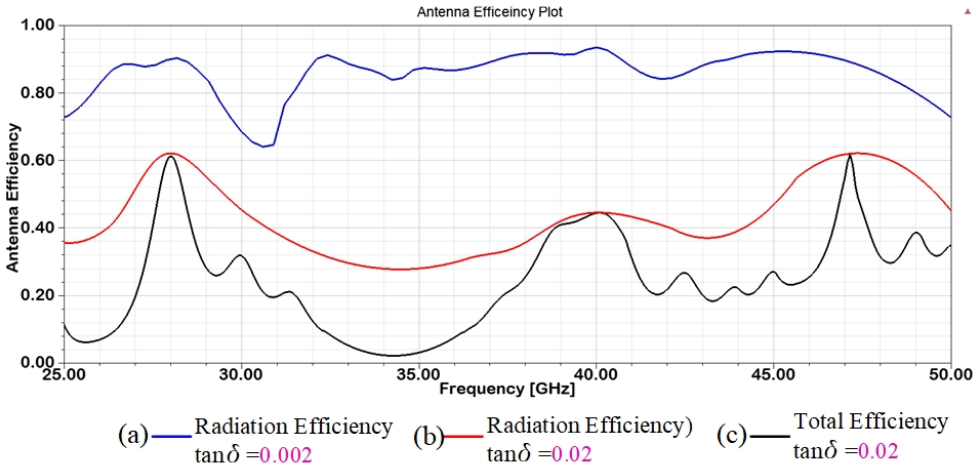

Figure 5.7: Optimized antenna total and radiation efficiency plot in different tangent loss.

The surface current distribution of the reference antenna and genetically engineered

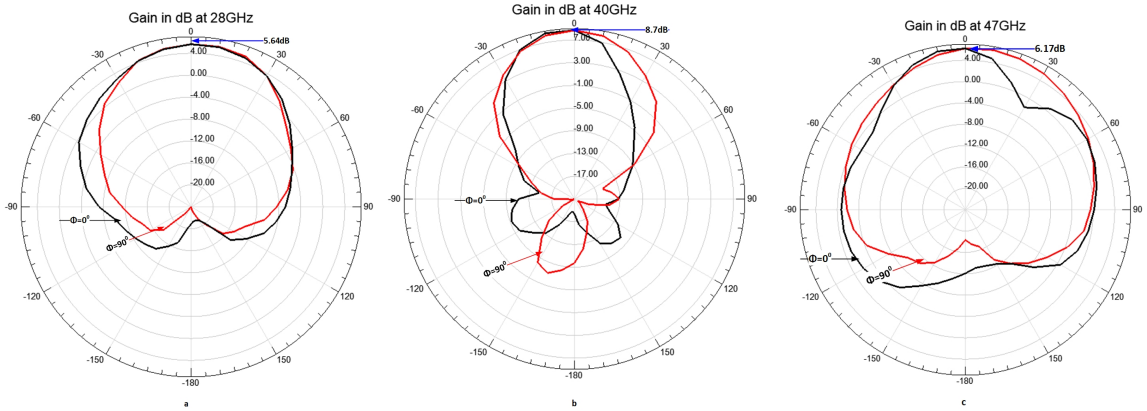

(a) at 28 GHz (b) at 40 GHz (c) at 47 GHz

Figure 5.8: Polar plot of gain in dB when $\phi = 0^0$ and $\phi = 90^0$

antenna at the intended frequency is presented in Figure 5.9. The engineered antenna operates in three frequency bands due to the availability of several current routes on the optimized patch shape. As the figure depicts the current distribution of the reference antenna at 28 GHz is greater closer to the microstrip line and patch edge. At 28 GHz, the edge of the cells on the left side of the optimized antenna has the highest current distribution, whereas, at 40 GHz, the edge of the cells on the right side has the highest current distribution. The current distribution is high on the center and right cells at 47 GHz.

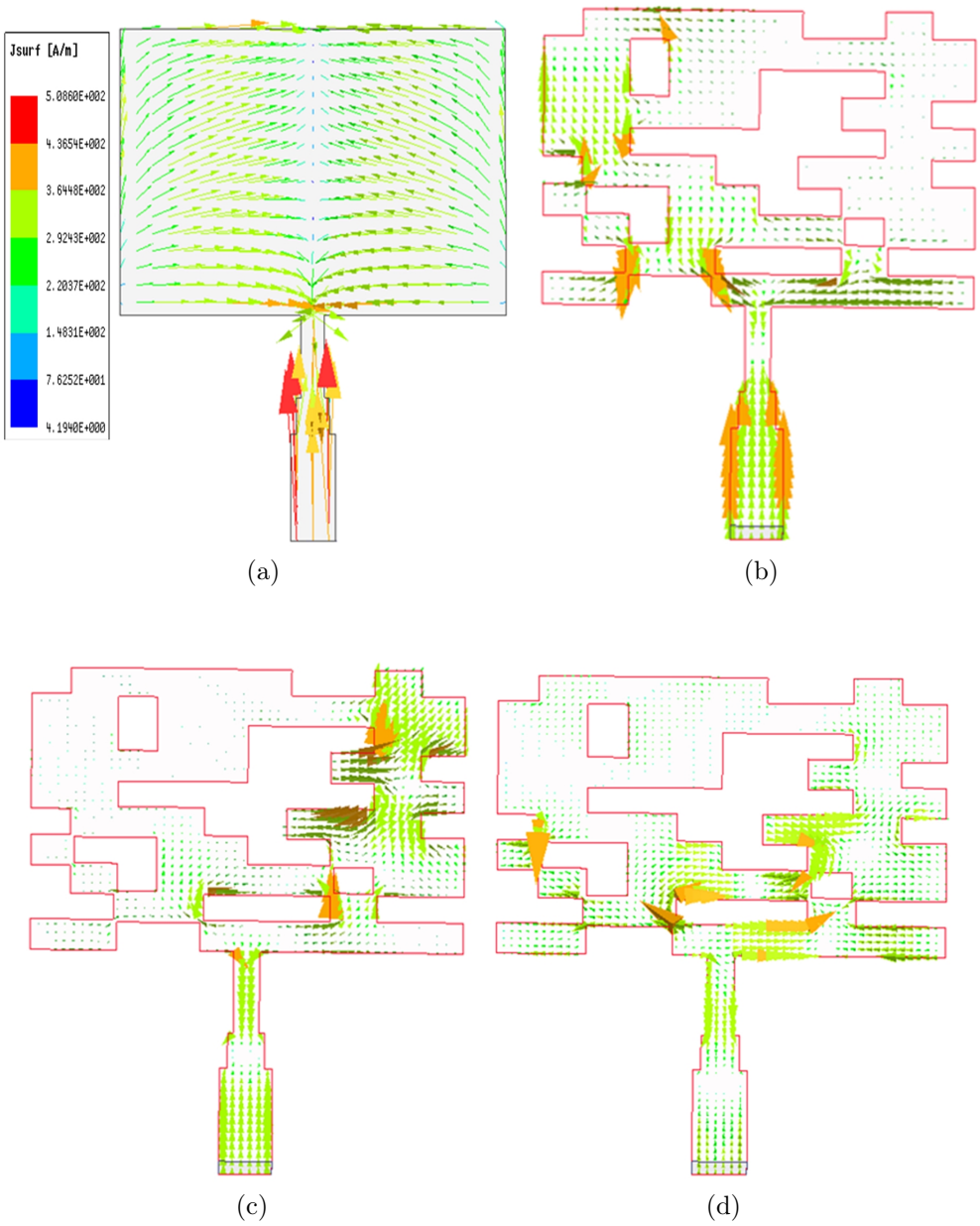

Figure 5.9: Surface current distribution of (a) reference antenna at 28GHZ and optimized antenna (b) at 28GHZ, (c) at 40GHz and (d) at 47GHz

5.2.4 Comparison with Related Works

The table below compares the findings of this study to those of other researchers in the literature (Table 5.4). As indicated in the table's remark section, these papers investigated a variety of techniques to increase antenna performance, while the antenna in this research utilizes a genetic algorithm. The proposed antenna is able to operate in three distinct bands and is compared to multiband related works. The comparison demonstrates that the proposed work outperforms the rest of the literature by more than 2 dB in directivity at 40 GHz resonance frequency. The survey also reports that the maximum

peak realized gain of a single antenna achieved by fractal shaped structure is 7.67 dB in the microwave frequency range while the gain of the proposed antenna is higher than nearly 1 dB in mm-wave frequency at one of the operating frequency. In addition, the antenna has a wide bandwidth in all three working bands when compared to others. The antenna's performance was realized by employing a binary-coded genetic algorithm for patch geometry optimization. To the best of my knowledge up until the completion of this dissertation report, no research has been conducted utilizing genetic algorithms to enhance the performance of microstrip antennas operating in the millimeter-wave frequency range.

Table 5.4: performance comparison of this work with other related works

Papers	Patch size in λ^2	Reson. freq. (GHz)	BW (GHZ)	Gain(dB)	Directivity(dB)	Remark
[129]	0.48x0.48	14.66 23.25 28.9	– – –	$5.44\|_{max}$	10.0 $\|_{max}$	Inset feed + rectangular slit,
[141]	1.1 x0.95	25.4 34.6 38	7.34 4.04 3.3	6.4 5.88 7.04	6.9 6.3 7.5	Semi-circular slot,
[130]	0.24x0.26	11.65 13.96 17	0.8 1.8 0.6	– – –	7.41 7.99 7.3	Slit position optimization
[156]	0.43x0.43	2.6 6 8.2	0.410 0.840 4.84	5.42 6.52 7.67		elliptical shape fractal geometry
[213]*	1.75x1.68	42 51.5 60	5 8.4 5.5	5.8 3.9 5.3		PSO
[214]	0.53x0.57	23.9 35.5 70.9	– – –	4.43 3.66 5.64	– – –	Inset feed Low gain and directivity
This work	0.41x0.61	28 40 47	1.8 5.5 0.85	5.64 8.7 6.17	7.7 12.15 8.25	Genetic algorithm

* The results are based on prototype measurement

5.3 Bandwidth Enhancement of Quad-band Antenna

It is easily observable that the dissertation has accomplished triple band operation in the preceding portion of this chapter. Let us now extend the study challenge to quad-band operation. As a result, it is critical to focus on antenna technology optimization to overcome propagation obstacles and enhance the quad-functionality, bandwidth, gain, and directivity of mm-wave antennas [131]. Low-profile quad-band antennas with high bandwidth, gain, and efficiency, in particular, can meet the requirements of current and next-generation wireless communication [215]. However, creating quad-band microstrip patch antennas is a difficult undertaking.

Numerous mechanisms in advancing a patch antenna for quad-band operation are published in the literature. Quad-band antenna for mobile communication was designed by a combination of three-quarter wavelength monopoles antenna resonates at 0.4 GHz, 0.9 GHz, 1.6 GHz, and 2.75 GHz [216]. A compact microstrip antenna with inverted T in combination with three L stubs resonated at 2.54/3.5/4.38/5.3 GHz quad-band frequencies is reported in [217]. A quad-band circularly polarized antenna was reported by combining ring and stubs on the patch and inserting an open-ended C-shaped gap in the ground surface [218]. A quad-band antenna which resonates at 1.78 GHz, 3.28 GHz, 4 GHz, and 4.3 GHz was configured by using a defected ground structure (DGS) inspired by meta-material [219]. A millimeter wave dielectric resonator antenna propagates at quad-band (28 GHz, 34 GHz, 38 GHz, and 42 GHz) with enhanced gain was proposed in [220]. In [221, 222], the authors introduced a four-port quad- band MIMO antenna that resonates at mm-wave frequencies (28 GHz, 43 GHz, 52 GHz, and 57 GHz). Three slanted strips and a square slot proximity feed were used to create a circularly polarized multi-band microstrip antenna for 5G applications that resonate at 28 GHz, 38 GHz, 60 GHz, and 73 GHz [223] and the use of a cross slot on the patch for multi-band operation was described in [224].

This particular study presents a quad-band patch antenna for mm-wave frequencies with improved impedance bandwidth with adequate gain and directivity using a binary-coded genetic algorithm. The method seeks the best-fitted antenna for diverse wireless applications based on the established anticipated operating center frequencies of 28.3 GHz, 38.1 GHz, 46.6 GHz, and 60.0 GHz. The reference and proposed antenna designs, the optimization process and settings, and the results of the proposed antenna will all be covered in this section. The paper also compares the proposed antenna to previous similar studies.

5.3.1 Antenna Modeling

A proposed microstrip patch antenna was designed on a 15 mm x 15 mm size RT/duriod-5880(tm) substrate. The substrate has a 2.2 dielectric constant, 0.0009 tangent loss, and

0.5 mm thickness. The initial dimension of the reference model was modeled based on the transmission line as presented in chapter two. However, the antenna with the estimated dimensions does not have sufficient antenna performance at the desired frequency bands. Therefore, a parametric study was used to fine-tune the dimension of the radiating patch. Accordingly, the patch's length was varied in four stages from 7.6 to 8.2 mm, while its width was adjusted in 0.2 mm increments from 9.2 to 9.8 mm. When the antenna resonates around 38 GHz, the optimal length is 0.73 λ and the width is 0.9λ. A 50 Ω microstrip feed line with dimensions of 3.4 mm x 0.9 mm is connected to the patch. The reference antenna model and its optimal size are presented in Figure 5.10. The reference antenna was used for patch geometry optimization with a binary-coded genetic algorithm.

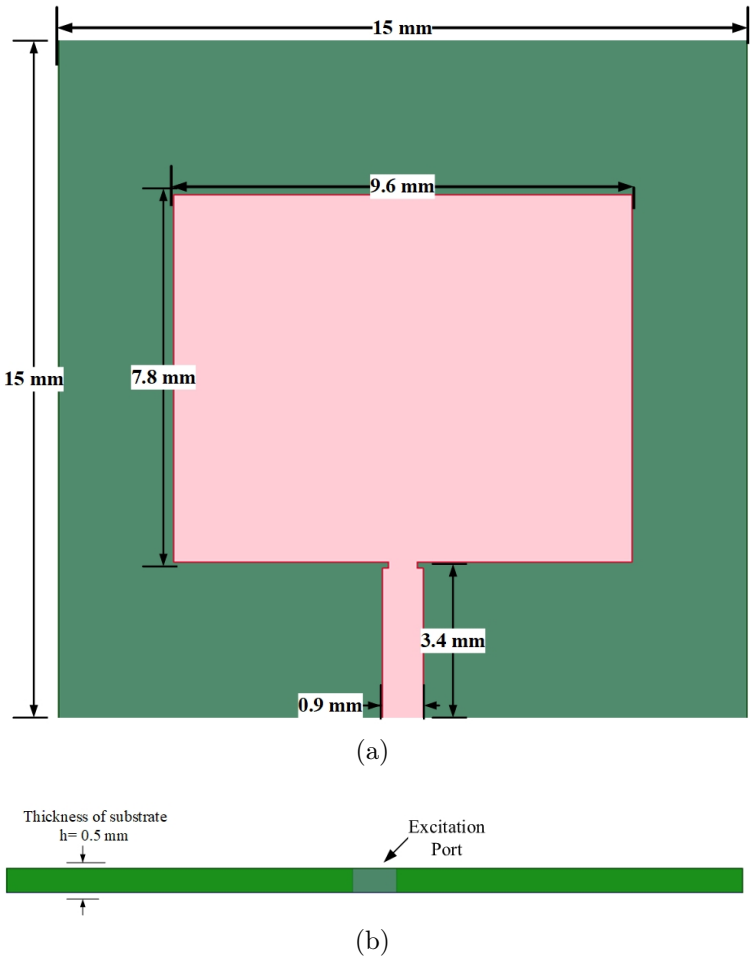

Figure 5.10: Reference patch antenna model on a substrate (h=0.5 mm,ϵr =2.2, tanδ= 0.0009) (a) top view, (b) side view.

5.3.2 GA Optimization Setup

The patch surface is segmented into 6 × 6 tiny random and uniform rectangular cells to optimize the patch shape, as illustrated in Figure 5.11. Table 5.5 organizes and

summarizes the genetic algorithm optimization setup.

The goal of this optimization is to look into the development of a quad-band resonance

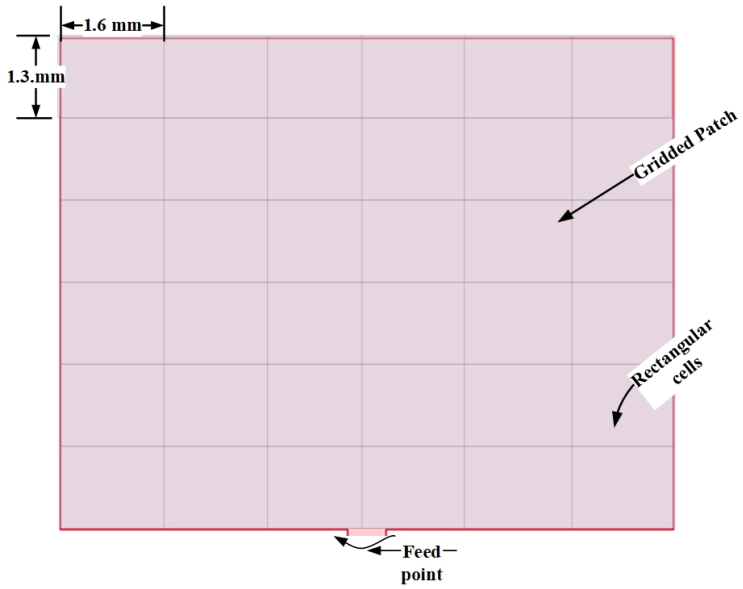

Figure 5.11: Divided patch surface in rectangular cells

Table 5.5: Optimization setup for genetic algorithm

No.	Parameters	Specified Values
1	population size	30
2	Genes in a chromosomes	36
3	Maximum number of generations	100
4	Type of crossover	Single-point
5	Crossover probability	0.8
6	Mutation	Single-bit
7	Rate of mutation	0.01
8	Selection method	Tournament

antenna. As a result, the fitness function is defined as increasing the negative reflection coefficient at four demanded frequencies.

$$Fittness\ Function = -\frac{1}{N}\sum_{i=1}^{N} S_{11}(f_i) \tag{5.3}$$

Where S_{11} (fi) is designed as.

$$S_{11}(f_i) = \begin{cases} S_{11}(f_i) & \text{if } S_{11}(f_i) \geq -10 \text{ dB} \\ -10 \text{ dB} & \text{if } S_{11}(f_i) \leq -10 \text{ dB} \end{cases} \tag{5.4}$$

Where

f_i: the sample frequency at each 100MHz interval

S_{11} (f_i): the reflection coefficient of the antenna

N: number of sample frequencies in each band

5.3.3 Results and Discussion

The simulation converged after 40 iterations, as shown in Figure 5.12-a, and the iteration continued for the next 60 generations to demonstrate the consistency of the convergence. Finally, Figure 5.12-b depicts the most fitted individual antenna based on the algorithm. The solution space has a capacity of 2^{36}=6.8x10^{10} individuals in it. If each individual computing time is 1 second, the overall computation time taken to find the best-fitting individual will be 2.1x10^3 years. However, thanks to a genetic algorithm, the best-fit individuals are picked in only 40.3 hours only by utilizing a RAM of 8 GB, core I7, and 2.7 GHz processing speed computer.

Both the reference model and the genetically engineered antenna were simulated using ANSYS HFSS. The reference antenna resonated at 38 GHz single frequency band and had a covered impedance bandwidth of 1.2 GHz. The peak S_{11} value of the reference model at 38 GHz is -38.4 dB, whereas the antenna's maximum directivity is 6.1 dB. On the other hand, the proposed genetically optimized antenna works at four distinct frequencies: 28.3 GHz, 38.1 GHz, 46.6 GHz, and 60.0 GHz. The outcomes demonstrated that the antenna's bandwidth has also improved.

As shown in Figure 5.13, the antenna operates in quad-band, with a peak value of return loss S_{11} = -21.4 dB at 28.3 GHz, S_{11} = -18.1 dB at 38.1 GHz, S_{11} = -13.8 dB at 46.6 GHz, and S_{11} = -22.1 dB at 60.0 GHz. When S_{11} < -10 dB is taken into account, bandwidth improvement of the antenna in the operating bands is visible. At 28.3 GHz center frequency, the antenna has a fractional bandwidth of 3.2 % or 0.9 GHz, 6.0 % or 2.3 GHz, 3.4 % or 1.6 GHz and 11.1 % or 6.7 GHz at 28.3, 38.1, 46.6, and 60.0 GHz, respectively.

All operational bands (27.9 GHz-28.8 GHz, 37.1 GHz-39.4 GHz, 45.9 GHz-47.5 GHz, and 57.8 GHz-64.5 GHz) have a voltage standing wave ratio (VSWR) of less than 2. Figure 5.14 illustrates that the VSWR is typically less than 1.5 at most resonant frequencies. According to the plot, the VSWR values at 28.3 GHz, 38.1 GHz, 46.6 GHz, and 60 GHz are respectively 1.18, 1.28, 1.51, and 1.45. As a result, it can be shown that

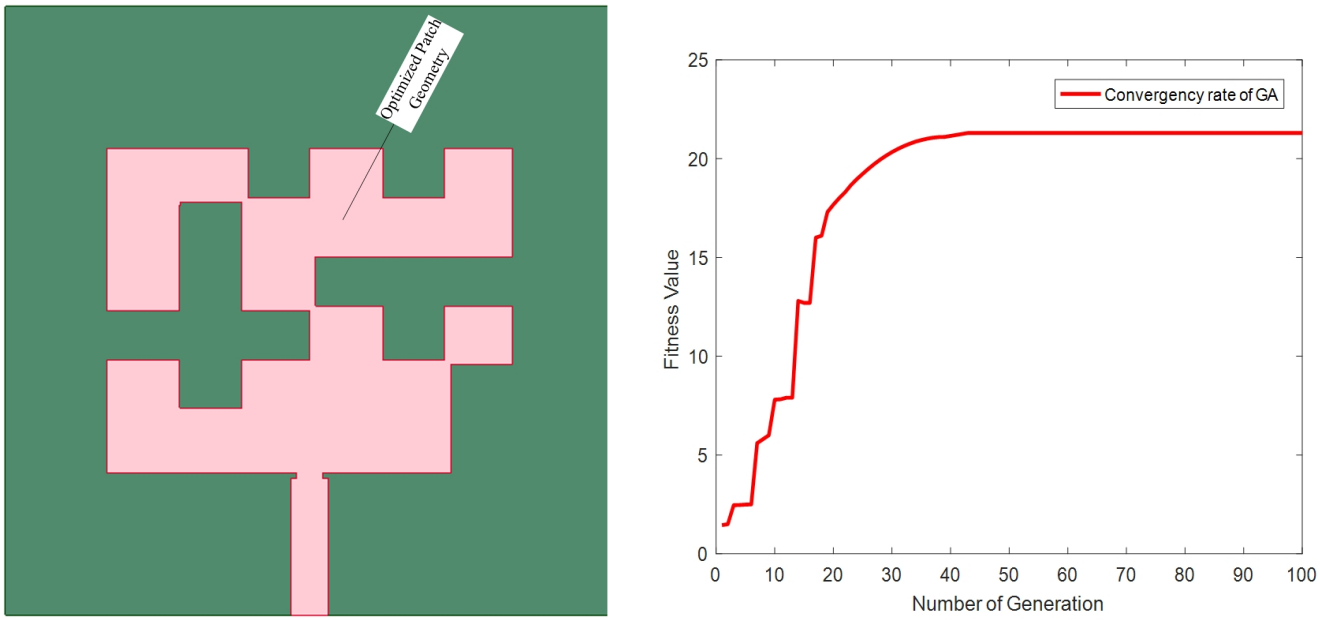

(a) (b)

Figure 5.12: a) genetically optimized proposed patch geometry, b) fitness value vs. number generation

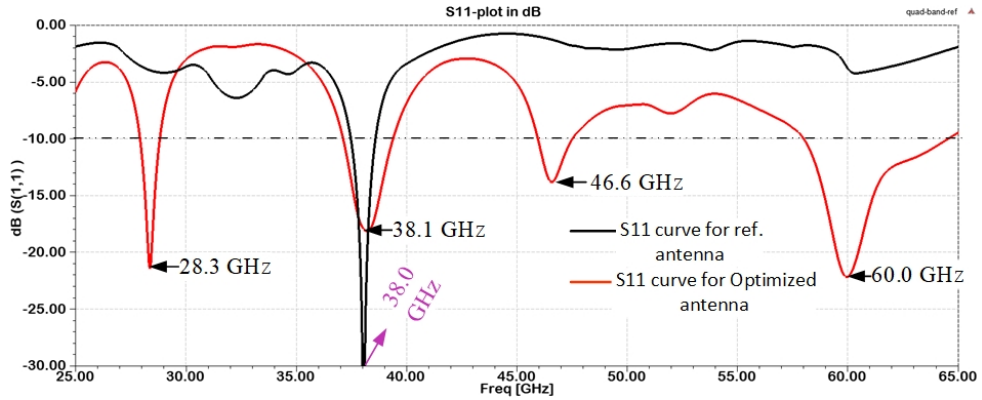

Figure 5.13: Simulated results of S11 for genetically optimized antenna and reference model

there is a good chance of matching or just a slight mismatch loss at the antenna's feed in four resonant bands.

Figure 5.15 displays the real and imaginary input impedance plot of the optimized antenna. It demonstrates that there are only minor differences between the antenna's input impedance and the characteristic impedance of the transmission line. The input impedance of the engineered patch antenna at 28.3 GHz is 44.31+j5.64, at 38.1 GHz is 44.1-j10.28, at 46.6 GHz is 65.65-j18.39, and at 60.0 GHz is 51.92+j7.95. Despite having a low reactance value, their real impedance value is close to the characteristic impedance. The findings indicate that the antenna and transmission line are nearly matched.

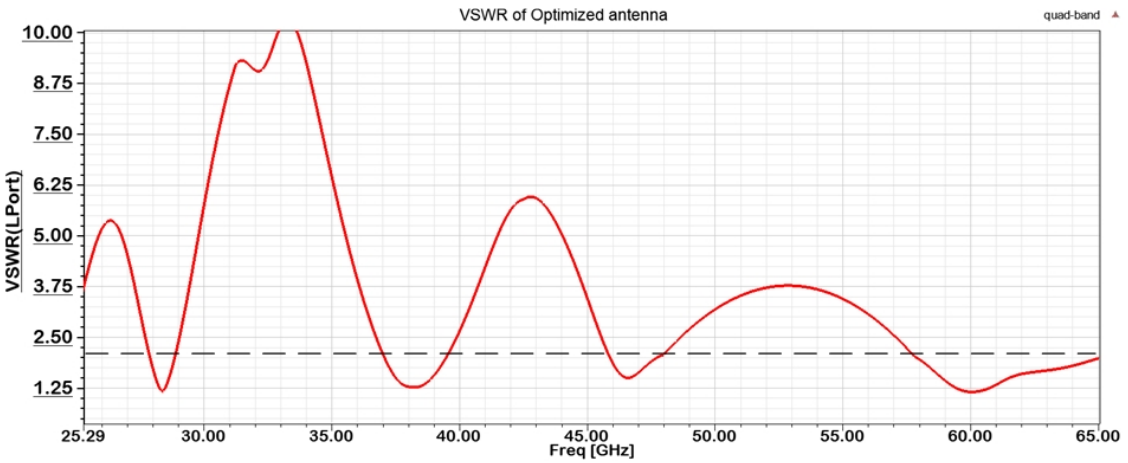

Figure 5.14: VSWR result of genetically optimized antenna

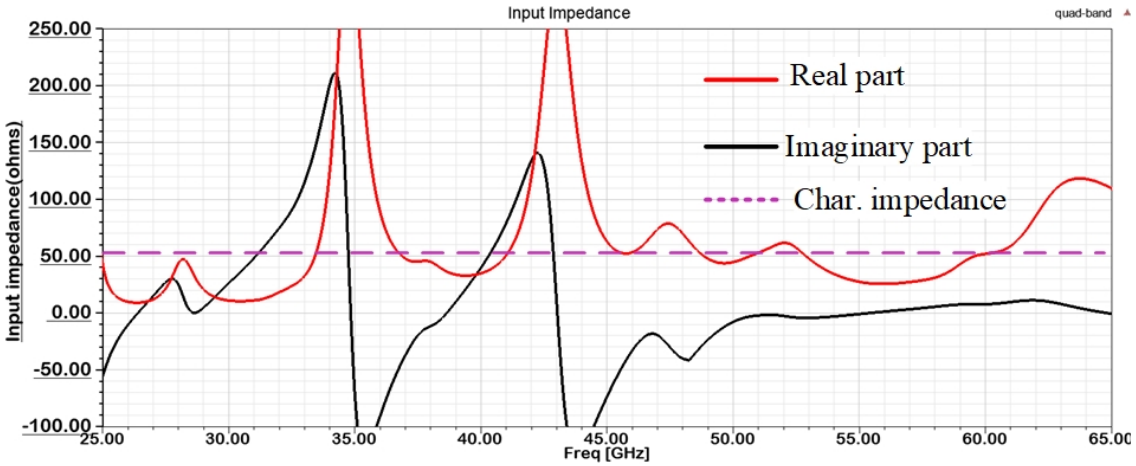

Figure 5.15: Real and imaginary impedance plot

The directivity and gain are better than the reference model and sufficient for mm-wave wireless applications. The antenna's 3D gain plot at four operational frequencies is shown in Figure 5.16. The optimized antenna demonstrates excellent performance characteristics. It achieves a maximum gain of 8.6 dB at a frequency of 38.1 GHz, outperforming the conventional microstrip antenna model. Even at 60.0 GHz, the optimized antenna maintains a minimum gain of 6.9 dB, which is superior to the conventional model. Furthermore, the proposed antenna exhibits impressive peak gains of 7.7 dB at 28.3 GHz and 7.2 dB at 46.6 GHz.

Figure 5.17 depicts the antenna's directivity pattern in the planes of $\theta = 0^0$ and $\phi = 90^0$, which is almost projected in a broadside orientation. Furthermore, the directivity enhancement in all working bands was observed. At 38.1 GHz, the maximum peak directivity of the optimized antenna is visualized as 8.8 dB at $\theta = 0^0$, while at 28.3 GHz, 46.6 GHz, and 60.0 GHz, peak broadside directivity of 7.8 dB, 7.3 dB, and 7.1 dB were observed, respectively.

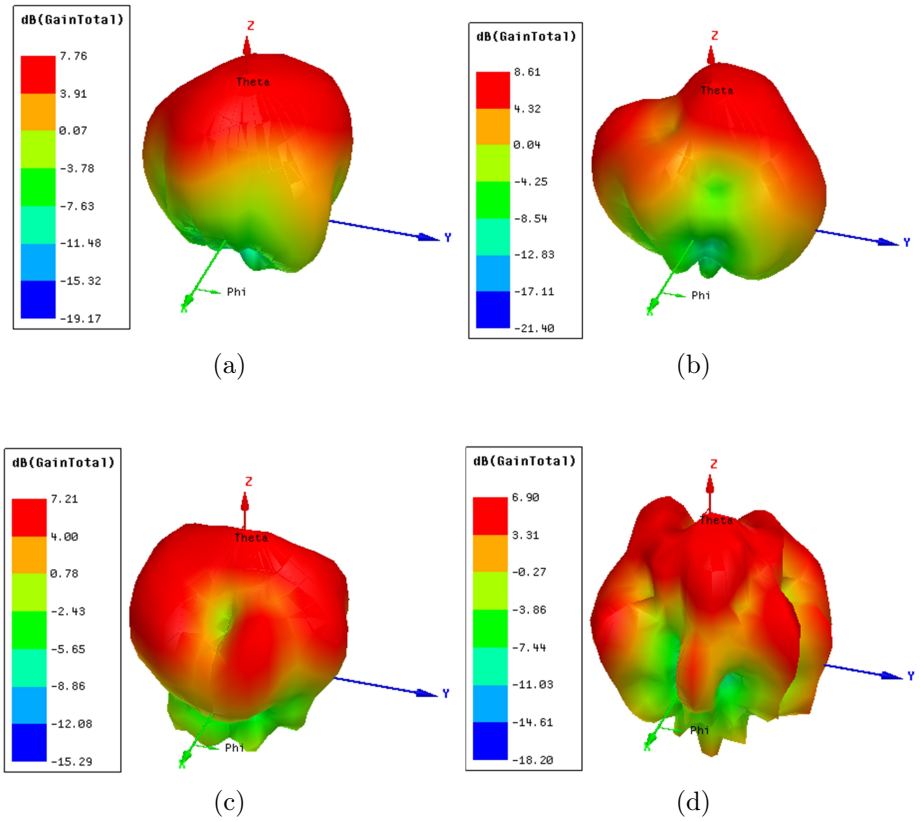

Figure 5.16: The 3D gain plot of the proposed antenna in dB (a) at 28.3 GHz (b) at 38.1 GHz, (c) at 46.6 GHz, (d) at 60.0 GHz.

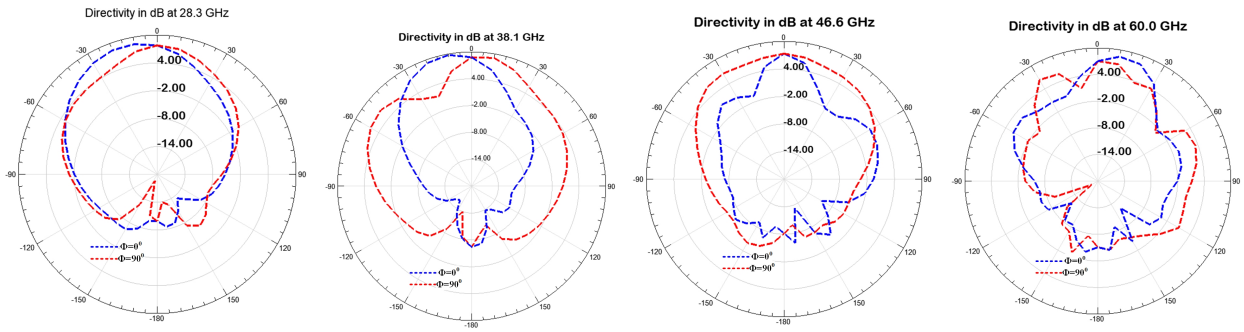

Figure 5.17: The 2D radiation pattern plot of the proposed antenna in dB (a) at 28.3 GHz (b) at 38.1 GHz, (c) at 46.6 GHz, (d) at 60.0 GHz.

The antenna's total efficiency and radiation efficiency are additional crucial metrics to describe antenna performance. Mismatch loss is not taken into consideration by radiation efficiency; however, it is by total efficiency, which is the product of radiation efficiency and mismatch loss. The radiation efficiency of the improved antenna is 96.3 %, 95.4 %, 97.7 %, and 94.8 %, respectively, at 28.3 GHz, 38.1 GHz, 46.6 GHz, and 60.0 GHz, as depicted in Figure 5.18. However, the mismatch loss at resonant frequencies has little impact on the antenna efficiency since the reflection coefficient is small relative to other

frequencies. In light of this, the improved antenna has a total efficiency of 95.8% at 28.3 GHz, 93.8 % at 38.1 GHz, 93.4 % at 46.6 GHz, and 94.2 % at 60.0 GHz, respectively. It is evident from these radiation properties that the genetically engineered antenna is able to meet the needs of mm-wave wireless communication systems terminals in quad-band applications.

Figure 5.19 depicts the surface current distributions of the entire patch antenna to

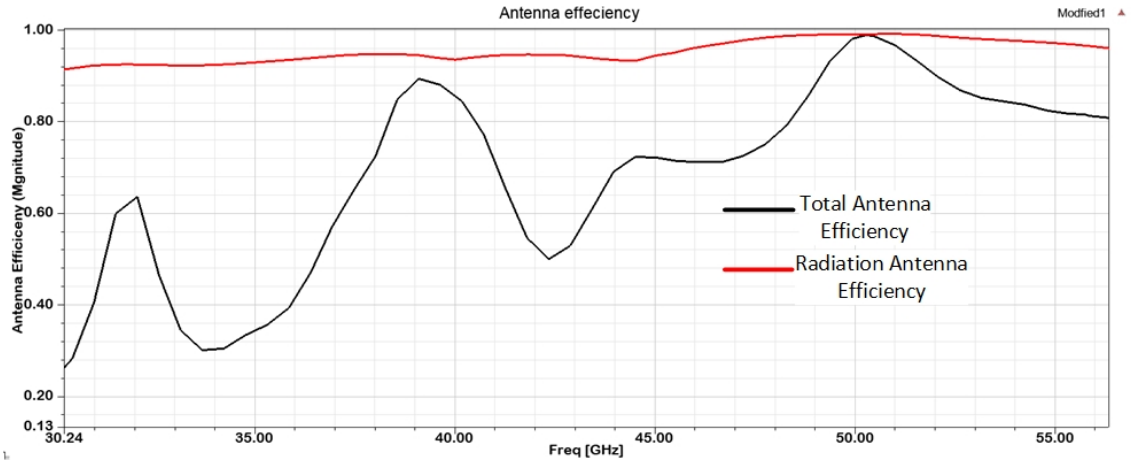

Figure 5.18: Total efficiency and radiation efficiency of the optimized antenna

further clarify the quad-band operation properties of the optimized antenna at 28.3, 38.1, 46.6, and 60.0 GHz. The graphic clearly shows that the current distributions differ across the four bands. The majority of current distributions are located near the feed point and the cell's edges on the optimized patch surface.

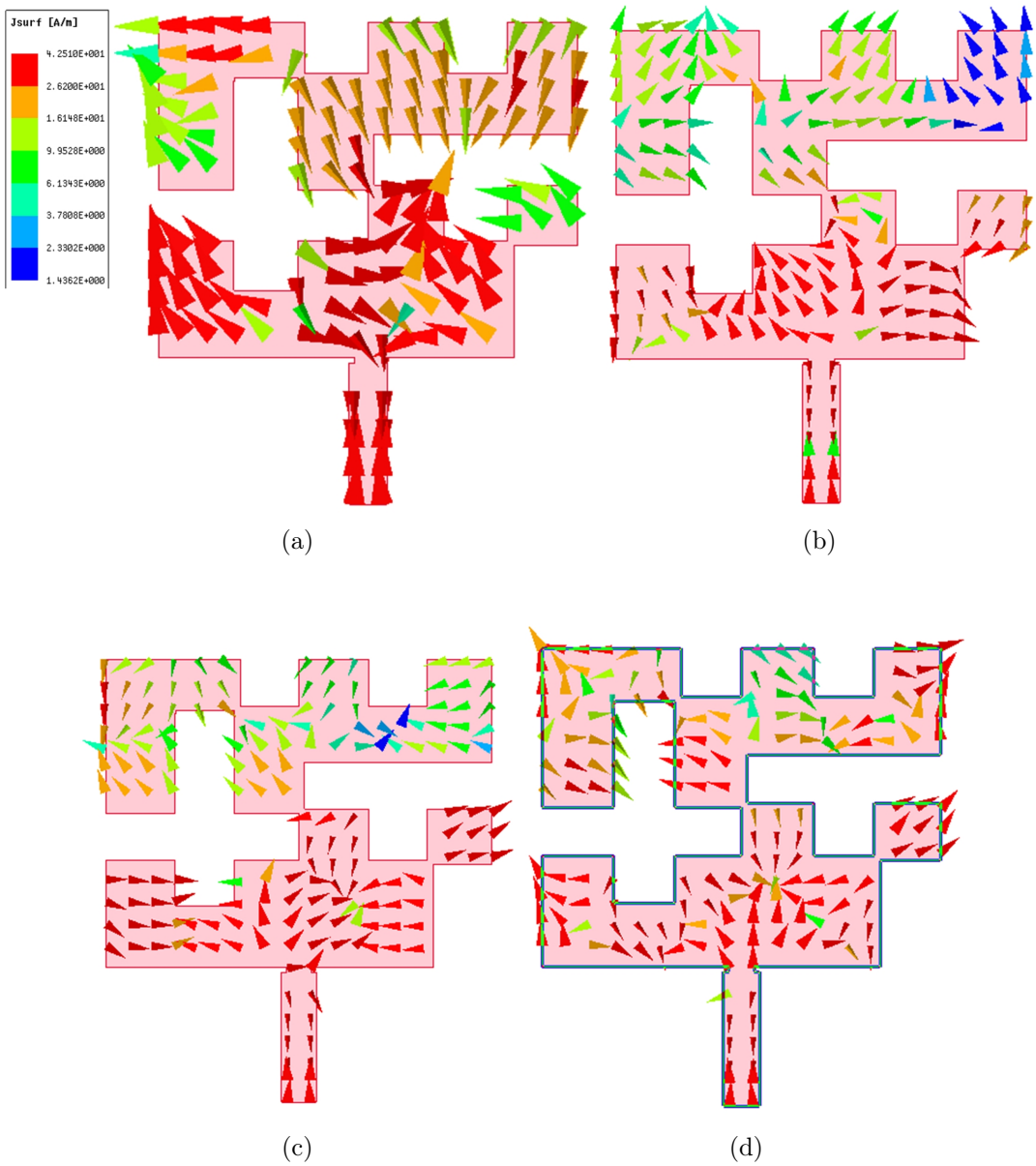

Figure 5.19: Current distribution on the surface of the optimized antenna (a) 28.3GHz (b) 38.1GHz, (c) 46.6 GHz, (d) 60.0 GHz.

5.3.4 Comparison with Related Works

Almost all of the related works mentioned in the literature employ a complex antenna structure to generate a quad-band. For instance, [218] and [220] are employed sophisticated superstrate and slots structures for quad-band creation. In contrast, this work employs a very simple antenna structure that is simple to model and manufacture. The optimized antenna performance was compared with several relevant works in the literature, as shown in Table 5.6. As presented in the table, a 4x4 hexagonal patch MIMO antenna operating in quad-band achieves a peak gain of 8.0 dB [222]. The bandwidth of the antenna, on the other hand, receives less attention. At the same time, that antenna

has low directivity in comparison to this study. Furthermore, using a single optimized antenna, this study achieves a gain slightly higher than its maximum gain. A work presented in [217] achieves a peak gain of 1.98 dB in microwave frequency, but the gain is significantly lower than that of this optimized antenna. When compared to previous relevant studies, the uniqueness of this work can be seen in the improvement of bandwidth, gain, and directivity of a single antenna with quad-band resonance frequency using a binary-coded genetic algorithm optimization. Moreover, the antenna performance is sufficient for mm-wave wireless communication

Table 5.6: Performance comparison of this work with related simulated works

Paper	Patch size in λ^2	Reson. freq. (GHz)	BW (GHz) (S11≤-10 dB)	Directivity(dB)	Gain (dB)	Techniques
[217]	0.2x0.25	2.54 3.51 4.38 5.3	0.24 0.28 0.2 0.57	- - - -	Max. gain 1.98	By adding inverted L and T stub
[220]	1.12x1.02	28 34 38 42	Total around 10	- - - -	6.9 7.4 8.5 7.5	DRA with slotted ground and superstrate
[222]	0.93x1.68	28 45 51 57	0.6 2 1.8 1.3	- - - -	7.3 7.03 7.2 8.0	4x4 hexagonal patch MIMO
This work	0.73x0.9	28.3 38.1 46.6 60.0	0.9 2.3 1.6 6.7	7.8 8.8 7.3 7.1	7.7 8.6 7.2 6.9	Genetic algorithm

5.4 Penta-band Antenna with Bandwidth Improvement for Wearable Applications

In recent years, there have been a number of investigations on wireless monitoring of human attributes. Several services are anticipated from wearable devices addressing the ever-growing customer requirements. Designers and researchers in the field of wearable antennas continue exploiting antenna technology to meet client needs. Globally, extensive research has been undertaken towards innovative and tiny wearable antennas capable of wirelessly communicating human body parameters to a nearby accessible network. As wearable antenna technology advances, new and diverse applications such as medical monitoring, smart diagnosis, aging care, battle-field personal care, astronaut monitoring, child protection, and location-based services have emerged [204]. Such devices are used in sports medicine to track the characteristics of athletes in training. Wearable antennas are often employed in hazardous areas to manage the work environment [225]. The wearable antenna in a well-designed system has appropriate operating bandwidth, acceptable radiation characteristics for human tissue, and high enough gain and directivity to suit the requirements [226]. The antenna, on the other hand, must be light, flexible, compact in size, inexpensive, resistant to damage, and comfortable to wear. Microstrip antennas are an attractive option for mm-wave multi-band wearable antennas [227]. Even though the microstrip antenna has low gain and narrow bandwidth with some other deficiencies in its performance, the antenna is advantageous over other antennas due to its low profile, easy manufacturing, and planar structure.

The dynamic development of wireless communication derives coexisted multiple standards that increase the demand for multi-functional antennas. Refereeing to Chapter One, mm-wave bands are part of the radio frequency spectrum between 30 and 300 GHz, corresponding to a free space wavelength ranging from 10 to 1 mm. Because of the plenty of bandwidth available at mm-wave frequency, numerous applications such as wireless networks, mobile communication, and internet of things, wireless human monitoring systems, and machine-to-machine communications will be facilitated and become more prevalent in the band for the next-generation technologies [228]. In the case of human monitoring systems, networks in the band are critical because they allow data transmission over small ranges of cellular systems. As the photon energy is insufficient to take an electron from an atom at the mm-wave spectrum, the radiation from this band is not ionized. Instead, the absorption of electromagnetic mm-wave energy by tissues results in the primary physiologic consequence of heat [229]. Thus, antennas in mm-wave for a body-centric network should be optimized according to the rules and guidelines of specific absorption rate to protect the human tissue from injuries.

This section of the chapter presents a wearable penta-band mm-wave microstrip antenna

using a binary-coded genetic algorithm for the wireless human monitoring system. For operational reasons, antennas of this type should use fabric substrates for easy integration with clothes [230]. Simultaneously, the bandwidth of such an antenna should be as broad as possible to allow for abundant data transfer in the link in all operating bands. The research will discuss the optimized antenna in free space simulation by varieties of the fabric substrate, on body simulation with different distances from the human phantom model.

5.4.1 Antenna Modeling

An appropriate wearable antenna design should be considered to minimize losses in wearable scenarios. The geometric configuration of the reference rectangular microstrip antenna suitable for GA optimization is illustrated in Figure 5.20. The antenna's radiating patch and ground plane are composed of a 0.035 mm thick perfect electric conductor (PEC). A 0.6 mm thick fabric Polytetrafluoroethylene (PTFE) substrate with a dielectric constant of 2.05 and loss tangent of 0.0017 is employed. It is advantageous to minimize the surface wave losses by utilizing a substrate with a low dielectric constant, which simultaneously enhances impedance bandwidth [50]. The overall dimension of the textile substrate is 18 x 18 x 0.6 mm^3. The antenna radiating patch is 10.8 mm x 14.6 mm in size and is fed by a 50 Ω microstrip line that is 3.6 mm long and 0.9 mm wide. Besides the standard procedures used to calculate these dimensions presented in chapter two, the parametric analysis was utilized to articulate the patch dimensions in the interest of appropriate reference antenna performance at 39.5 GHz center frequency. The antenna was modeled and simulated using HFSS software. The dimensions of the reference model are summarized in Table 5.7.

Table 5.7: Summary of the size of reference antenna

	Antenna component		
Parameter	Substrate	Radiating Patch	Feed Line
Width (mm)	18	14.6	0.9
Length (mm)	18	10.8	3.6
Thickness (mm)	0.6	0.035	0.035
Material type	PTFE	PEC	PCE

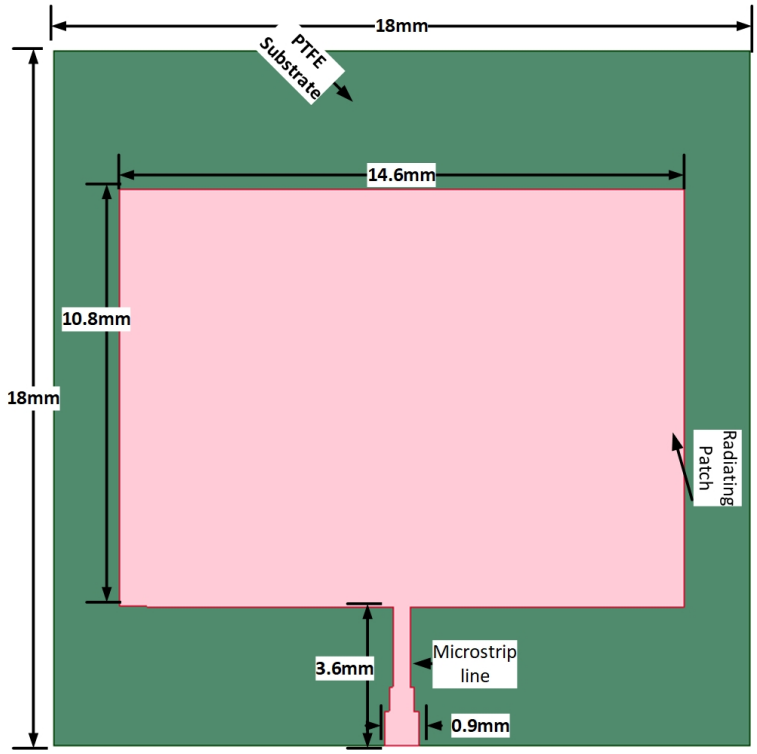

Figure 5.20: Proposed reference microstrip antenna model on finite ground plane

5.4.2 GA Optimization Setup

In this research, GA optimization is used to optimize the patch geometry. In the proposed solution space, the radiating patch geometry has a variety of shapes, and only a few of these configurations perform well. The GA is greedy since it continually seeks the best-fitting individual to ensure the continuation of the generation. In this optimization problem, the surface of the patch is gridded into 8 x 8 small rectangular cells having the size of 1.3 x 1.82 mm^2, as shown in Figure 5.21. When using a binary-coded genetic algorithm, it is evident that 2^{64} unique candidates are available in the solution space. Every rectangular cell on the surface has its corresponding conducting and non-conducting properties. During the "on" and "off" stages of the cell, vertical overlapping was employed to protect the infinitesimal connection between cells on the patch surface as presented in chapter three. The geometry of the patch surface is varied in each iteration, resulting in a new antenna with a new fitness value for each. Therefore, the performance of the antenna is updated.

The crucial role in the GA optimization process is the formulation of a good fitness function while considering the desired performance criteria. This work formulated the fitness function considering all the performance factors and their target values. The primary goal is to develop a penta-band mm-wave microstrip antenna that can operate at five unique frequencies with broad bandwidth for wearable devices. As a result, the fitness function is designed to minimize the reflection coefficient and increase the antenna's working

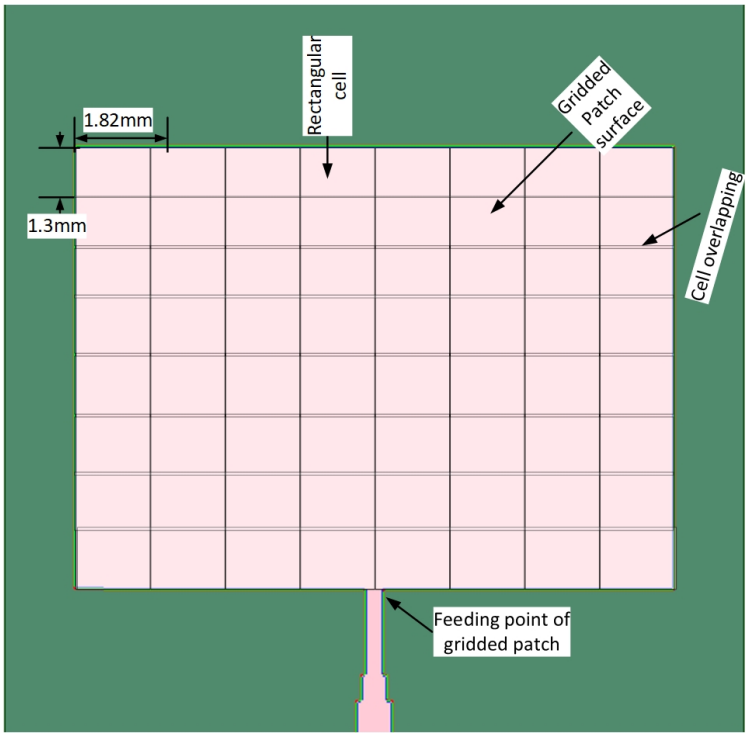

Figure 5.21: Division of patch surface for binary-coded genetic algorithm

bandwidth. The fitness function, as depicted in Equation 5.5, is formulated by summing the total operating bandwidth within the available frequency range and minimizing the reflection coefficient within each individual band. This fitness function is designed to optimize the antenna's performance by simultaneously enhancing the bandwidth and reducing the reflection coefficient across multiple frequency bands. By combining these two objectives, the fitness function ensures that the antenna operates effectively over a wide range of frequencies while minimizing signal reflections and maximizing signal transmission efficiency. To expedite the computation process, an upper bound of 8 GHz is imposed on the maximum bandwidth allowed for a single band. This limitation helps reduce the computational time required for optimization. Weighting coefficients (C_k) are also utilized to eliminate any overlaps or interference between the operating bands of the antenna. These coefficients are determined by dividing the band of interest by the upper bound of the bandwidth. The resulting value of the weighting coefficient ensures that each band is appropriately prioritized and contributes to the overall optimization process. By computing and assigning an appropriate weighting coefficient for each band, the optimization algorithm can effectively balance the performance across different frequency bands: 27.5-28.5 GHz, 31.0-31.5 GHz, 38.5-40.5 GHz, 46.5-48.0 GHz, and 54.0-62.0 GHz, mitigating overlaps and achieving desired performance characteristics.

$$Fittness\ function = \sum_{k=1}^{M} \left(C_k Bw\,(k) - \frac{1}{N} \sum_{i=1}^{N} \rho(f_i) \right) \tag{5.5}$$

$$Bw(k) = \begin{cases} Bw(k)\ if\ Bw \leq 8\ \text{GHz} \\ 8\ \ \text{GHz}\ \ if\ Bw > 8\ \text{GHz} \end{cases} \tag{5.6}$$

$$\rho\,(f_i) = \begin{cases} \rho\ (fi) & \text{if } \rho \geq -10\ \text{dB} \\ -10\ \text{dB} & \text{if } \rho \leq -10\ \text{dB} \end{cases} \tag{5.7}$$

Where N is the number of sampling frequencies in a given band and M is the number of the operating band. The sampling frequency (f_i) is in the 50 MHz used with the analysis sweep and $\rho(f_i)$ is the reflection coefficient value in dB at each sampling frequency. C_k assigns the k^{th} bandwidth weighting factor, and Bw(k) is bandwidth at the k^{th} band in GHz.

The patch surface of the reference model is optimized using the following algorithm configurations. The total number of population clusters in a particular generation is 15 individuals. In a population, a single chromosome is represented by 64 genes. Single-point crossover with a probability of 0.8 and single-bit mutation with a mutation rate of 0.01 were used. Throughout 250 generations, the selection operator employed the tournament selection approach.

5.4.3 Results and Discussion

The optimization and simulation of the proposed penta-band antenna were carried out using commercially available electromagnetic simulation software HFSS in combination with MATLAB. The geometry of the shape was optimized by providing 'on' and 'off' states for the rectangular cells on the patch surface until the final structure was obtained using a binary-coded genetic algorithm. The total computing performance of the multi-iterative optimization approach is influenced by the time required for electromagnetic simulation. GA returns the best out of 2^{64} = 1.84 x10^{19} solution space in 4.3 days at the 250 generations using core I7, 8 GB RAM, and 2.7 GHz processor speed, as shown in Figure 5.22-a. If we think a second for each aspirant solution, the computation time would be 5.85 x 10^{11} years. Hence, GA started to converge after 103 generations, as shown in Figure 5.22-b.

Free Space Simulation

The optimized antenna with a fabric PTFE substrate was simulated in free space. The simulated S_{11} curve for both the reference and optimized antennas is presented in Figure

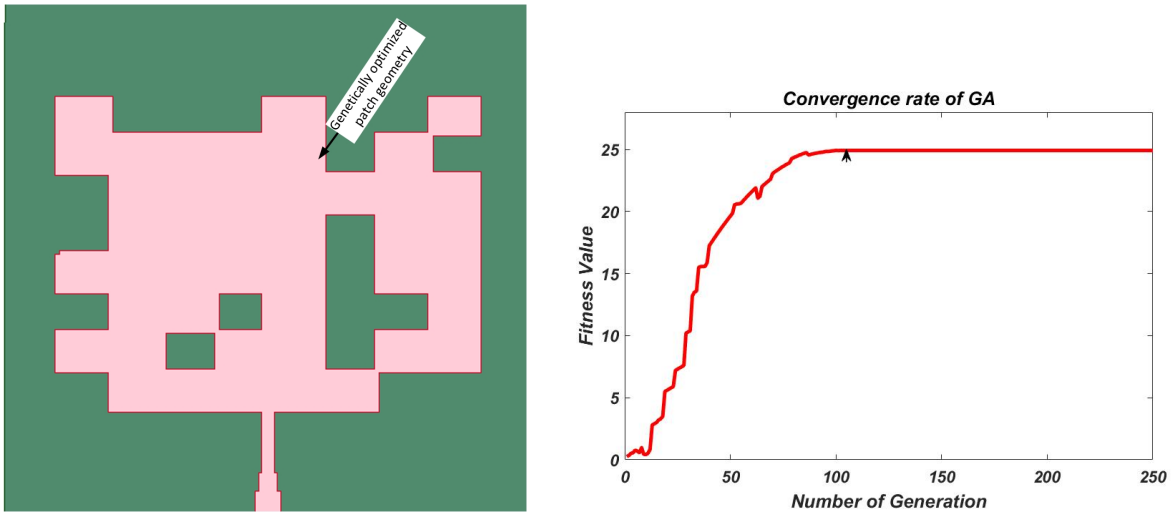

(a) (b)

Figure 5.22: (a) The fitted genetically optimized patch geometry (b) Fitness value versus number of generation

5.23. The figure demonstrated that the reference model resonated only at a single frequency of 39.5 GHz, with a minimum peak S_{11} value of -20.6 dB. Whereas, the optimized antenna resonates at five distinct bands with center frequencies of 27.7 GHz, 30.3 GHz, 40.0 GHz, 47.2 GHz, and 56.7 GHz and peaks S_{11} values of -34.5 dB, -20.1 dB, -35.2 dB, -22.4 dB, and -25.8 dB, respectively. The VSWR was determined to be less than 2 for all five operational bands, indicating that the proposed antenna was well matched to a 50 Ω microstrip line that transmits the maximum power between the feed line and antenna. The bandwidth of the reference model is 0.9 GHz since it operates in the range of (39.0-39.9 GHz) when considering S_{11} < -10 dB is considered. However, the optimized antenna achieved a better bandwidth in all five operating bands: 0.69 GHz (27.43 - 28.12 GHz), 2.32 GHz (28.94 - 31.26 GHz), 2.22 GHz (39.27 - 41.49 GHz), 1.76 GHz (46.44 - 48.2 GHz), and 8.11 GHz (53.83 - 61.94 GHz). These bandwidth improvements were made by employing genetic algorithm optimization.

The 3D gain pattern of the optimized antenna at all five resonant frequencies is presented in Figure 5.24. The antenna has achieved gain values of 10.2 dB, 8.4 dB, 7.7 dB, 9.5 dB, and 8.4 dB at resonating frequencies of 27.7 GHz, 30.3 GHz, 40.0 GHz, 47.2 GHz, and 56.7 GHz, respectively. As seen from the 3D pattern, they are almost in the broadside direction with slight distortions in higher frequency bands.

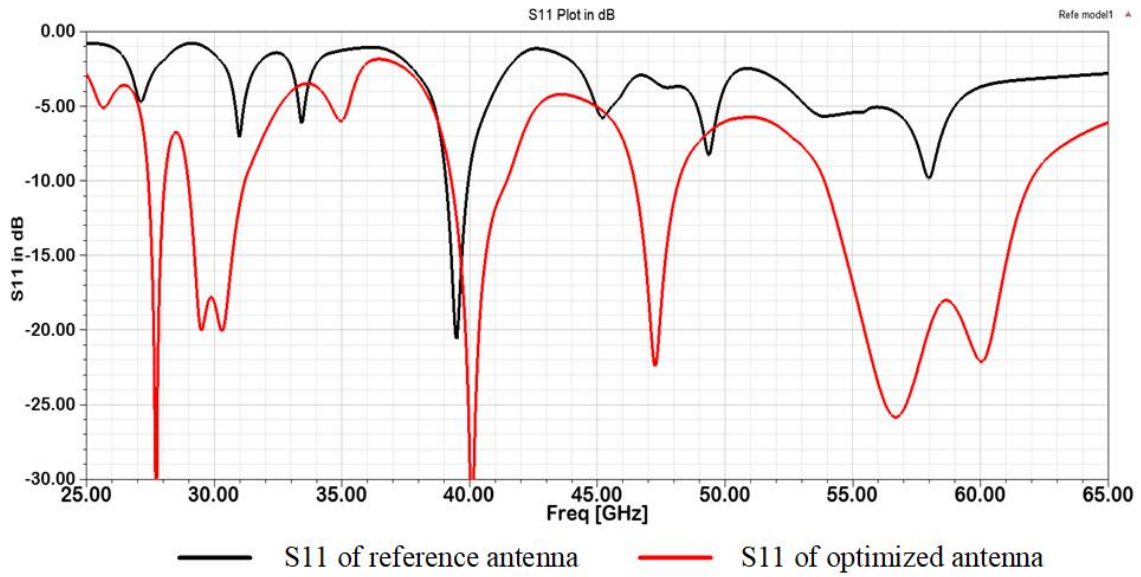

Figure 5.23: S11 curve for the genetically optimized antenna and the reference antenna

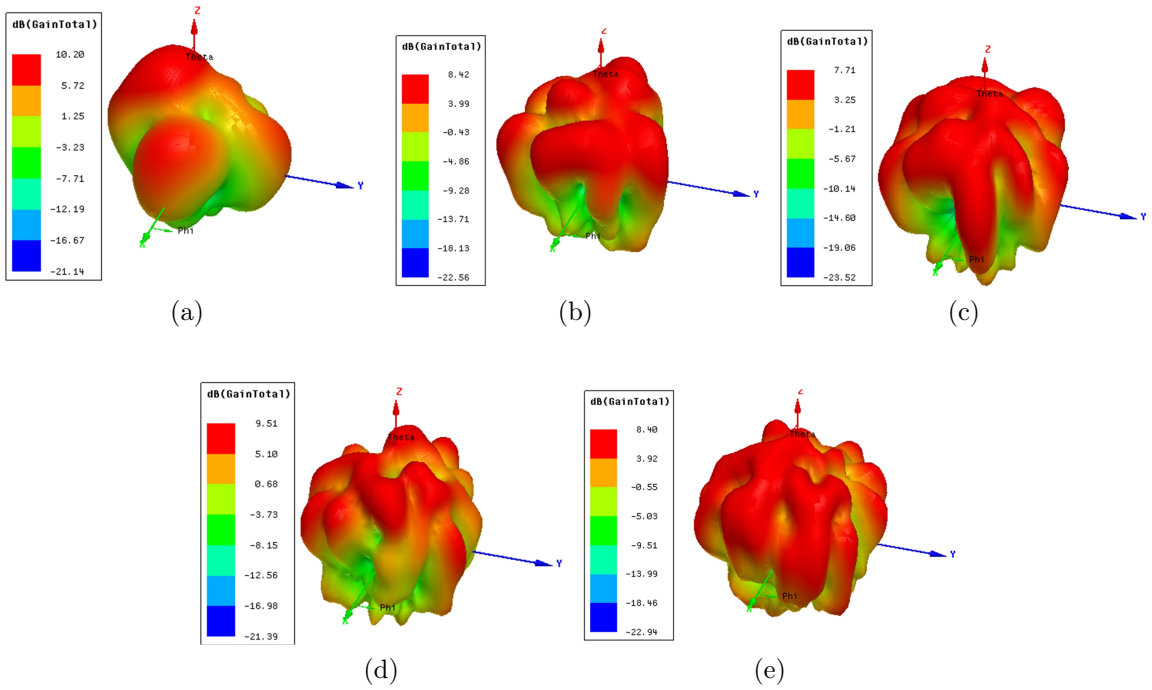

Figure 5.24: The 3D gain of the optimized antenna at all five resonance frequencies (a) 27.2 GHz, (b) 30.3 GHz, (c) 40.0 GHz, (d) 47.2 GHz, and (e) 56.7 GHz

Simulation with Different Substrate

For further analysis and investigation of the improved antenna's performance, the free space simulation was carried out by substituting the PTFE substrate with various textiles. Polyester, silk, jeans, and cotton fabrics were used as substrates with dimensions similar to PTFE. The dielectric constant and tangent loss parameters of fabric substrates are described in Table 5.8. Figure 5.25 displays the simulation result of their S_{11} values. The

results indicate that the optimized antenna operates in five frequency bands for all fabric substrates. When the dielectric constant decreases, the resonant frequency slightly shifts towards a higher frequency, and the total operating bandwidth of the antenna increases. The cotton-based optimized antenna has a bandwidth of 3 GHz more than the PTFE antenna. Polyester substrate performs closely to the initial PTFE optimized antenna due to the closer dielectric constants. According to simulation results, all of the evaluated substrates exhibited a gain of higher than 8 dB in each band. Table 5.9 summarizes the free space performance study of the improved antenna with various fabric substrates and the performance of the reference model.

Table 5.8: The dielectric constant and the loss tangent value of the selected fabric substrates

No.	Textile material	Dielectric constant	Loss Tangent
1	Cotton	1.6	0.04
2	Polyester	1.9	0.0045
4	Jeans	1.67	0.073
5	Silk	1.75	0.012
6	PTFE	2.05	0.0017

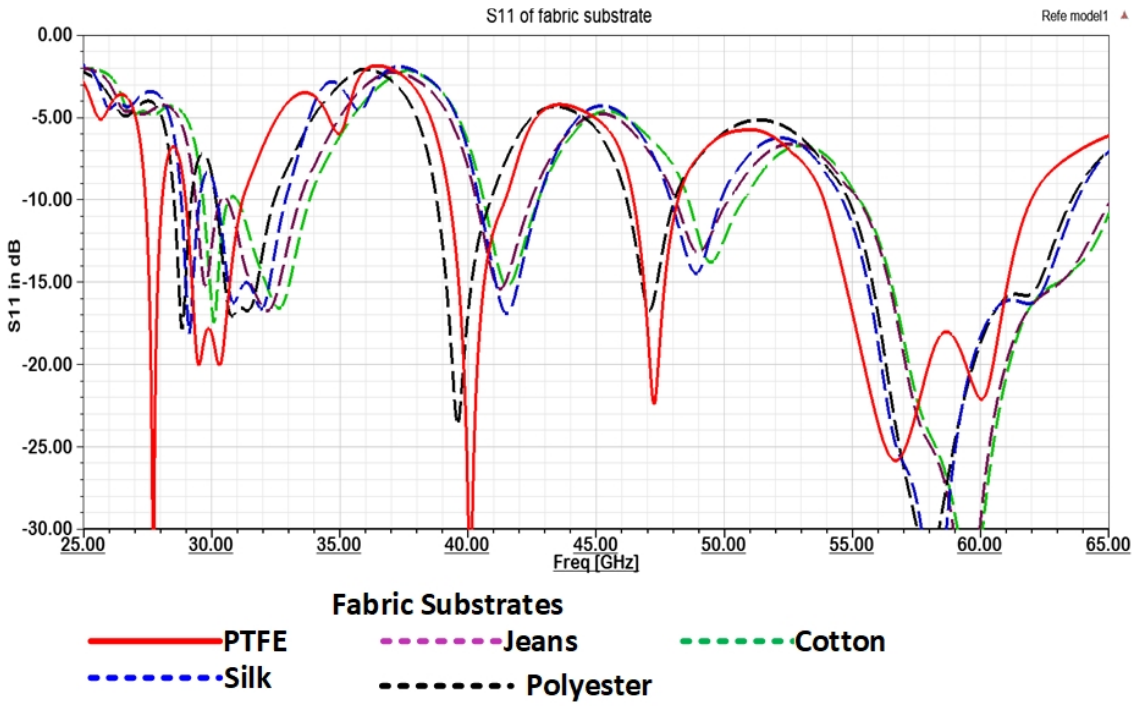

Figure 5.25: S11 result of the genetically optimized antenna with various fabric substrates

Table 5.9: performance of the optimized antennas

Substrate type	Resonance Frequency (GHz)	S11	Peak directivity	Peak gain	Bandwidth (GHz)
PTFE	27.8	-34.5	10.3	10.2	0.69
	30.3	-20.1	8.5	8.4	2.32
	40.1	-35.2	7.8	7.7	2.22
	47.2	-22.4	9.6	9.5	1.76
	56.7	-25.8	8.9	8.4	8.11
Silk	29.1	-18.1	9.5	9.3	0.75
	31.9	-16.6	9.6	9.3	2.72
	41.5	-16.9	8.9	8.7	2.35
	48.9	-14.5	8.4	8.2	2.01
	58.2	-38.6	8.3	8.1	9.23
Polyester	28.8	-17.8	8.8	8.7	0.68
	30.8	-17.1	8.7	8.4	2.3
	39.6	-23.6	7.8	7.5	2.12
	47.1	-16.7	8.9	8.7	1.89
	57.9	-32.2	8.8	8.1	8.74
Jeans	29.7	-15.2	9.3	8.9	1.06
	32.2	-16.7	9.4	9.0	3.02
	41.3	-15.4	7.7	7.4	2.16
	49.0	-13.2	9.0	8.9	2.02
	59.5	-38.6	8.7	8.3	9.78
Cotton	30.1	-17.3	9.6	9.1	0.99
	32.6	-16.6	8.9	8.6	2.76
	41.6	-15.2	9.5	9.3	2.22
	49.5	-13.7	8.1	7.8	2.35
	59.6	-34.8	8.8	8.4	9.82

Figure 5.26 (a-e) and Figure 5.27 (a-e) depict the optimized antenna's gain pattern in E and H planes with various fabric substrates, respectively. The gain patterns of the E and H planes exhibit only slight differences. The patterns guided in the broadside direction show a significant distortion at a few angles, particularly at higher frequencies.
Figure 5.28 (a-e) showcases the surface current distributions at resonance frequencies, emphasizing the electromagnetic radiation properties of the optimized antenna within its operating bands. Notably, when the proposed antenna operates at resonance frequencies, significant surface current density is observed at the junction of the feed line and patch, as well as the corner points of each slot. This indicates high energy distribution and strong radiation from these specific points. Additionally, there is a moderate current distribution over the surface of each active rectangular cell, which contributes slightly to the far-field radiation properties.

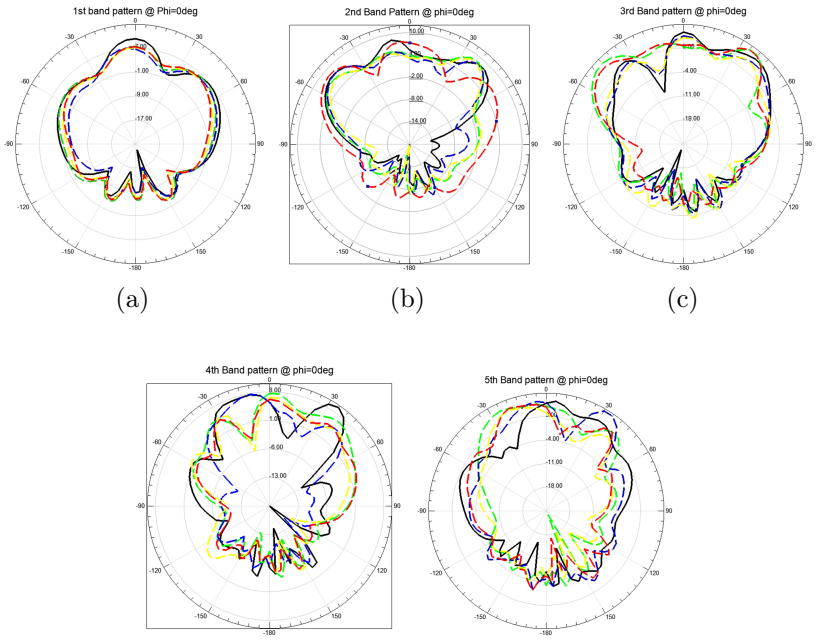

(a) (b) (c)

(d) (e)

Figure 5.26: 2D gain pattern in E-plane of the optimized antenna in various fabric substrate

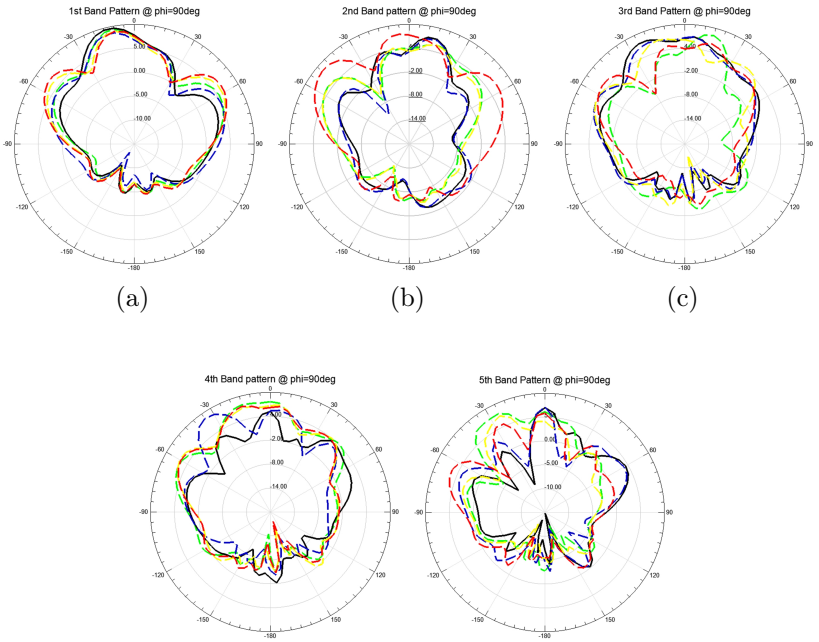

(a) (b) (c)

(d) (e)

Figure 5.27: 2D gain pattern in H-plane of the optimized antenna in various fabric substrate

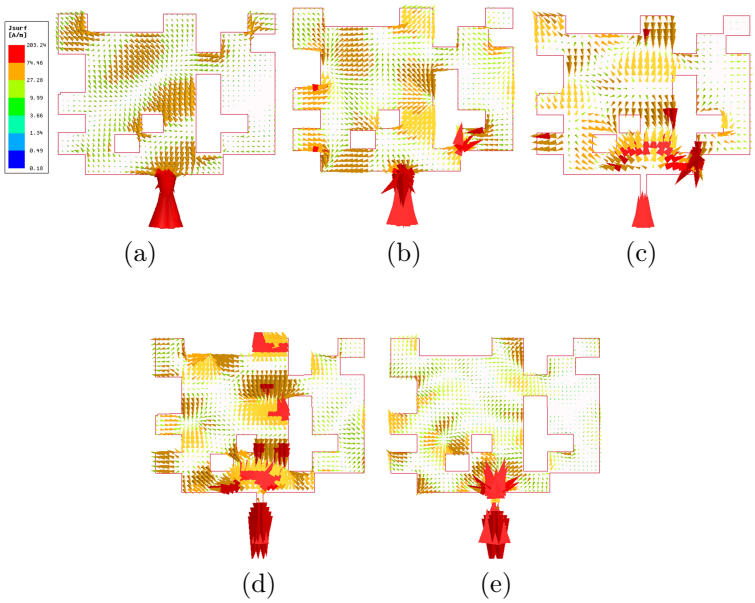

Figure 5.28: Current distribution on the patch surface of the optimized antenna with PTFE substrate at different resonance frequencies

On-body Simulation

In the case of wearable contrivances, the antenna should be simulated conjointly with the proximity of the human body model. The human body model should be discretized into small resolutions during the joint simulation. The computational time and memory requirement are high when the model's size is much larger than that of the operating wavelength. As mm-wave signals cannot penetrate human skin more than 0.5 mm, most research studies employ a three-layer phantom representation [231, 232]. The heterogeneous and lossy nature of the human body has a direct influence on the antenna performance when it works nearby.

A three-layered phantom that consists of muscle, fat, and skin is designed in HFSS, as shown in Figure 5.29-a. At 40 GHz, the average permittivity and conductivity of these layers are specified for muscle (ϵ_r=52.79; tanδ =1.705), fat (ϵ_r=5.28; tanδ =0.1) and skin (ϵ_r=31.29; tanδ =5.0138) [233]. In this model, the thickness of muscle, fat, and skin layers are 5mm, 3 mm, and 2 mm, respectively. The proposed optimized wearable antenna is fixed on a 20 x 20 x 10 mm flat body phantom to study its radiation characteristics in three proximity levels to the human body. The antenna was positioned at three different distances from the phantom to analyze the antenna performance in wearable scenarios. Starting from 2 mm, the antenna gradually moved away to 10 mm from the phantom. Figure 5.29-b shows the antenna's position at variable proximity from the model.

Figure 5.30 shows the S_{11} performance curves of the optimized PTFE substrate antenna corresponding to various proximity placements from the human body model. When the antenna is placed 2 mm, 5 mm, and 10 mm away from the phantom, the center frequency

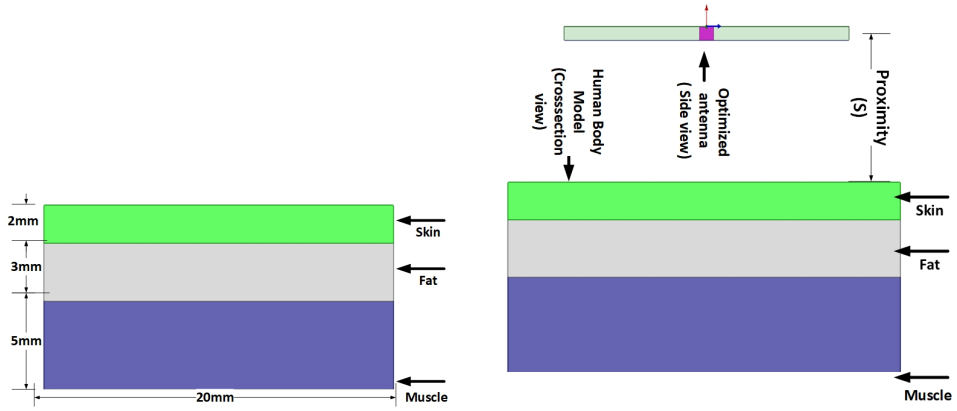

(a) (b)

Figure 5.29: (a) Human body model and its dimensions [229] (b) placement of the optimized antenna in variable proximity(S)

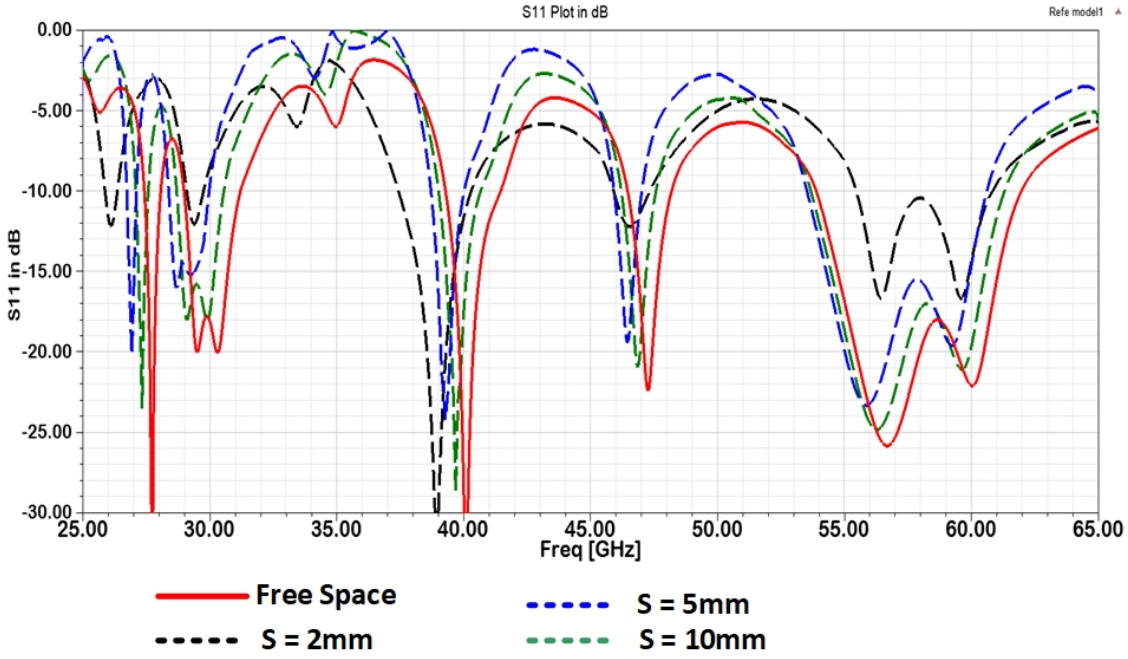

Figure 5.30: S_{11} performance of the optimized antenna at various proximity from the human model

shifts toward lower, as shown in the graph. At the same time, the antenna resonates at five distinct frequencies in each level of proximity. The shifting was not noticeable when the antenna was close to free space at 10 mm proximity. The bandwidth of the optimized antenna was highly affected at 2 mm placement, resulting in about 10.9 GHz over all penta-band operations, which is 28 % lower than the free space bandwidth coverage.
The gain and radiation efficiency were adversely affected when the antenna operated close to the human body model. When the gap between the antenna and the phantom model gradually increases, radiation efficiency and gain also increase. At a distance of 2 mm, the minimum gain value was observed, which is 4.7 dB. The maximum gain in the on-body

simulation was 8.4 dB at 10 mm proximity. However, this value was substantially lower when compared to the free space findings due to the lossy nature of human tissues. Table 5.10 summarizes the results of the on-body simulation of the optimized antenna with a PTFE substrate. The gain pattern of the antenna in the E-plane and H-plane for various distances are shown in Figure 5.31 and Figure 5.32, respectively. The radiation patterns don't change much with multiple antenna placements except for power level variations.

Table 5.10: On-body simulation performance of the optimized antenna at various distances from the body model

Placement	Resonance Frequency (GHz)	Bandwidth (GHz)	Gain (dB)	Directivity (dB)
On-body 2 mm	26.1	0.4	5.1	7.4
	29.4	0.8	5.2	7.6
	38.9	2.9	4.8	6.3
	46.6	1.4	4.7	6.5
	56.4	5.4	5.8	8.1
On-body 5 mm	26.9	0.4	5.8	7.3
	28.7	1.7	5.7	7.1
	39.2	1.3	5.2	6.4
	46.5	1.1	6.0	8.2
	55.9	7	6.2	7.8
On-body 10 mm	27.3	0.4	6.7	8.0
	29.1	1.9	7.2	8.4
	39.7	1.6	6.1	6.8
	46.8	1.3	8.4	8.9
	56.2	7.6	7.5	8.8
Free space	27.8	0.69	10.2	10.3
	30.3	2.32	8.4	8.5
	40.1	2.22	7.7	7.8
	47.2	1.76	9.5	9.6
	56.7	8.11	8.4	8.9

5.4.4 Comparison with Related Works

Table 5.11 summarizes the results of genetically improved antennas and some other similar research studies. The originality of this work has been recognized in terms of its pentaband operation and other performance metrics. For example, in reference [230] a wearable UWB antenna for mm-wave devices was proposed. The antenna was only capable of operating in a single band with a bandwidth of 12.1 GHz. However, this genetically modified wearable antenna can operate in five frequency bands with a total bandwidth

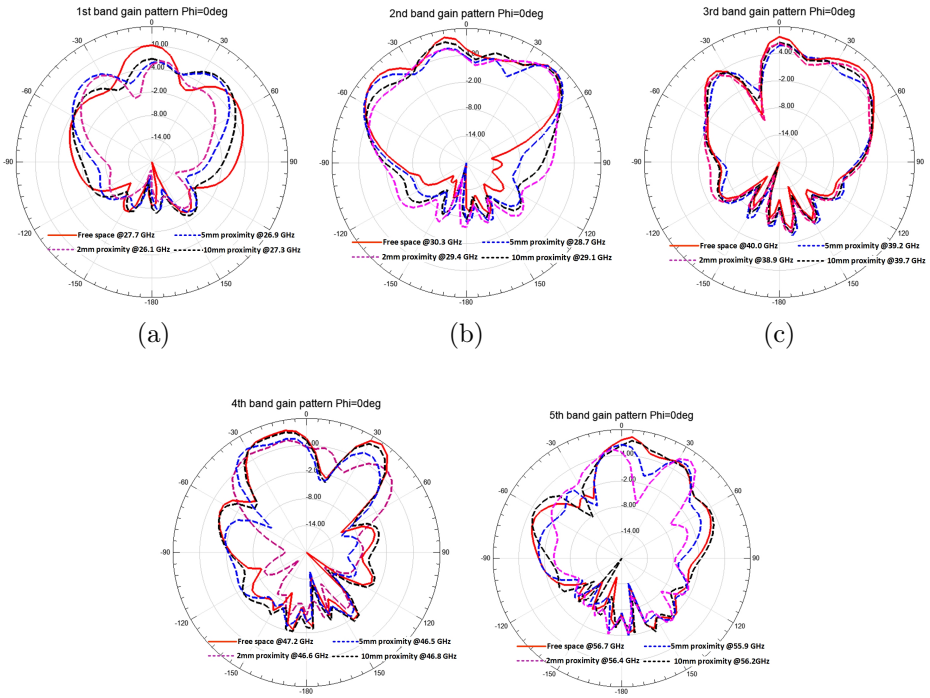

(a) (b) (c)

(d) (e)

Figure 5.31: On-body H-plane 2D gain pattern of in various distances from human body model

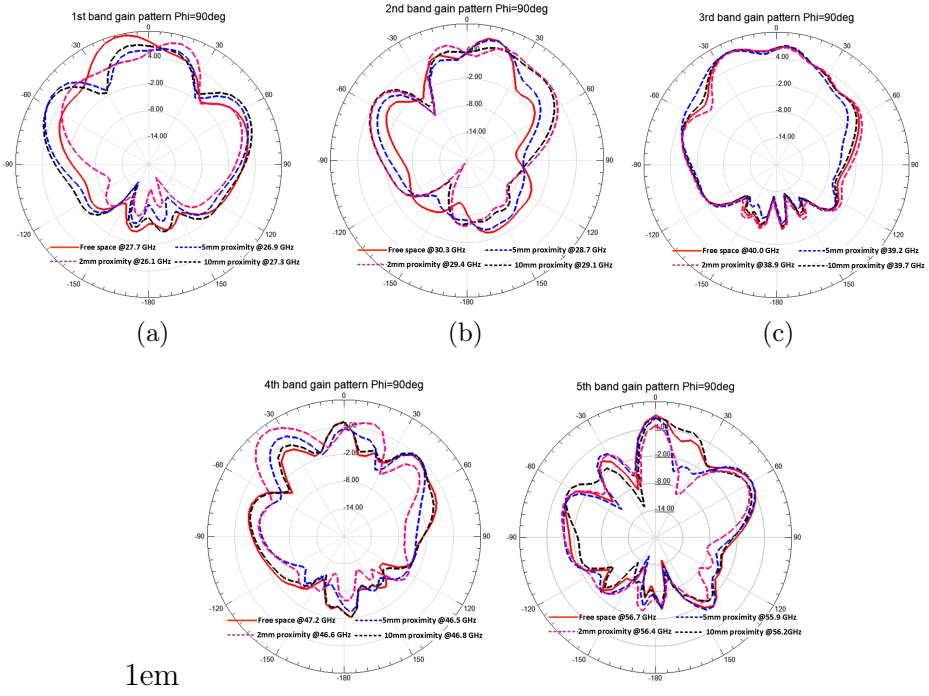

(a) (b) (c)

1em

(d) (e)

Figure 5.32: On-body H-plane 2D gain pattern of in various distances from human body model

of 15.1 GHz. Nevertheless, the proposed antenna has a maximum gain of 10.2, which indicates its superiority. Aside from the fact that the improved antenna utilizes a flexible textile-based substrate, it also outperforms related works in both free space and on-body simulations, making the optimized antenna a strong choice for wearable devices.

Table 5.11: Performance comparison of this work with similar works in the literature

Papers	Size of the patch	Resonance Frequency (GHz)	Bandwidth (GHz)	Gain(dB) Free space	Optimizing Method	Material
[230]	53.6x46	2.403	0.17	5.94	Parametric	Jeans
[228]*	11x6.5	60	12.1	8.62	Parametric	FR4-epoxy
[225]	40x34	2.4	0.6	3.8	U shape slites	Cotton
[226]	43.2x43.2	5.2 5.8	0.36 0.15	8.0 8.2	Metasurface based	RO4003
[227] *	50mm diame-ter	1.8 2.5 3.6 5.8	- - - -	2.5 6 2.6 5.9	Pareto–Estra algo-rithm	DuPont Pyralux
This work	14.6x10.8	27.8 30.3 40.1 47.2 56.7	0.69 2.32 2.22 1.76 8.11	10.2 8.4 7.7 9.5 8.4	Genetic algorithm	PTFE

* Results are based on prototype measurement

5.5 Chapter Summary

This chapter contains a compilation of completed works based on the dissertation's core objectives: which are multi-band, bandwidth, and directivity improvement. The computations and simulations were done using a combination of MATLAB and HFSS. The optimization procedure and the comparison of results with relevant previous studies were discussed. The algorithm has demonstrated the capacity of increasing a single antenna to function in several bands, as presented in tri-band, quad-band, and penta-band microstrip antennas.

The proposed tri-band antenna operates at 27.8-28.3 GHz, 38.4-40.6 GHz, and 46.8-47.2 GHz with peak directivity of 7.7 dB, 12.1 dB, and 8.2 dB at the center frequency, respectively. In optimization of a quad-band microstrip antenna for mm-wave wireless communication, the proposed antenna resonates at four distinct bands: 27.9 GHz–28.8 GHz, 37.1 GHz–39.4 GHz, 45.9 GHz–47.5 GHz, and 57.8 GHz–64.5 GHz. In all the

operating bands, a genetically optimized microstrip antenna performs admirably. The penta-band antenna work aimed to optimize and analyze a novel mm-wave textile-based antenna for wearable applications. A binary-coded genetic algorithm was utilized to optimize the reference patch geometry targeted to enhance the multi-band operation and widen the bandwidth. The improved antenna was simulated in free space and at various distances from a phantom human body model. In free space simulation, the antenna operates in five bands: 27.43-28.12 GHz, 28.94-31.26 GHz, 39.27-41.49 GHz, 46.44-48.2 GHz, and 53.83-61.94 GHz a total bandwidth of 15.11 GHz. The broadside directivity was 10.3, 8.5, 7.8, 9.6, and 8.9 dB in the respective bands. The gain was highly affected when the antenna was close to the human body model compared to free space findings. In addition, the antenna was tested on various flexible textile substrates such as cotton, jeans, silk, and polyester. The result shows that the antenna has adequate bandwidth coverage in all five distinct bands with sufficient gain.

In a nutshell, genetic algorithms were applied for the optimization of a multi-band microstrip antenna to maximize directivity and minimize return losses at desired frequencies by avoiding complicated feeding systems and losses caused by the antenna array.

Chapter 6

Conclusion and Recommendation for Future work

6.1 Conclusions

The need for high directive, broadband, multi-band microstrip antennas to accommodate the exponential increase in mm-wave wireless communication at a small size, affordable price, and acceptable performance served as the driving force behind the research detailed in this dissertation. The primary focus of this dissertation is the synthesis, optimization, and analysis of multi-band, high directive, and broadband microstrip patch geometry structures for mm-wave wireless communications applications.

The dissertation starts by outlining the reader via motivational points and research problems surrounding the mm-wave antenna. The research then provided a comprehensive review of the low-profile, low-cost, simply integrated, and well-built microstrip antenna. The antenna is investigated from various perspectives, including performance indicators, design principles, analytical approaches, and performance improvement strategies. Numerous optimization strategies and methods for increasing performance have been reported. Furthermore, the dissertation focuses on how to use a binary-coded representation in genetic algorithm optimization approaches. It describes phases of a genetic algorithm and optimization processes for microstrip antennas, as well as HFSS and MATLAB interface.

The proposed optimization algorithm has proven to be a feasible method for reducing design time while merely boosting the provided performance parameter of a microstrip antenna. The convergence of the optimization technique records a better understanding of the influence of the microstrip patch antenna design variables by providing an evaluation of the performance impact compared to candidate variables. As a result, many multi-band microstrip patch antennas with varying performance are synthesized using the optimization technique, and parametric analysis is carried out to ensure the optimal design of the reference antenna from a single element. In this dissertation, six distinct multi-band antenna designs are synthesized with bandwidth and directivity improvement. Throughout the study time, the author's original work included a full set of binary-coded genetic algorithm optimization algorithms suited for improving microstrip patch antennas modeled in the HFSS simulation software. Using a combination of MATLAB and HFSS,

the algorithm can create and evaluate advanced microstrip patch antenna configurations. The binary-coded genetic algorithm optimizer was successful in driving microstrip antennas to resonate at the desired frequencies while also enhancing operating bandwidths and directivities. Different binary-coded GA runs revealed that the patch surface division size of the antenna, position of conducting and non-conducting cells on the patch surface, and dimensions of cells in the radiating element all play an important role in determining the microstrip patch antenna performance. The binary-coded GA optimizer exhibited significant advantages in quickly assessing whether the provided parameters are suitable for optimization and what is possible with antenna configurations. The optimizer liberates researchers from the time-consuming and unpredictable trials of manual optimization, allowing them to be faster, more inventive, and more efficient when optimizing antennas for future mm-wave wireless communications.

The dissertation proposes and investigates three dual-band microstrip antennas with diverse patch geometry layouts for mm-wave wireless applications. The GA optimizer was developed to generate a high-directional dual-band patch antenna element from a range of cell shapes, including rectangular and circular cells. The circular cells model resulted in a high-directivity antenna with a directivity of 8.6 dB and 10.9 dB at resonance frequencies of 28.0 GHz and 31.1 GHz, respectively. The proposed antenna, which was designed by small rectangle cells, achieved 8.6 dB and 9.0 dB at their respective center frequencies of 28.0 GHz and 46.6 GHz. Patch geometry optimization is heavily influenced by the distribution of genes used to represent an individual. There is also a research task to establishing a dual-band microstrip antenna with bandwidth improvement. It was achieved by optimizing a 0.73 x 0.86 λ^2 patch antenna. The overall operational bandwidth is 4.9 GHz across both working bands (38.5 GHz - 40.1 GHz and 49.0 GHz - 52.3 GHz), with adequate additional performance. To summarize, a binary-coded genetic algorithm was effectively applied to increase the directivity and bandwidth of a dual-band mm-wave microstrip patch antenna.

An extension of optimization was conducted for a tri-band mm-wave rectangular microstrip patch antenna using a binary-coded genetic algorithm with the added quality of a high directive investigation. In the finding, a genetically engineered antenna was achieved with a triple band operation at working bands of 27.8-28.3 GHz, 38.4-40.6 GHz, and 46.8-47.2 GHz. The tri-band antenna operates at the center frequency of 28 GHz, 40 GHz, and 47 GHz with peak directivity of 7.7 dB, 12.15 dB, and 8.25 dB, respectively. The corresponding total efficiencies of a proposed antenna were 61.2 % at 28 GHz, 44.5 % at 40 GHz, and 59.3 % at 47 GHz. However, the efficiencies of the antenna can be enhanced by employing a low-loss tangent substrate. The study also reveals that a lossy substrate isn't recommended for mm-wave antennas. Another study in the dissertation was conducted by employing GA with a small number of genes and forcing them to resonate at quad-band using a simplified fitness function and low processing time. The

quad-band microstrip antenna was developed via 36 genes in 40.3 hours over 100 generations. The quad-band antenna could work at four distinct frequencies: 27.9 GHz-28.8 GHz, 37.1 GHz-39.4 GHz, 45.9 GHz-47.5 GHz, and 57.8 GHz-64.5 GHz. It has a maximum total bandwidth of 11.5 GHz with broadside directivity of 7.8 dB, 8.8 dB, 7.3 dB, and 7.1 dB at resonance frequencies of 28.3GHz, 38.1GHz, 46.6GHz, and 60.0GHz. The proposed antennas have adequate bandwidth, gain, and radiation patterns. As a result, the improved antennas are a viable option for wireless mm-wave applications.

This dissertation described a novel genetically generated penta-band mm-wave microstrip antenna configuration with increased bandwidth. The synthesized antenna is particularly optimized for mm-wave wearable wireless applications. The radiating patch was 10.8 mm long by 14.6 mm wide and placed on a PTFE flexible fabric substrate. The study was carried out in both free space and on-body simulation. In free space simulation, the antenna operates in five bands: 27.43-28.12 GHz, 28.94-31.26 GHz, 39.27-41.49 GHz, 46.44-48.2 GHz, and 53.83-61.94 GHz. At five resonance center frequencies of 27.8 GHz, 30.3 GHz, 40.1 GHz, 47.2 GHz, and 56.7 GHz, the optimized antenna attained peak broadside directivity of 10.3, 8.5, 7.8, 9.6, and 8.9 dB, respectively. It implies that the optimized antenna achieves the bandwidth augmentation objective besides the penta-band operating stipulation on the fabric substrate with acceptable directivity.

The study was expanded to evaluate the enhanced antenna performance in other flexible fabric substrates such as cotton, silk, polyester, and jeans. The results reveal that the optimized antenna resonated in five distinct frequency bands across all textiles, notwithstanding a little shift caused by the dielectric properties of other fabrics compared to the PTFE substrate. The optimized antenna has enough bandwidth coverage and good directivity in all working bands. The on-body simulation was also performed to assess the modified antenna's performance. It was accomplished by building a human phantom model with three distinct layers: skin, fat, and muscle, each with thicknesses of 2 mm, 3 mm, and 5 mm. The simulation was carried out at various distances from the phantom model. The finding indicated that the human body's lossy nature drastically impacted the performance of wearable antennas when simulated close to the phantom model against free space simulation. In general, the optimized antenna is suitable for wireless penta-band mm-wave wearable device

Finally, the dissertation investigated the different structures of microstrip antennas by employing a binary-coded genetic algorithm that can be most appropriate for mm-wave wireless communication. It is believed that this research is vital and can assist researchers, antenna designers, and engineers to easily synthesize, optimize, analyze, and design microstrip antennas for mm-wave wireless communication. In summary, a binary-coded genetic algorithm was applied to improve the performance of the microstrip antenna in terms of its multi-band properties for multi-functionality, bandwidth improvement, and high directivity from a single antenna element. The algorithm greedily searches for the

best-fitted individual antenna based on the designed cost function, which will minimize the design complexity and losses caused by different structures added to enhance the performance of the microstrip antenna.

6.2 Challenges and Limitations

The study of practical wireless system design and measurement at mm-wave frequencies is still in its infancy. The AAiT laboratory does not have the RF testing equipment for mm-wave wireless systems, such as a Vector Network Analyzer (VNA), connectors, adapters, cables, an echo chamber, etc. Even yet, this dissertation has only offered simulation findings since laboratory materials are both too expensive and unavailable. Even in the country, there is no opportunity for the prototype fabrication and testing of the optimized antenna. This issue has prevented testing and actual measurements at mm-wave frequencies from validating improved antennas and their uses for the current study.

6.3 Recommendation for Future Work

For future work, the investigation and conclusions acquired in this thesis may be separated into two sections. Some work remains to be done in phase one to improve the optimization effectiveness and efficiency of the established genetic algorithm. In phase two, various potential future research pathways for improving the performance of microstrip antennas in the mm-wave frequency range and beyond will be investigated

6.3.1 Increasing Efficiency and Effectiveness of GA

Despite the fact that the suggested binary-coded genetic algorithm optimization strategy is insufficient to deal with the increasing complexity of antenna challenges, it remains a promising tool that might be improved in the future by upgrading the methodology to fit more demanding applications. Many of the expansions and adjustments published in the literature may be used for this optimization approach to strengthen its resilience and ability to optimize more complicated antenna designs and challenges, such as multi-band, high directive, and broadband antennas. As a result, the following ideas and concepts may be used to explain future work on the proposed algorithm:

Parallel genetic algorithm:

The concept of parallel GA has been proposed in the literature that using multiple populations increases the quality of genetic algorithm findings and reduces computational time when compared to results generated using a single population genetic algorithm. A parallel genetic algorithm model divides the population into several sub-populations that

are assigned to different processors. A typical basic genetic algorithm is applied individually to each processor's subgroup. Individuals periodically move among sub-populations to exchange between the group. However, the concept of parallel GA hasn't been implemented yet, particularly in antenna optimization. Hence, the future studies of this dissertation will include multiple parallel populations processed at a time to increase the qualities and search accuracy, and to decrease the processing time of genetic algorithm in optimization microstrip antenna.

Multi-objective GA:

In complicated problems, it isn't possible to include many objective functions into a single cost function. So it is demanded to use multi-objective optimization instead of the usual single-objective cost function. In the context of antenna refinement, multiple objectives may be incorporated in terms of improving multi-band, gain, bandwidth, radiation efficiency, antenna size, input impedance, and directivity. Rather than addressing antenna problems separately using single objective methods as usual, it is preferable to improve the notion of GA through multi-objective optimization in order to tackle more antenna problems at once in the future.
Incorporating other feasible approaches to the binary-coded genetic algorithm may be improved further to minimize computing time and boost searching speed. To solve increasingly complex issues rapidly and with greater computational efficiency, the ideas of multi-objective genetic algorithm and parallel genetic algorithm were created. Future work will concentrate on the high-level genetic algorithm-based optimizations required to handle increasingly complicated problems with varying objective costs utilizing computationally efficient machines.

6.3.2 Further Improving Performance of mm-wave antenna

The mm-wave antennas examined throughout this research have been made using the microstrip patch antenna technique with a finite metallic ground plane. Even though mm-wave wireless communication uses microstrip antennas because of their many benefits, these technologies still need to be improved in terms of gain and directivity, bandwidth, and multiband operation in various techniques. Alternative concepts outside genetic algorithms or approaches in combination can be taken into consideration as future work to minimize the complexity and size of the antenna without suffering a penalty for decreasing bandwidth and directivity. Beyond what this dissertation has accomplished, future studies need to focus on expanding the number of operational bands beyond penta-band with outstanding performance and improving the directivity and bandwidth of microstrip antennas.
Future research will need to focus on improving antenna performance by combining ge-

netic algorithms with other performance-improving techniques, such as changing the ground plane with electromagnetic bandgap (EBG) structures, applying the idea of a high impedance surface with a photonic band gap (PBG), or using metamaterial structures, which are periodic structures that may stop electromagnetic waves from traveling in specific directions and frequency ranges. A great contender for creating low-profile, high-efficiency antennas is the high-impedance surface because it aids in suppressing surface waves on the ground plane of the antennas. This results in high radiation efficiency with minimal backward radiation.

As an outstanding contender for next-generation communication, terahertz frequencies could be included in our future study. In order to further increase microstrip antenna performance in the terahertz region, particularly for multi-band behavior, terahertz antenna difficulties, and performance improvement strategies could be studied during a future phase of research.

References

[1] P. Popovski, "A perspective on time toward wireless 6g," *Proceedings of the IEEE*, vol. 110, pp. 1116–1146, 2022.

[2] H. Tataria, M. Shafi, A. F. Molisch, M. Dohler, H. Sjöland, and F. Tufvesson, "6g wireless systems: Vision, requirements, challenges, insights, and opportunities," *Proceedings of the IEEE*, vol. 109, pp. 1166–1199, 2021.

[3] X.You, "Towards 6g wireless communication networks: Vision, enabling technologies, and new paradigm shifts," *China Information Sciences*, vol. 64, pp. 1–74, 2021.

[4] Agrawal, S. Kumar, and K. Sharma, "5g millimeter wave (mmwave) communications," *in 3rd International Conference on Computing for Sustainable Global Development*, vol. India, 2016.

[5] Dicandia, F. Alessio, N. J. Fonseca, M. Bacco, S. Mugnaini, and S. Genovesi, "Space-air-ground integrated 6g wireless communication networks: A review of antenna technologies and application scenarios," *Sensors*, vol. 22, pp. 31–36, 2022.

[6] M. A. Ullah, R. Keshavarz, M. Abolhasan, J. Lipman, K. P. Esselle, and N. Shariati, "A review on antenna technologies for ambient rf energy harvesting and wireless power transfer: Designs, challenges and applications," *IEEE Access*, vol. 10, pp. 17 231–17 267, 2022.

[7] Shareef, O. Ahmed, A. M. A. Sabaawi, K. S. Muttair, M. F. Mosleh, and M. B. Almashhdany, "Design of multi-band millimeter wave antenna for 5g smartphones," *Indonesian Journal of Electrical Engineering and Computer Science*, vol. 25, pp. 382–387, 2022.

[8] A. S. Omar, A. A. Saraira, Q. H. Alsafasfeh, and A. Arfoa, "Bio-inspired algorithms applied on microstrip patch antennas: A review," *International Journal on Communications Antenna and Propagation*, vol. 6, pp. 336–347, 2016.

[9] Ahmad, Iftikhar, W. Tan, Q. Ali, and H. Sun, "Latest performance improvement strategies and techniques used in 5g antenna designing technology, a comprehensive study," *Micromachines*, vol. 13, pp. 7–17, 2022.

[10] Haupt and R. L., "Antenna design with a mixed integer genetic algorithm," *IEEE Transactions on Antennas and Propagation*, vol. 55, pp. 577–582, 2007.

[11] Y. Choongil, G. D. Jo, Y.-J. Ko, and H. K. Chung, "Perspectives on 6g wireless communications," *ICT Express*, vol. 2022, 2022.

[12] L. Xinying, J. Yu, and G.-K. Chang, "Photonics-aided mm-wave communication for 5g," *in Optical Fiber Communications Conference and Exhibition (OFC)*, 2019.

[13] N. A. Hussain and S. Lim., "Review of recent phased arrays for millimeter-wave wireless communication," *Sensors*, vol. 18, p. 3194, 2018.

[14] M.-B. Marja, S. Yrjölä, and P. Ahokangas, "Spectrum management in the 6g era: The role of regulation and spectrum sharing," *in the 2nd 6G Wireless Summit*, 2020.

[15] F. Rob, "Why has multilateral space and spectrum resource management become more difficult," *Available at SSRN: http://dx.doi.org/10.2139/ssrn.4180784*, 2022.

[16] F. Team, "Fcc online table of frequency allocations," *Federal Communications Commission Office Of Engineering And Technology Policy And Rules Division*, 2022.

[17] K. Guoqin, H. Liu, and K. Li, "Analysis on the new progress of spectrum planning of imt-2020 (5g)," *Journal of Physics: Conference Series*, vol. 1437, pp. 12–16, 2020.

[18] P. Natale, S. Lagén, B. Bojović, and L. Giupponi, "Nr-u and ieee 802.11 technologies coexistence in unlicensed mm-wave spectrum: Models and evaluation," *IEEE access*, vol. 8, pp. 71 254–71 271, 2020.

[19] I. Team, "Studies on frequency-related matters for international mobile telecommunications identification including possible additional allocations to the mobile services on a primary basis in portion (s) of the frequency range between 24.25 and 86 ghz," *in for the future development of International Mobile Telecommunications for 2020 and beyond, Resolution 238*, vol. Geneva, 2015.

[20] W. Xiong, L. Kong, F. Kong, F. Qiu, M. Xia, S. Arnon, and G. Chen, "Millimeter wave communication: A comprehensive survey" ieee communications surveys & tutorials," *in for the future development of International Mobile Telecommunications for 2020 and beyond, Resolution 238*, vol. 20, pp. 1616–1653, 2018.

[21] K. Juha, M. Nekovee, H. Benn, W. Kim, J. Park, and H. Sungsoo, "Challenges and opportunities of mm-wave communication in 5g networks," *in 9th international conference on cognitive radio oriented wireless networks and communications*, 2014.

[22] C.Seker, M.T.Güneser, and T.Ozturk, "A review of millimeter wave communication for 5g," *in 2nd International Symposium on Multidisciplinary Studies and Innovative Technologies*, 2018.

[23] Y. Xing, T. S. Rappaport, and A. Ghosh, "Millimeter wave and sub-thz indoor radio propagation channel measurements, models, and comparisons in an office environment," *IEEE Communications Letters*, vol. 25, pp. 3151–3155, 2021.

[24] A. Ayham, "A survey on the effects of human blockage on the performance of mm wave communication systems," *in IEEE International Black Sea Conference on Communications and Networking (BlackSeaCom)*, 2022.

[25] K. M. Muhammad, "Infinity shell shaped mimo antenna array for mm-wave 5g applications," *Electronics*, vol. 10, 2022.

[26] W. Haichaoa, N. Deng, and M. Haenggi, "Performance analysis of inter-cell interference coordination in mm-wave cellular networks," *IEEE Transactions on Wireless Communications*, vol. 21, pp. 726–738, 2022.

[27] A. Dejen, M. Ridwan, J. Anguera, and J. Jayasinghe, "Millimeter wave cellular communication performances and challenges: A survey," *EAI Endorsed Transactions on Mobile Communications and Applications*, vol. 7, 2022.

[28] Q. Xue, X. Fang, M. Xiao, and L. Yan, "Multiuser millimeter wave communications with nonorthogonal beams," *IEEE Transactions on Vehicular Technology*, vol. 66, pp. 5675–5688, 2017.

[29] A. Dejen, J. Anguera, M. Ridwan, and J. Jayasinghe, "Genetically engineered dual-band microstrip antenna with improved directivity for 5g mm-wave mobile applications," *in 1st IEEE International Women in Engineering Symposium*, vol. SRI LANKA, 2020.

[30] A. Dejen, J. Jayasinghe, M. Ridwan, and J. Anguera, "Optimization of dualband microstrip mm-wave antenna with improved directivity for mobile application using genetic algorithm," *in 9th International Conference on Advances of Science and Technology*, vol. Bahir Dar, 2021.

[31] A. Dejen, J.Jayasinghe, M. Ridwan, and J. Anguera, "Genetically engineered triband microstrip antenna with improved directivity for mm-wave wireless application," *AIMS Electronics and Electrical Engineering*, vol. 6, pp. 1–15, 2022.

[32] A. Dejen, J. Anguera, J. Jayasinghe, and M. Ridwan, "Bandwidth improvement of dual-band microstrip mm-wave antenna using genetic algorithm," *International Journal of Computing and Digital Systems*, vol. 13(1), pp. 1–7, 2023.

[33] A. Dejen, J. Jayasinghe, M. Ridwan, and J. Anguera, "Genetically optimized quadband mm-wave microstrip patch antenna," *In 7th International Conference on Micro-Electronics, Electromagnetics and Telecommunications*, vol. presented, 2023.

[34] A. Dejen, M. Ridwan, J. Jayasinghe, and J. Anguera, "Multi-band mm-wave wearable antenna synthesized with a genetic algorithm," *International Journal of Antennas and Propagation*, vol. 2022, pp. 1–17, 2022.

[35] D. John and L. Volakis, "Antenna engineering handbook," *McGraw-Hill*, vol. fourth edithion, New York, USA, 2007.

[36] J. C. Maxwell, "A treatise on electricity and magnetism," *Oxford Univ. Press*, vol. London, U.K, 1904.

[37] C. Balanis, "Antenna theory: A review," *Proceedings of the IEEE*, vol. 80, 1992.

[38] T. A. Milligan, "Modern antenna design," *A JOHN WILEY & SONS, INC*, vol. Canada, 2005.

[39] B. D. Patel, "Microstrip patch antenna a historical perspective of the development," *in Conference on Advances in Communication and Control Systems*, vol. CAC2S 2013, Atlantis Press, 2013.

[40] S. I. Naqvi, "An integrated antenna system for 4g and millimeter-wave 5g future handheld devices," *IEEE Access*, vol. 7, 2019.

[41] M. Sharma., "Design of multiband circularly/linearly polarized antenna for multiple wireless (wwan/bluetooth/wimax/wlan/downlink satellite system)," *International Journal of Microwave and Wireless Technologies*, vol. 11, p. 967–974, 2019.

[42] E. P.Ogherohwo, S. D. Mado, and M. Y. Eggah, "Design and analysis of meander microstrip antenna at wireless band," *Journal of Natural Science and Integration*, vol. 5, pp. 112–117, 2015.

[43] AL-Amoudi and M. Abdulrahman, "Study, design, and simulation for microstrip patch antenna," *International Journal of Applied Science and Engineering Review (IJASER)*, vol. 2, pp. 1–29, 2021.

[44] S. Indrasen and V. S. Tripathi, "Micro strip patch antenna and its applications: a survey," *International Journal of Applied Science and Engineering Review*, vol. 2, pp. 1595–1599, 2011.

[45] M. Anuj, "Microstrip antenna," *International Journal Of Scientific & Technology Research*, vol. 4, pp. 54–57, 2015.

[46] A. S.Mohammed, S. Kamal, M. F. Ain, Z. A. Ahmad, U. Ullah, M. Othman, and R. Hussin, "Microstrip patch antenna: A review and the current state of the art," *Journal of Advanced Research in Dynamical and Control Systems*, vol. 11, pp. 510–524, 2019.

[47] L. Warren and G. A. Thiele., "Antenna theory and design," *John Wiley & Sons*, 2012.

[48] T. F. A. Nayna, A. K. M. Baki, and F. Ahmed, "Comparative study of rectangular and circular microstrip patch antennas in x band," *in International Conference on Electrical Engineering and Information & Communication Technology*, vol. Dhaka, Bangladesh, 2014.

[49] K. Anzar and R. Nema, "Analysis of five different dielectric substrates on microstrip patch antenna," *International journal of computer applications*, vol. 55, 2012.

[50] P. L. Chandra, M. S. Hosain, S. Sarker, M. H. Prio, M. Morshed, and A. K. Sarkar, "The effect of changing substrate material and thickness on the performance of inset feed microstrip patch antenna," *American Journal of Networks and Communications*, vol. 4, pp. 54–58, 2015.

[51] A.Bansal and R. Gupta, "A review on microstrip patch antenna and feeding techniques," *International Journal of information technologies*, vol. 12, pp. 149–154, 2020.

[52] James and J. R, "Handbook of microstrip antennas," *IET*, 1989.

[53] G. Ramesh, P. Bhartia, I. J. Bahl, and A. Ittipiboon, "Microstrip antenna design handbook," *Artech house*, 2001.

[54] C. A. Balanis, "Modern antenna handbook," *Artech house*, vol. John Wiley & Sons, 2011.

[55] M. Ranjan, "An overview of microstrip antenna," *HCTL Open International Journal of Technology Innovations and Research (IJTIR)*, vol. 21, pp. 39–55, 2016.

[56] H. Mohamed, J. P. Daniel, and C. Terret, "Analysis of aperture-coupled microstrip antenna using cavity method," *Electronics Letters*, vol. 25, p. 391, 1989.

[57] R. Mishra, "An overview of microstrip antenna," *HCTL Open International Journal of Technology Innovations and Research (IJTIR)*, vol. 21, pp. 39–55, 2016.

[58] H. L. Peng, Z. Tang, Y. P. Zhang, and J. F. Mao, "Cavity model analysis of a dual-probe-feed circular microstrip patch antenna," *IEEE Antennas and Wireless Propagation Letters*, vol. 15, pp. 44–47, 2016.

[59] J. Gomez-Tagle and C. G. Christodoulou, "Extended cavity model analysis of stacked microstrip ring antennas," *IEEE Transactions on Antennas and Propagation*, vol. 45(11), pp. 1626–1635, 1997.

[60] C. J. Joseph and W. George, "Practical antenna handbook," *McGraw-Hill Education*, 2012.

[61] J. Geng and R. Jin, "Antenna optimization and design based on binary coding," *Springer Nature*, 2022.

[62] G. C. Walton, "The method of moments in electromagnetics," *Chapman and Hall/CRC*, 2021.

[63] E.Newman and P. Tulyathan, "Analysis of microstrip antennas using moment methods," *IEEE Transactions on Antennas and Propagation*, vol. 29(1), pp. 47–53, 1981.

[64] R. C. M. Pimenta, M. V. Africano, R. Adriano, and C. Resende, "3d cuda fdtd based method for analysis of microstrip antennas," *in 2017 SBMO/IEEE MTT-S International Microwave and Optoelectronics Conference (IMOC)*, 2017.

[65] N. Eisuke, M. Aikawa, and S. Egashira, "Fdtd analysis of stacked microstrip antenna with high gain," *Progress in electromagnetic research*, vol. 33, pp. 29–43, 2001.

[66] E. S. Khabbat, S. O. Hasan, and M. M. Ameen, "Microstrip patch antenna design, simulation and fabrication for 5g applications," *Simulation Modelling Practice and Theory*, vol. 116, p. 102497, 2022.

[67] S. Angana, K. Sarmah, and K. K. Sarma, "Low return loss slotted rectangular microstrip patch antenna at 2.4 ghz," *in 2nd International Conference on Signal Processing and Integrated Networks (SPIN)*, 2015.

[68] C. John and R. Lohani, "Design and implementation of microstrip patch antenna for 5g applications," *in 5th International Conference on Communication and Electronics Systems (ICCES)*, 2020.

[69] H. Sonia, C. C. Tripathi, and R. Rishi, "Impedance matching techniques for microstrip patch antenna," *Indian Journal of Science and Technology*, vol. 10(28), pp. 1–16, 2017.

[70] S. Gurdeep and J. Singh, "Comparative analysis of microstrip patch antenna with different feeding techniques," *in International Conference on Recent Advances and Future Trends in Information Technology*, 2012.

[71] Y. Huang and K. Boyle, "Antennas from theory to practice," *John Wiley & sons*, 2008.

[72] J. Anguera, C. Puente, C. Borja, and J. Soler, "Fractal-shaped antennas: a review," *Wiley Encyclopedia of RF and Microwave Engineering*, vol. 2, pp. 1620–1635, 2005.

[73] P. M. Teresa and G. Umamaheswari, "Compact slotted microstrip antenna for 5g applications operating at 28ghz," *IETE Journal of Research*, vol. 68(5), pp. 3778–3785, 2022.

[74] C. Borja, G. Font, S. Blanch, and J. Romeu, "High directivity fractal boundary microstrip patch antenna," *Electronics Letters*, vol. 36(9), 2000.

[75] J. Anguera, A. Andújar, and J. Jayasinghe, "High-directivity microstrip patch antennas based on tmodd-0 modes," *IEEE Antennas and Wireless Propagation Letters*, vol. 19(1), pp. 39–43, 2020.

[76] L.Hakim and M. Faisal, "Design and simulation of a multiband millimeter wave microstrip patch antenna array for 5g wireless communication," *in 22nd International Conference of Computer and Information Technology (ICCIT)*, 2019.

[77] L. Antti, J. Säily, J. Ala-Laurinaho, J. de Cos, and V. Ermolov, "Patch antenna and antenna array on multilayer high-frequency pcb for d-band," *IEEE Open Journal of Antennas and Propagation*, vol. 1, pp. 396–403, 2020.

[78] S. Wangyu, Y. Li, L. Chang, H. Li, X. Qin, and H. Wang, "Dual-band dual-polarized microstrip antenna array using double-layer gridded patches for 5g millimeter-wave applications," *IEEE Transactions on Antennas and Propagation*, vol. 69(10), pp. 6489–6499, 2021.

[79] T. Shaw, D. Bhattacharjee, and D. Mitra, "Gain enhancement of slot antenna using zero-index metamaterial superstrate," *Int. J. RF Microw.Comput.-Aided Eng*, vol. 27(4), pp. 1–10, 2017.

[80] Ziolkowski and R. W, "Electrically small antenna advances for current 5g and evolving 6g and beyond wireless systems," *Antenna and Array Technologies for Future Wireless Ecosystems*, pp. 335–391, 2022.

[81] A. Bakhtiari, "Investigation of enhanced gain miniaturized patch antenna using near zero index metamaterial structure characteristics," *IETE Journal of Research*, vol. 68(2), pp. 1–8, 2019.

[82] Sağık, A. M., and e. a. O., "Optimizing the gain and directivity of a microstrip antenna with metamaterial structures by using artificial neural network approach," *Wireless Pers Commun*, vol. 118, pp. 109–124, 2021.

[83] R. Kumar and M. Kartikeyan, "Design and simulation of multi band compact microstrip patch antenna," *in IEEE Indian Conference on Antennas and Propogation (InCAP)*, vol. Ahmedabad, India, pp. 26–43, 2019.

[84] H. Suthar, D. Sarkar, K. Saurav, and K. Srivastava, "A high gain and wideband directional antenna using z-shaped near zero-index metamaterial," *in IEEE UP Section Conference on Electrical Computer and Electronics (UPCON)*, 2015.

[85] Ucar and M. HB, "Complementary srr-based reflector to enhance microstrip antenna performance," *The Applied Computational Electromagnetics Society Journal (ACES)*, vol. 36(6), pp. 779–789, 2021.

[86] M. S. Ahmad, C. Y. Kim, and J. G. Park, "Multishorting pins pifa design for multiband communications," *International journal of Antenna and propagation*, pp. 1–10, 2014.

[87] X. Zhang and L. Zhu, "High-gain circularly polarized microstrip patch antenna with loading of shorting pins," *IEEE Transactions on Antennas and Propagation*, vol. 64(6), pp. 2172–2178, 2016.

[88] J. Liu, Z. Tang, Z. Wang, H. Li, and Y. Yin, "Gain enhancement of a broadband symmetrical dual-loop antenna using shorting pins," *IEEE Antennas and Wireless Propagation Letters*, vol. 17(8), pp. 1369–1372, 2018.

[89] H. Errifi, A. Baghdad, and A. S. Abdelmajid Badri, "Directivity enhancement of aperture coupled microstrip patch antenna using two layers dielectric superstrate," *in IEEEProceedings of 2014 Mediterranean Microwave Symposium (MMS2014)*, vol. Marrakech, Morocco, 2014.

[90] K. J. Hee, C.-H. Ahn, and J.-K. Bang, "Antenna gain enhancement using a holey superstrate," *IEEE Transactions on Antennas and Propagation*, vol. 64(3), pp. 1164–1167, 2016.

[91] A. K. Singh, M. P. Abegaonkar, and S. K. Koul, "High-gain and high-aperture-efficiency cavity resonator antenna using metamaterial superstrate," *IEEE Antennas and Wireless Propagation Letters*, vol. 16, pp. 2388–2391, 2017.

[92] H. Niamat, U. Azimov, M. Jeong, S. Rhee, S. W. Lee, and N. Kim, "A high-gain microstrip patch antenna using multiple dielectric superstrates for wlan applications," *The Applied Computational Electromagnetics Society Journal (ACES)*, vol. 35(2), pp. 187–193, 2020.

[93] W. Abdul, A. Ahmad, S. Ullah, D. you Choi, and F. U. Islam, "Performance analysis of wearable dual-band patch antenna based on ebg and srr surface," *MDPI Sensors*, vol. 22(14), p. 5208, 2022.

[94] M. M. Mohanna, "A novel high directive willis-sinha tapered slot antenna for gpr application in detecting landmine," *Progress In Electromagnetics Research C*, vol. 80, pp. 181–198, 2018.

[95] L. Xiang-yu, J. Li, J. jun Tang, X. liang Wu, and Z. xiang Zhang, "High gain microstrip antenna design by using fss superstrate layer," *in 4th International Confer-*

ence on Computer Science and Network Technology (ICCSNT), vol. Harbin, China, 2015.

[96] R. Krishna, R. V. S., and R. Kumar, "Slotted ground microstrip antenna with fss reflector for high-gain horizontal polarisation," *Electronics Letters*, vol. 51(8), pp. 599–600, 2015.

[97] L. Kurra, M. P. Abegaonkar, A. Basu, and S. K. Koul, "Fss properties of a uniplanar ebg and its application in directivity enhancement of a microstrip antenna," *IEEE Antennas and Wireless Propagation Letters*, vol. 15, pp. 1606–1609, 2016.

[98] J. Anguera, E. Martínez, C. B. Carles Puente, and J. Soler, "Broad-band triple-frequency microstrip patch radiator combining a dual-band modified sierpinski fractal and a monoband antenna," *IEEE Transactions on Antennas and Propagation*, vol. 54(11), pp. 3367–3373, 2006.

[99] Y.Ghazaoui, A. E. Alami, M. E. Ghzaoui, D. B. S. Das, and S. Mohapatra, "Millimeter wave antenna with enhanced bandwidth for 5g wireless application," *Journal of Instrumentation*, vol. 15(1), p. T01003, 2020.

[100] A.-A. Ahmad and Y. S. Khraisat, "Bandwidth enhancement of microstrip patch antenna," *Applied Physics Research*, vol. 11(1), pp. 35–40, 2019.

[101] W. Y. Yong, A. Haddadi, T. Emanuelsson, and A. A. Glazunov, "A bandwidth-enhanced cavity-backed slot array antenna for mmwave fixed-beam applications," *IEEE Antennas and Wireless Propagation Letters*, vol. 19(11), pp. 1924–1928, 2020.

[102] J. Anguera, C. Puente, C. Borja, and J. Soler, "Dual frequency broadband stacked microstrip antenna using a reactive loading and a fractal-shaped radiating edge," *IEEE Antennas and Wireless Propagation Letters*, vol. 6, pp. 309–312, 2007.

[103] Abdelaziz and Abdelmonem, "Bandwidth enhansment of microstrip antenna," *Progress In Electromagnetics Research*, vol. 63, pp. 311–317, 2006.

[104] K. D. Xu, H. Xua, Y. Liu, J. Li, and Q. H. Liu, "Microstrip patch antennas with multiple parasitic patches and shorting vias for bandwidth enhancement," *IEEE Access*, vol. 6, pp. 11 624–11 633, 2018.

[105] Y. Sumin, D.-Y. Kim, and S. Nam, "Bandwidth and efficiency enhancement of cavity-backed slot antenna using a substrate removal," *IEEE Antennas and Wireless Propagation Letters*, vol. 11, pp. 1458–1461, 2012.

[106] J. M. Kovitz and Y. Rahmat-Samii, "Using thick substrates and capacitive probe compensation to enhance the bandwidth of traditional cp patch antennas," *IEEE Transactions on Antennas and Propagation*, vol. 62(10), 2014.

[107] M. A. SB, S. Kamal, M. F. bin Ain, R. Hussin, Z. A. Ahmad, U. Ullah, M. Othman, and M. F. A. Rahman, "Mathematical modelling on the effects of conductive material and substrate thickness for air substrate microstrip patch antenna," *The Applied Computational Electromagnetics Society Journal (ACES)*, vol. 35(6), pp. 674–683, 2020.

[108] A. S. Mohammed, S. Kamal, M. F. B. Ain, F. Najmi, Z. A. Ahmad, Z. Zahar, R. Hussin, I. A. Zubir, and M. F. A. Rahman, "Improving the gain performance of air substrate patch antenna array using the effect of conductive material thickness study for 5g applications," *Journal of Physics: Conference Series*, vol. 1529(5), pp. 1–9, 2020.

[109] L. Sun, Y. Lu, and G. Ou, "Axial ratio analysis of a multiple-feed microstrip antenna," *in Asia-Pacific Microwave Conference*, 2008.

[110] V. Gatti, Roberto, R. Rossi, and M. Dionigi, "Single-layer line-fed broadband microstrip patch antenna on thin substrates," *Electronics*, vol. 10(1), p. 37, 2020.

[111] L. Wang and Y. F. En, "A wideband circularly polarized microstrip antenna with multiple modes," *IEEE Open Journal of Antennas and Propagation*, vol. 1, pp. 413–418, 2020.

[112] K. M. Kumar, S. Kumar, and B. K. Kanaujia, "Design, modeling and analysis of dual-feed defected ground microstrip patch antenna with wide axial ratio bandwidth," *Journal of Computational Electronics*, vol. 17(3), pp. 1019–1028, 2018.

[113] T. N. Berna, C. Tangel, and A. Y. Teşneli, "Performance improvement of a microstrip patch antenna by using electromagnetic band gap and defected ground structures," *in 2020 International Conference on Electrical, Communication, and Computer Engineering (ICECCE)*, 2020.

[114] A. Ashyap, "Robust and efficient integrated antenna with ebg-dgs enabled wide bandwidth for wearable medical device applications," *IEEE Access*, vol. 8, pp. 56 346–56 358, 2020.

[115] M. Esa, U. Jamaluddin, and M. S. Awang, "Antenna with dgs for improved performance," *in IEEE Asia-Pacific Conference on Applied Electromagnetics (APACE)*, 2010.

[116] J. M. J. W. Jayasinghe and D. Uduwawala, "A novel multiband miniature planar inverted f antenna design for bluetooth and wlan applications," *International Journal of Antenna and Propagation*, 2015.

[117] K. Galib, N. Sarker, and H. Mondal, "Two compact multiband millimetre wave antennas for wireless communication," *in IEEE International Conference on Telecommunications and Photonics (ICTP)*, vol. Dhaka, Bangladesh, 2019.

[118] P. Roy, R. Vishwakarma, A. Jain, and R. Singh, "Multiband millimeter wave antenna array for 5g communication," *in International Conference on Emerging Trends in Electrical, Electronics and Sustainable Energy Systems (ICETEESES–16)*, 2016.

[119] T. Okan, "Design and analysis of a quad-band substrate-integrated waveguide cavity backed slot antenna for 5g applications," *Int.J. RF Microw. Comput.-Aided Eng*, vol. 30(7), 2020.

[120] W. Layla, S. Ibnyaich, and M. M. Hassani, "The study of the ground plane effect on a multiband pifa antenna by using genetic algorithm and particle swarm optimization," *Journal of Microwaves, Optoelectronics and Electromagnetic Applications*, vol. 15, pp. 293–308, 2016.

[121] S. B. a nd S. Sahu, "Frequency reconfigurable antenna inspired by metamaterial for wlan and wimax application," *in IEEE International Conference*, 2014.

[122] won Jung C, L. MJ, and D. F. F. Li GP, "Reconfigurable scan-beam single-arm spiral antenna integrated with rf-mems switches," *IEEE Trans Antennas Propagation*, vol. 54(2), pp. 455–463, 2006.

[123] R. I, F. JM, R. H, and T. H, "Design of a frequency reconfigurable patch antenna using capacitive loading and varactor diode," *in IEEE 9th European Conference*, 2015.

[124] T. H. Karimian R, "Multiband mimo antenna system with parasitic elements for wlan and wimax application," *International Journal of antenna and propagation*, 2013.

[125] K. Y, Shimizu, and M. H., "A small tunable multiband antenna with parasitic elements for mobile applications," *in IEEE-APS Topical Conference*, 2015.

[126] J.-W. Kim, T.-H. Jung, and H.-K. Ryu, "Compact multiband microstrip antenna using inverted-l- and t-shaped parasitic elements," *IEEE Antennas And Wireless Propagation Letters*, vol. 12, pp. 1299–1302, 2013.

[127] S. Asif, A. Iftikhar, M. S. Khan, and D. E. Anagnostou, "A compact multiband microstrip patch antenna with u-shaped parasitic elements," *IEEE antenna transaction and propagation*, vol. 1(15), pp. 617–618, 2015.

[128] F. N. M. Redzwan, M. Ali, M. M. Tan, and N. Miswadi, "Design of tri-band planar inverted f antenna (pifa) with parasitic elements for umts2100, lte and wimax mobile applications," *in IEEE 2015 International Conference on Computer, Communication, and Control Technology*, vol. Malaysia, 2015.

[129] U. Venkateshkumar, S.Kiruthiga, H.Mihitha, K.Maheswari, and M.Nithiyasri, "Multiband patch antenna design for 5g applications," *in Proceedings of the Fourth International Conference on Computing Methodologies and Communication (ICCMC 2020)*, 2020.

[130] R. Kumar and M. Kartikeyan, "Design and simulation of multi band compact microstrip patch antenna," *in 2019 IEEE Indian Conference on Antennas and Propogation (InCAP)*, vol. Ahmedabad, India, 2019.

[131] W. Hussain, M. Khattak, and M. A.K.Khattak, "Multiband microstrip patch antenna for 5g wireless communication," *International Journal of Engineering Works*, vol. 7(1), pp. 15–21, 2020.

[132] A. A, O. Y, and Abdulguddoos, "A low profile multiband microstrip patch antenna for 5g mm-wave wireless application," *in International Conference of Technology, Science and Administration*, 2021.

[133] M. I. Khattak, A. Sohail, U. Khan, Z. Ullah, and G. Witjaksono, "Elliptical slot circular patch antenna array with dual band behaviour for future 5g mobile communication networks," *Progress In Electromagnetics Research C*, vol. 89, pp. 133–147, 2019.

[134] H.-C. Huang, R. Ma, X. Jian, Y. Wang, and Z. Zhu, "A miniaturized band-switching multiband dual-polarized 5g mm-wave antenna-in-package (aip) array for cellular phones," *in 2019 International Symposium on Antennas and Propagation (ISAP)*, 2019.

[135] P. Sunthari and R. Veeramani, "Multiband microstrip patch antenna for 5g wireless applications using mimo techniques," *in 2017 First International Conference on Recent Advances in Aerospace Engineering (ICRAAE)*, 2017.

[136] s.Punith, S. K. Praveenkumar, A. A. Jugale, and M. R. Ahmed, "A novel multiband microstrip patch antenna for 5g communications," *in Third International Conference on Computing and Network Communications (CoCoNet'19)*, 2020.

[137] A.Nadeem, Haraza, and M. Ali, "Optimized broadband and dual-band printed slot antennas for future millimeter wave mobile communication," *in International Journal of Electronics and Communications*, 2015.

[138] J. W. Jayasinghe and D. N. Uduwawala, "A novel miniature multi-frequency broadband patch antenna for wlan applications," *in IEEE 8th International Conference on Industrial and Information Systems*, 2013.

[139] M. Lamsalli, E. Hamichi, M. Boussouis, A. Touhami, and T. Elhamadi, "Genetic algorithm optimization for microstrip patch antenna miniaturization," *Progress In Electromagnetics Research Letters*, vol. 60, pp. 113–120, 2016.

[140] P. Jain, V. Maheshwari, and V. Thakre, "Micro strip patch antenna optimization using genetic algorithm," *International Journal of Engineering Applied Sciences and Technology*, vol. 2(2), pp. 30–33, 2016.

[141] W. Jayasinghe, J. Anguera, and D. N. Uduwawala, "A high-directivity microstrip patch antenna design by using genetic algorithm optimization," *Progress In Electromagnetics Research C*, vol. 37, pp. 131–144, 2013.

[142] D. U. J.M.J.W. Jayasinghe and J. Anguera, "Design of dual band patch antennas for cellular communications by genetic algorithm optimization," *International Journal of Engineering and Technology*, vol. 1, pp. 26–43, 2012.

[143] S. Behera and Y. Choukiker, "Design and optimization of dual band microstrip antenna using particle swarm optimization technique," *Journal of Infrared, Millimeter, and Terahertz Waves*, vol. 31(11), pp. 1346–1354, 2010.

[144] L. Zhang, Z.Cui, Y. C. Jiao, and F. S.Zhang, "Broadband patch antenna design using differential evolution algorithm," *Microwave and Optical Technology Letters*, vol. 51, pp. 1692–1695, 2009.

[145] S. Karimkashi and A. Kishk, "Invasive weed optimization and its features in electromagnetics," *IEEE Transactions on Antennas and Propagation*, vol. 58, pp. 1269–1278, 2010.

[146] Z. Bayraktar, M. Komurcu, Z. H. Jiang, D. H. Werner, and P. L. Werner, "Stub-loaded inverted-f antenna synthesis via wind driven optimization," *in IEEE International Symposium on Antennas and Propagation (APSURSI)*, 2011.

[147] C. M. Coleman, E. J. Rothwell, and J. E. Ross, "Investigation of simulated annealing, ant-colony optimization, and genetic algorithms for self-structuring antennas," *IEEE Transactions on Antennas and Propagation*, vol. 52(4), pp. 1007–1014, 2004.

[148] B. Navaamsini, A. K. Ramasamy, and F. H. Nagi, "Faulty antenna detection in a linear array using simulated annealing optimization," *Indonesian Journal of Electrical Engineering and Computer Science*, vol. 19(3), pp. 1340–1347, 2020.

[149] D. He and Y. Hong, "An improved tabu search algorithm based on grid search used in the antenna parameters optimization," *Mathematical Problems in Engineering*, vol. 2015, pp. 1–8, 2015.

[150] J. Jayasinghe, D. Uduwawala, and J. Anguera, "Increasing the directivity of a microstrip patch array by genetic optimization," *Journal of the National Science Foundation of Sri Lanka*, vol. 43, pp. 83–89, 2015.

[151] T. Orankitanun and S. Yaowiwat, "Application of genetic algorithm in tri-band u-slot microstrip antenna design," *in 2020 17th International Conference on Electrical Engineering/Electronics, Computer, Telecommunications and Information Technology (ECTI-CON)*, vol. 43, pp. 83–89, 2020.

[152] M. R. Gaurav, R. Mishra, P. Kuchhal, and N. P. Kumari, "Analysis of the microstrip patch antenna designed using genetic algorithm based optimization for wide-band applications," *iInternational Journal of Pure and Applied Mathematics*, vol. 118(11), pp. 841–849, 2018.

[153] A. Wyant and J. Venkataraman, "Optimization of reduced size microstrip patch with slots using a genetic algorithm," *in proceeding Computer Science and Business*, 2009.

[154] D. R.Jackson and J. L. Volakis, "Microstrip antennas: Antenna engineering handbook, digital engineering library," *McGraw-Hill*, vol. 80(1), pp. 7–23, 2007.

[155] H. Cheng-Nan, D.-C. Chang, C.-H. Yu, T.-W. Hsaio, and D.-P. Lin, "Millimeter-wave microstrip antenna array design and an adaptive algorithm for future 5g wireless communication systems," *International Journal of antennas and Propagation*, vol. 2016, p. 10, 2016.

[156] A. H.Jabire, A. Abdu, and S. Salisu, "Multiband millimeter wave t-shaped antenna with optimized patch parameter using particle swarm optimization," *Nigerian Journal of Technology*, vol. 36(3), pp. 904–909, 2017.

[157] K.Sastry, D. Goldberg, and G.Kendall, "Genetic algorithms," *in Search Methodologies*, vol. Boston, Springer, pp. 97–126, 2005.

[158] Goldberg and D. Edward, "The design of innovation: Lessons from and for competent genetic algorithms," *Kluwer Academic Publishers*, vol. Boston, Springer, 2002.

[159] Srivastava, P. Ranjan, and T. hoon Kim, "Application of genetic algorithm in software testing," *International Journal of software Engineering and its Applications*, vol. 3(4), pp. 87–96, 2009.

[160] A. V. Mokshin, V. V. Mokshin, and L. M. Sharnin, "Adaptive genetic algorithms used to analyze behavior of complex system," *Communications in Nonlinear Science and Numerical Simulation*, vol. 71, pp. 174–186, 2019.

[161] Hettiarachchi, D. Suresh, N. Noman, and H. Iba, "Messy genetic algorithm for evolving mathematical function evaluating variable length gene regulatory networks," *in 2013 IEEE Congress on Evolutionary Computation*, vol. Cancun, Mexico, 2013.

[162] T. A. El-Mihoub, A. A. Hopgood, L. Nolle, and A. Battersby, "Hybrid genetic algorithms: A review," *Engineering Letters*, vol. 13(2), pp. 124–137, 2006.

[163] Huang and Chien-Feng, "Independent sampling genetic algorithms," *In GECCO*, 2001.

[164] D. Kusum, K. P. Singha, M. L. Kansal, and C. Mohan, "A real coded genetic algorithm for solving integer and mixed integer optimization problems," *Applied Mathematics and Computation*, vol. 212, pp. 505–518, 2009.

[165] J. JM and R.-S. Y, "Genetic algorithms in engineering electromagnetic," *IEEE Antenna and Propagation*, vol. 39, pp. 7–21, 1997.

[166] B. Clayton and D. E. Goldberg, "An analysis of reproduction and crossover in a binary-coded genetic algorithm," *Grefenstette*, 1987.

[167] Kozeny and Vaclav, "Genetic algorithms for credit scoring: Alternative fitness function performance comparison," *Expert Systems with applications*, vol. 42(6), pp. 2998–3004, 2015.

[168] Jayasinghe, J. Anguera, and Uduwawala, "On the behavior of several fitness functions for genetically optimized microstrip antennas," *International Journal of Scientific World*, vol. 3(1), 2015.

[169] Jayasinghe, J. Windhya, D. N. Uduwawala, and J. Anguera, "Increasing the directivity of a microstrip patch array by genetic optimization," *Journal of the National Science Foundation of Sri Lanka*, vol. 43, pp. 904–909, 2015.

[170] K. Sourabh, S. S. Chauhan, and V. Kumar, "A review on genetic algorithm: past, present, and future," multimedia tools and applications," *International Journal of Scientific World*, vol. 80(5), pp. 8091–8126, 2021.

[171] S. Mirjalili., "Genetic algorithm. in: Evolutionary algorithms and neural networks," *Cham, Springer*, vol. 2019, pp. 43–55, 2019.

[172] R. N. Mohd and J. Geraghty., "Genetic algorithm performance with different selection strategies in solving tsp," *in Proceedings of the world congress on engineering*, vol. Hong Kong, China, pp. 43–55, 2011.

[173] A. Shukla, H. M. Pandey, and D. Mehrotra, "Comparative review of selection techniques in genetic algorithm," *in 2015 International Conference on Futuristic Trends on Computational Analysis and Knowledge Management (ABLAZE)*, vol. Greater Noida, India, 2015.

[174] Blickle and Tobias, "Tournament selection in evolutionary computation," *CRC Press*, pp. 181–186, 2000.

[175] H. Ahmad, K. Almohammadi, E. Alkafaween, E. Abunawas, A. Hammouri, and V. S. Prasath, "Choosing mutation and crossover ratios for genetic algorithms a review with a new dynamic approach," *MDPI Information*, vol. 10(12), p. 390, 2019.

[176] Vekaria and K.Clack, "Selective crossover in genetic algorithms: An empirical study," *in Parallel Problem Solving from Nature, Berlin, Heidelberg, Springer*, vol. 10(12), pp. 438–447, 1998.

[177] Abuljadayel and F. Wedyan, "An approach for the generation of higher order mutants using genetic algorithms," *International Journal of Intelligent Systems and Applications*, vol. 12(10), p. 34, 2018.

[178] H. John, "Genetic algorithms," *Scholarpedia*, vol. 7(12), p. 1482, 2012.

[179] G. David and K. Sastry, "A practical schema theorem for genetic algorithm design and tuning," *in Proceedings of the 3rd Annual Conference on Genetic and Evolutionary Computation*, 2001.

[180] A. Wyant and J. Venkataraman, "Optimization of reduced size microstrip patch with slots using a genetic algorithm," *International Journal of Antenna and Propagation*, 2008.

[181] P. Jain, V. Maheshwari, and V. Thakre, "Micro strip patch antenna optimization using genetic algorithm," *International Journal of Engineering Applied Sciences and Technology*, vol. 2(2), pp. 30–33, 2016.

[182] M. Lamsalli, E. Hamichi, M. Boussouis, A. Touhami, and T. Elhamadi, "Genetic algorithm optimization for microstrip patch antenna miniaturization," *Progress In Electromagnetics Research Letters*, vol. 60, pp. 113–120, 2016.

[183] R. G. Mishra, R. Mishra, P. Kuchhal, and N. P. Kumari, "Analysis of the microstrip patch antenna designed using genetic algorithm based optimization for wide-band applications," *International Journal of Pure and Applied Mathematics*, vol. 118(11), pp. 841–849, 2018.

[184] J. Jayasinghe, J.Anguera, and Uduwawala, "Genetic algorithm optimization of a high-directivity microstrip patch antenna having a rectangular profile," *Radioengineering*, vol. 22(3), 2013.

[185] E. David., "Hfss 13: Hybrid fe-bi for efficient simulation of radiation and scattering," *ANSYS Inc*, vol. 22(3), 2011.

[186] Silvestro and John, "Hybrid finite element boundary integral method," *Ansys, Inc.[online]*, vol. Available: https://support. ansys. com , online, 2010.

[187] S. Wang and H. Gao, "A dual-band wearable conformal antenna based on artificial magnetic conductor," *International Journal of Antennas and Propagation*, vol. 2022, p. 8, 2022.

[188] T. Xie, J. Yu, Z. Lin, Y. Li, and a. Z. Y. Guodong Zhang, "A novel dual-band "c+o" structure antenna," *International Journal of Antennas and Propagation*, vol. 2021, p. 8, 2021.

[189] X. Ran, Z. Yu, T. Xie, Y. Li, XiuxiaWang, and P. Huang, "A novel dual-band binary branch fractal bionic antenna for mobile terminals," *International Journal of Antennas and Propagation*, vol. 2020, 2020.

[190] S. Z. R. Rodríguez-Cano and G. F. Pedersen, "Beam-steerable multi-band mm-wave bow-tie antenna array for mobile terminals," *in 12th European Conference on Antennas and Propagation (EuCAP 2018)*, 2018.

[191] U. Rafique, H. Khalil, and Saif-Ur-Rehman, "Dual-band microstrip patch antenna array for 5g mobile communications," *in 2017 Progress in Electromagnetics Research Symposium*, vol. Singapore, pp. 26–43, 2017.

[192] R. Dwivedi and D. Upadhyay, "High gain dual band antenna using fractal geometry for mobile communication," *in 2nd International Conference on Signal Processing and Integrated Networks (SPIN)*, vol. Delhi-NCR, India, 2015.

[193] J. W. Jayasinghe and D. N. Uduwawala, "A novel miniature multi-frequency broadband patch antenna for wlan applications," *in IEEE 8th International Conference on Industrial and Information Systems*, vol. 118(11), 2013.

[194] A. Ghalib, M. U. Khan, M. S. Sharawi, and R. Mittra, "A dual-band frequency selective surface for antenna applications in 5g mobile terminals," *in 2020 IEEE International Symposium on Antennas and Propagation and North American Radio Science Meeting*, vol. Montreal, Canada, 2020.

[195] J. Anguera, G. Montesinos, C. Puete, C. Borja, and J. Soler, "An undersampled high-directivity microstrip patch array with a reduced number of radiating elements

inspired on the sierpinski fractal," *Microwave and Optical Technology Letters*, vol. 37(2), pp. 100–103, 2003.

[196] M. E. Hossain, P. Kirtonia, and M. F. Samad, "A low cost dual-band patch antenna array for future 5g communication applications," *in 1st International Conference on Advances in Science, Engineering and Robotics Technology (ICASERT)*, vol. Dhaka, Bangladesh, 2019.

[197] Z. Haider, M. U. Khan, and H. M. Cheema, "A dual-band metamaterial superstrate for antenna gain enhancement," *in 2018 IEEE International Symposium on Antennas and Propagation USNC/URSI National Radio Science Meeting*, vol. Boston, MA, USA, 2018.

[198] S. J. Franson and R. W. Ziolkowski, "Confirmation of zero-n behavior in a high gain grid structure at millimeter-wave frequencies," *IEEE Antennas And Wireless Propagation Letters*, vol. 8, pp. 387–390, 2009.

[199] M. John and M. J. Ammann, "Design of a wide-band printed antenna using a genetic algorithm on an array of overlapping sub-patches," *in IEEE International Workshop on Antenna Technology Small Antennas and Novel Metamaterials*, 2006.

[200] W.-T. Ding, F. Meng, Y.-B. Tian, and H.-N. Yuan, "Antenna optimization based on auto-context broad learning system," *International Journal of Antennas and Propagation*, vol. Article ID 7338164, p. 10, 2022.

[201] X.-Y. Zhang, Y.-B. Tian, and X. Zheng, "Antenna optimization design based on deep gaussian process model," *International Journal of Antennas and Propagation*, vol. Article ID 2154928, p. 10, 2020.

[202] A. Kapoor and R. Mishra, "Genetic algorithm optimized gain augmented dual band printed antenna for cognitive ehealth care (iomt) applications," *in 2022 IEEE 11th International Conference on Communication Systems and Network Technologies (CSNT)*, 2022.

[203] H.-C. Huang, R. Ma, Y. W. Xianjin Jian, and Z. Zhu, "A miniaturized band-switching multiband dual-polarized 5g mm-wave antenna-in-package (aip) array for cellular phones," *in 2019 International Symposium on Antennas and Propagation (ISAP)*, 2019.

[204] M. B.Almashhdany, O. A. Al-Ani, and A. M. A. Sabaawi, "Design of multi-band slotted mmwave antenna for 5g mobile applications," *in 3rd International Conference on Sustainable Engineering Techniques (ICSET 2020)*, vol. Canada, 2020.

[205] M. I. Khattak, A. Sohail, U. Khan, Z. Ullah, and G. Witjaksono, "Elliptical slot circular patch antenna array with dual band behaviour for future 5g mobile commu-

nication networks," *Progress In Electromagnetics Research C*, vol. 89, pp. 133–147, 2019.

[206] Y. Lv, F. Cao, X. Feng, and H. Li, "Improved binary particle swarm optimization and its application to beamforming of planar antenna arrays," *Progress In Electromagnetics Research C*, vol. 114, pp. 217–231, 2021.

[207] J. Claudio, "Optimized corrugated tapered slot antenna for mm-wave applications," *IEEE Transactions on Antennas and Propagation*, vol. 66(3), pp. 1227–1235, 2018.

[208] M. F. Mohammad Lutful Hakim, "Design and simulation of a multiband millimeter wave microstrip patch antenna array for 5g wireless communication," *in 22nd International Conference of Computer and Information Technology ICCIT-2019*, vol. Bangladesh, pp. 257–264, 2019.

[209] P. A. Dzagbletey, Young-Bae, and J. Member, "Stacked microstrip linear array for millimeter-wave 5g baseband communication," *IEEE Antennas and Wireless Propagation Letters*, vol. 1(1), pp. 780–783, 2018.

[210] J. Anguera, A. Andujar, S. Benavente, J. Jayasinghe, and S. Kahng, "High-directivity microstrip antenna with mandelbrot fractal boundary," *IET Microwaves, Antennas and Propagation*, vol. 12(4), pp. 569–575, 2018.

[211] J. Anguera, E. Martínez, C. Puente, C. Borja, and J. Soler, "Broadband dual-frequency microstrip patch antenna with modified sierpinski fractal geometry," *IEEE Transactions on Antennas and Propagation*, vol. 52(1), pp. 66–73, 2004.

[212] K. S. K. S. H. Suthar, D. Sarkar, "A high gain and wideband directional antenna using z-shaped near zero-index metamaterial," *in IEEE UP Section Conference on Electrical Computer and Electronics (UPCON)*, 2015.

[213] M. Anab, M. I. Khattak, S. M. Owais, A. A. Khattak, and A. Sultan, "Design and analysis of millimeter wave dielectric resonator antenna for 5g wireless communication systems," *Progress In Electromagnetics Research C*, vol. 98, pp. 239–255, 2020.

[214] H. Errifi, A. Baghdad, A. Badri, and A. Sahel, "Directivity enhancement of aperture coupled microstrip patch antenna using two layers dielectric superstrate," *in IEEEProceedings of 2014 Mediterranean Microwave Symposium (MMS2014)*, vol. Marrakech, Morocco, 2014.

[215] W. Hussain, M. Khattak, and M. A.K.Khattak, "Multiband microstrip patch antenna for 5g wireless communication," *International Journal of Engineering Works*, vol. 7(1), pp. 15–21, 2020.

[216] M.Ur-Rehman, M.Adekanye, and Chattha, "Tri-band millimeter wave antenna for body-centric networks," nano communication net-works," *International Journal of Engineering Works*, vol. 18, pp. 72–81, 2018.

[217] A. E. S. Ahmad and J.-M. Floch, "Quad-band antenna for mobile communication," *in 6th European Conference on Antennas and Prop- agation (EUCAP)*, vol. Prague, Czech Republic, 2012.

[218] K. Galav and M. Meena, "Design and analysis of quad band antenna for wieless systems," *Microelectronics Journal*, vol. 5(4), pp. 886–871, 2020.

[219] K. Srivastava, A. Kumar, B. Kanaujia, S. Dwari, and S.Kumar, "Low profile single feed monopole antenna for quad-band circularly polarised applications," *International Journal of Electronics*, vol. 106(2), pp. 318–331, 2019.

[220] M. A. Abdalla, W. W. Wahba, and M. E. Atrash, "A quad-band miniaturised compact ϕ-shaped csrr-based metamaterial- inspired dg resonator antenna," *International Journal of Electronics*, vol. 1, 2021.

[221] M. Sana, S. Ahmad, F. Abrar, and M. A. Qasim, "Millimeter-wave quad-band dielectric resonator antenna for 5g applications," *in IEEE EUROCON 2021 - 19th International Conference on Smart Technologies*, vol. Lviv, Ukraine, 2021.

[222] M. A. El-Hassan, A. E. Farahat, and K. F. A. Hussein, "Compact-size quad-band patch and mimo antenna system for 5g mobile handsets," *Progress In Electromagnetics Research C*, vol. 112, pp. 221–238, 2021.

[223] M. Hassan, Farahat, and Hussein, "Millimetric-wave quad-band mimo antennas for future generations of mobile communications," *Progress In Electromagnetics Research B*, vol. 95, pp. 41–60, 2022.

[224] N. Abdelatif, H. Zamel, A. Attiya, and A. Awamry, "Multi- band mm-wave antenna for 5g-wigig communication systems," *Progress In Electromagnetics Research C*, vol. 99, pp. 133–143, 2020.

[225] M. Rahim, M. Samsuri, N. Elbasheer, and M.E.Ali, "Textile uwb antenna bending and wet performances," *International Journal of Antennas and Propagation*, vol. 2012, p. 12, 2012.

[226] S.Karthikeyan, Y.V.Gopal, V. Kumar, and T.Ravi, "Design and analysis of wearable antenna for wireless body area network," *in International Conference on Frontiers in Materials and Smart System Technologies*, 2019.

[227] G.Mu and P. Ren, "A compact dual-band metasurface-based antenna for wearable medical body-area network devices," *Journal of Electrical and Computer Engineering*, vol. 2020, 2020.

[228] L.Januszkiewicz, P.D.Barba, and Kawecki, "Design optimization of wearable multiband antenna using evolutionary algorithm tuned with dipole benchmark problem," *MDPI Electronics*, vol. 10(18), pp. 22–49, 2021.

[229] M. Khan, A. S. Islam and, M. Nakib, M.Baz, and M. Masud, "Design of a novel 60 ghz millimeter wave q-slot antenna for body-centric communications," *International Journal of Antennas and Propagation*, vol. 2021, 2021.

[230] T. Wu, T. S. Rappaport, , and C. M. Collins, "Safe for generation," *IEEE Microwave Megazine*, vol. Focus issue feature, pp. 65–84, 2015.

[231] B. Almohammed, A. Ismail, and A. Sali, "Electro-textile wearable antennas in wireless body area networks: Materials, antenna design, manufacturing techniques, and human body consideration—a review," *Textile Research Journal*, vol. 61(5), pp. 646–663, 2021.

[232] M. Khan, K. Islam, M. Shovon, N. Alam, M. Masud, M. Baz, and M. AlZain, "Various textiles-based comparative analysis of a millimeter wave miniaturized novel antenna design for body-centric communications," *International Journal of Antennas and Propagation*, vol. 2021, 2021.

[233] T. Wu, T. S. Rappaport, and C. M. Collins, "The human body and millimeter-wave wireless communication systems: Interactions and implications," *in IEEE International Conference on Communications (ICC)*, vol. London, UK, pp. 2423–2429, 2015.